TAMPEREEN TEKNILLINEN YLIOPISTO
TAMPERE UNIVERSITY OF TECHNOLOGY

Sanna Ranta

Wavelength Extension of Visible VECSELs by Structural Engineering

Julkaisu 1256 • Publication 1256

Tampere 2014

Tampereen teknillinen yliopisto. Julkaisu 1256
Tampere University of Technology. Publication 1256

Sanna Ranta

Wavelength Extension of Visible VECSELs by Structural Engineering

Thesis for the degree of Doctor of Science in Technology to be presented with due permission for public examination and criticism in Sähkötalo Building, Auditorium S1, at Tampere University of Technology, on the 31st of October 2014, at 12 noon.

Tampereen teknillinen yliopisto - Tampere University of Technology
Tampere 2014

ISBN 978-952-15-3391-4 (printed)
ISBN 978-952-15-3415-7 (PDF)
ISSN 1459-2045

Abstract

Optically-pumped vertical external-cavity surface-emitting lasers (VECSELs), also called semiconductor disk lasers, are versatile laser devices that are capable of emitting high output powers in a circular, low-divergence beam at emission wavelengths adjustable by the semiconductor gain medium. This unique combination of laser characteristics makes the VECSEL a desirable laser source for various applications ranging from biophotonics and spectroscopy to laser projection. Although VECSELs can emit fundamentally in a wide spectral range, the visible part of the electromagnetic spectrum cannot be fully accessed with direct VECSEL emission. This is due to lack of suitable gain and substrate materials as well as cost-effective pump lasers that are able to emit high optical powers. Thus, the wavelengths below 630 nm have to be generated typically via nonlinear frequency conversion.

This thesis is concerned with the development of VECSEL technology enabling extension of the emission range in the visible part of the spectrum, particularly in the yellow-orange (around 560–590 nm) range and at the red wavelength of 675 nm. Yellow-orange light is generated via frequency doubling near-infrared radiation emitted by GaInAs/GaAsP/GaAs VECSELs, whereas red light is directly generated from a GaInP/AlGaInP/GaAs VECSEL. The thesis reveals the design and growth procedures utilized to obtain high-quality GaInAs/GaAsP/GaAs VECSEL gain medium, and reports the first demonstration of a passively mode-locked GaInP/AlGaInP/GaAs VECSEL emitting at 675 nm. The use of reduced growth temperature and addition of strain compensation are shown to be effective methods in obtaining high quality GaInAs/GaAsP/GaAs gain mirrors. Consequently, over 20 W of frequency-doubled emission has been reached with the GaInAs/GaAsP/GaAs gain mirrors in subsequent studies.

Acknowledgments

The work presented in this thesis has been carried out at the Optoelectronics Research Centre (ORC) in collaboration with the Areté Associates, USA during the years 2010–2014. The research has been financially supported by the Areté Associates, the European Union, the Academy of Finland, and the Finnish funding Agency for Technology and Innovations (Tekes). On a personal level, I gratefully acknowledge the TUT's graduate school (previous the TUT President's Doctoral Programme), the National Doctoral Programme in Nanoscience (NGS-NANO), the Emil Aaltonen Foundation, as well as the Jenny and Antti Wihuri Foundation for granting me personal financial support.

The research presented in this thesis has been obtained as teamwork. Thus, I am grateful to a large group of individuals and co-workers who made the work possible. First of all, I would like to acknowledge my supervisor Prof. Mircea Guina, for the guidance and financial support. Thank you for believing in me and for pushing me forward. I am especially grateful to Dr. Tomi Leinonen, my closest supervisor, for guiding me to the world of semiconductors and lasers. Thank you for giving me your time and energy. I wish to thank also Dr. Antti Härkönen for the guidance given during the mode-locked laser experiment. Thank you for sharing your ideas and thoughts with me. I would like to thank Prof. Emeritus Markus Pessa, the founder of ORC, and Dr. Pekka Savolainen, the current director of ORC, for giving me the opportunity to perform the research and work at ORC. I thank also the development manager Anne Viherkoski and secretary Eija Heliniemi for helping me to struggle through all the administrative issues.

I have had the privilege to work with many experts in their field to whom I wish to express my gratitude. I wish to thank Dr. Jari Lyytikäinen for his comprehensive knowledge and experience in molecular beam epitaxy. A big thanks goes to Miki Tavast for helping me in my research in many ways. I am grateful to Dr. Teemu Hakkarainen for his contribution in the characterization work. I wish to thank Dr. Lasse Orsila and Prof. Günter Steinmeyer for their guidance in the mode-locked VECSEL experiment. I wish to acknowledge Emmi Kantola and Jussi-Pekka Penttinen for their excellent results obtained with the near-IR/yellow VECSELs. I am grateful to Jari Nikkinen for evaporating the antireflective coatings for the VECSELs, and to Dr. Antti Laakso for providing the energy level simulations. Big thanks belong to Jukka Lindfors and Ilpo Suominen as well for helping me to get the research started.

The collaborators at the Areté Associates are gratefully acknowledged for their VECSEL characterization work. The pre-examiners of this thesis Dr. Stéphane Calvez and Dr. Keith Wilcox are thanked for their insightful comments.

Besides the colleagues directly related to this research work, I wish to thank all the co-workers who are currently or have previously been working at ORC. Particularly, I acknowledge the MBE group members Dr. Mika Saarinen, Dr. Antti Tukiainen, Dr. Soile Suomalainen, Dr. Jonna Paajaste, Dr. Lauri Toikkanen, Ville-Markus Korpijärvi, Riku Koskinen, Arto Aho and Janne Puustinen for their help in growth and MBE related issues. I am also grateful to Ilkka Hirvonen, Bengt Holmström and Timo Lindqvist for their technical support. Especially, I wish to thank my roommate Dr. Turkka Salminen for the bright discussions we have had, and for mentally supporting me as well. Thanks for expanding my musical knowledge!

Finally, I wish to thank my parents Riitta and Kari for encouraging me to study. Thanks Dad for being so enthusiastic about technology and Mum for bringing so much excitement and action in our family! I thank my brother Jan for all the great times we have spent together in Tihusniemi. You are the best! I also thank my friends for giving me time to time something else to think about than work. I wish to show my deepest gratitude to my beloved significant other Toni for being always there for me, supporting me in my ‘ups’ and ‘downs’, and for loving me with all of his heart.

Tampere, October 2014
Sanna Ranta

Contents

Abstract i

Acknowledgments ii

Contents iv

List of Publications vi

Author's Contribution vii

List of Abbreviations and Symbols viii

1 Introduction 1

1.1 Background 1

1.2 Objectives and motivation 5

1.3 Thesis outline 6

2 Optically-pumped VECSELs 7

2.1 Gain mirror 8

2.1.1 Design 8

2.1.2 Epitaxial growth 12

2.1.3 Thermal management 13

2.2 Optical cavity 16

2.3 Optical pumping 17

2.4 Ultra-short pulse generation 18

3 Highly strained GaInAs/GaAsP/GaAs QW structures 21
3.1 Strain relaxation 22
3.2 Single QW growth temperature optimization 25
3.3 Strain compensation analysis 26
3.3.1 Structural quality 30
3.3.2 Optical quality 34
3.3.3 Thermal stability 38

4 Gain and absorber structures for near IR and red emission 41
4.1 GaInAs/GaAsP/GaAs gain mirrors for continuous wave near IR emission 41
4.2 GaInP/AlGaInP/GaAs gain mirror and SESAM structures for red mode-locked emission 50
4.3 Gain mirror processing 55

5 Characterization of VECSELs 61
5.1 Near IR continuous wave characteristics 61
5.1.1 Stable narrow-linewidth operation 62
5.1.2 Wavelength tuning 64
5.1.3 High power operation 66
5.2 Red mode-locked operation 68

6 Conclusions 73

Bibliography 77

List of Publications

The following publications are included in this thesis as appendices. In the text they are referred to as [P1]–[P5].

[P1] S. Ranta, T. Hakkarainen, M. Tavast, J. Lindfors, T. Leinonen, and M. Guina, “Strain compensated 1120 nm GaInAs/GaAs vertical external-cavity surface-emitting laser grown by molecular beam epitaxy,” *Journal of Crystal Growth*, vol. 335, no. 1, pp. 4–9, 2011.

[P2] S. Ranta, M. Tavast, T. Leinonen, R. Epstein, and M. Guina, ”Narrow linewidth 1118/559 nm VECSEL based on strain compensated GaInAs/GaAs quantum-wells for laser cooling Mg-ions,” *Optical Materials Express*, vol. 2, no. 8, pp. 1011–1019, 2012.

[P3] W.J. Alford, G.J. Fetzer, R.J. Epstein, Sandalphon, N. Van Lieu, S. Ranta, M. Tavast, T. Leinonen, and M. Guina, “Optically pumped semiconductor lasers for precision spectroscopic applications,” *IEEE Journal of Quantum Electronics*, vol. 49, no. 8, pp. 719–727, 2013.

[P4] S. Ranta, M. Tavast, T. Leinonen, N. Van Lieu, G. Fetzer, and M. Guina, “1180 nm VECSEL with output power beyond 20 W,” *Electronics Letters*, vol. 49, no. 1, pp. 59–60, 2013.

[P5] S. Ranta, A. Härkönen, T. Leinonen, L. Orsila, J. Lyytikäinen, G. Steinmeyer, and M. Guina, “Mode-locked VECSEL emitting 5 ps pulses at 675 nm,” *Optics Letters*, vol. 38, no. 13, pp. 2289–2291, 2013.

Author's Contribution

This thesis is a compilation of five research articles, which are published in international peer-reviewed journals. The research has been carried out as teamwork. The author has contributed mostly in the design, growth and characterization of the GaInAs/GaAsP/GaAs VECSEL gain mirrors [P1], [P2], [P3], [P4]. Moreover, the author has performed most of the passive mode-locking experiments for the GaInP/AlGaInP/GaAs VECSEL reported in [P5]. The author is the main author in [P1], [P2], [P4] and [P5], and has participated as a co-author in the preparation of the manuscript [P3]. A more detailed description about the author's role in preparing each article is given below.

In [P1], [P2], and [P3], the author has designed the passive optical properties of the gain mirror, and participated in the epitaxial growth and gain chip fabrication process. The author has performed the material characterization and the basic VECSEL measurements reported in [P1]; the co-authors have performed the VECSEL measurements shown in [P2] and [P3]. The co-authors have assisted in the gain chip fabrication process and in the material characterization described in [P1]. In [P4], the author has performed the gain chip fabrication process and all the VECSEL measurements; the co-authors have grown the gain mirror.

In [P5], the author has participated in the growth of the absorber structure and in the material characterization of the gain and absorber structures. The author performed the mode-locking experiments under supervision of senior co-authors. The co-authors have also contributed to the design, epitaxial growth and fabrication of the structures, and in the simulation of the laser pulse structure.

List of Abbreviations and Symbols

AcR	Active region sample
Al	Aluminum
AlAs	Aluminum arsenide
AlGaAs	Aluminum gallium arsenide
AlGaInP	Aluminum gallium indium phosphide
AlInP	Aluminum indium phosphide
As	Arsenic
AR	Antireflective
ASE	Amplified spontaneous emission
Au	Gold
AuSn	Gold-tin alloy
BEP	Beam equivalent pressure
BRF	Birefringent filter
Cu	Copper
DBR	Distributed Bragg reflector
DPSS	Diode-pumped solid-state laser
FM	Frank van der Merwe growth mode
FWHM	Full width at half maximum
Ga	Gallium
GaAs	Gallium arsenide
GaAsP	Gallium arsenide phosphide
GaInAs	Gallium indium arsenide

GaInP	Gallium indium phosphide
GaN	Gallium nitride
H_2O	Water
H_2O_2	Hydrogen peroxide
In	Indium
IR	Infrared
LBO	Lithium triborate
MBE	Molecular beam epitaxy
Mg	Magnesium
MOCVD	Metalorganic chemical vapor deposition
MOVPE	Metalorganic vapor phase epitaxy
Na	Sodium
NH_4OH	Ammonium hydroxide
Ni	Nickel
OC	Output coupler
OPL	Optical path length
ORC	Optoelectronics Research Centre
P	Phosphorus
PL	Photoluminescence
Pt	Platinum
PZT	Piezoelectric transducer
QD	Quantum dot
QW	Quantum well
RF	Radio frequency
RoC	Radius of curvature
RPG	Resonant periodic gain
RTA	Rapid thermal annealing
SC	Strain compensation
SDL	Semiconductor disk laser
SESAM	Semiconductor saturable absorber mirror
SHG	Second harmonic generation
SiO_2	Silicon dioxide
SK	Stranski-Krastanov growth mode

TEM_{00}	Fundamental transverse electromagnetic mode
Ti	Titanium
TiO_2	Titanium dioxide
UV	Ultraviolet
VECSEL	Vertical external-cavity surface-emitting laser
VW	Volmer-Weber growth mode
YAG	Yttrium aluminum garnet

Symbols, Greek Alphabet

α, and β	Angles related to the geometry of dislocation
$\Delta\lambda$	Bandwidth
ε	Elastic strain
λ	Wavelength
λ_{PL}	Photoluminescence wavelength
λ_{SB}	Center wavelength of the distributed Bragg reflector's reflectance band
λ_0	Design wavelength
ν	Poisson ratio
ω	Incident angle for the incoming x-rays in an x-ray diffractometer
$2\Delta g$	Bandwidth of the distributed Bragg reflector's reflectance band
θ	Diffraction angle

Symbols, Other

a	Lattice constant
a_s	Lattice constant of substrate
a_o	Lattice constant of overlayer
b	Burgers vector
E	Electric field
E_g	Bandgap
f	Lattice mismatch
f_{REP}	Pulse repetition rate
h_c	Critical thickness for plastic relaxation

k_B	Boltzmann constant
n	Index of refraction
n_H	Index of refraction of high index layer
n_L	Index of refraction of low index layer
n_s	Index of refraction of substrate
N	Number of layers
Q	Reciprocal space vector
R	Reflectance
t	Thicknesses
t_r	Pulse round-trip time
T	Temperature
x, y, and z	Spatial coordinates

Chapter 1

Introduction

The aim of the doctoral research was to develop light sources for the visible part of the electromagnetic spectrum based on a relatively new type of a semiconductor laser concept, called as the vertical external-cavity surface-emitting laser (VECSEL), or the semiconductor disk laser (SDL) [1]–[4]. Conceptually such a laser was described already in the sixties by Basov [5] in his Nobel lecture, but its full potential was not recognized until the nineties when the first high-power optically-pumped VECSEL was demonstrated to operate at room temperature [6], [7]. Since then, VECSELs have been constantly developed in various aspects: nowadays, the VECSEL can cover a wide range of emission wavelengths from ultraviolet (UV) to the mid-infrared (mid-IR) [8], [9] (though not without gaps); generate over 100 W of optical power [10]; and emit ultra-short pulses in the range from picoseconds to a few hundred femtoseconds [11], [12] with high average power levels [13]–[15] and repetition rates spanning from megahertz to gigahertz [16], [17]. Typically, VECSELs utilize optical excitation to achieve lasing, since optical pumping is easier to implement than electrical injection [18]–[20], and it provides uniform excitation over a large area. This uniform excitation enables optically-pumped VECSELs to reach much higher output powers than would be achievable with their electrically-pumped counterparts. This thesis concentrates only on optically-pumped VECSELs.

1.1 Background

Optically-pumped VECSEL is a versatile laser device that is able to generate high output powers in low-divergence circular beam at emission wavelengths, which can be tailored by the choice and composition of the semiconductor gain medium (bandgap engineering). Moreover,

the output power of the optically-pumped VECSEL can be scaled up without sacrificing the beam quality. This combination of power and good beam quality is hard to achieve with laser diode or any other type of semiconductor laser (although not impossible [21]–[23]), but is common for solid-state lasers [24]. Compared to traditional diode-pumped solid-state lasers (DPSS lasers), VECSELs are though more versatile in terms of emission wavelength. Furthermore, VECSELs typically have less limitation for the pump wavelength due to the naturally broad absorption of the semiconductor gain medium; semiconductors namely absorb radiation for all wavelengths shorter than their material bandgap. This property is especially exploited in barrier-pumped VECSEL designs (see Chapter 2). Due to their versatility, VECSELs can be used in a wide range of applications. The external cavity exploited by the VECSEL allows for manipulation of the output beam, which further increases the flexibility of the device. The external cavity enables, for example, intra-cavity frequency conversion as well as ultra-short pulse generation via passive mode locking.

In the visible part of the spectrum optically-pumped VECSELs can generate emission over the whole wavelength range with either direct emission or indirectly via intra-cavity second harmonic generation (SHG), also called frequency doubling, of VECSELs emitting fundamental radiation at near-infrared (near-IR). VECSELs with direct emission have been reported only at the red (650–740 nm [25]–[32]) and quite recently also at the violet part (440–445 nm [33], [34]) of the visible spectrum, whereas frequency-doubled VECSELs have so far covered the 460–675 nm wavelength range [8], [35]–[58], [P2], [P3]. **Figure 1.1** represents the demonstrated power performance of the optically-pumped VECSELs in the visible part of the spectrum.

In addition to the mentioned VECSEL demonstrations, some optically-pumped VECSELs are already being fabricated for commercial use, emitting mainly at the blue, green and yellow wavelengths [59]. Yet, the performance and wavelength span of these VECSELs are limited especially in the orange-red wavelength range. Overall, the optically-pumped VECSEL could be used for an even wider range of applications than it is currently being used if the device is developed further in terms of performance and wavelength span. Applications, for example, in the field of biophotonics and medical therapeutics, entertainment and laser display, spectroscopy, as well as scientific research would benefit from broader wavelength span in the visible spectrum [3], [4], [48], [59]–[61].

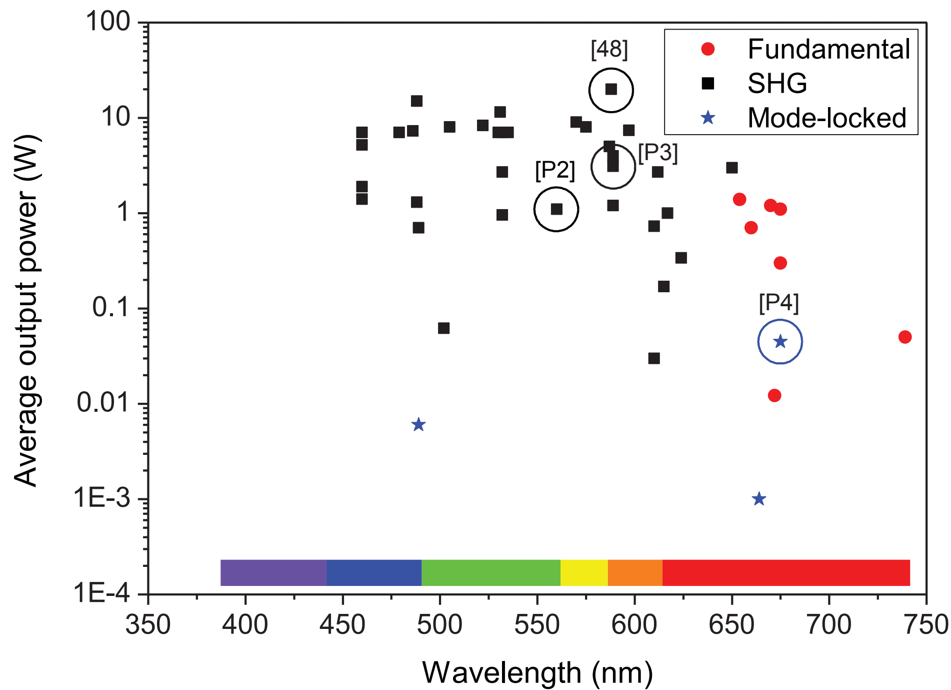

Figure 1.1: *State-of-the-art performance of optically-pumped VECSELs at visible part of the spectrum obtained via direct emission and second harmonic generation (SHG)* [8], [25], [27]–[32], [35]–[52], [54]–[58], [62], [63], [P2], [P3], [P5]. *The results linked to the doctoral work are marked with circles*.

Historically, continuous-wave high-power performance at blue (460–488 nm), green (505–535 nm) and red (650–675 nm) part of the spectrum were already achieved in years 2004–2007 using frequency-doubled GaInAs/GaAs VECSELs (blue and green), and fundamental GaInP/AlGaInP/GaAs VECSELs (red). The yellow-orange part of the spectrum remained as a challenge for a long time since the SHG process, which is needed to reach this spectral range, requires fundamental laser emission at 1140–1240 nm. This wavelength range is hard to access with the traditional GaInAs/GaAs quantum well (QW) material, which has been used most commonly to obtain emission around 1 µm. The difficulty in the manufacture of the required gain materials stems from the high lattice strain that complicates the epitaxial growth and deteriorates the crystalline quality. Various approaches have been developed to overcome this material constrain. The two most successful approaches, in terms of output power reported, involve an addition of a small amount of nitrogen (typically below 2%) in the GaInAs QW to decrease both the band-gap energy and the lattice constant of the material, or alternatively placing of tensile strained GaAsP material layers on both sides of the highly-strained GaInAs QWs. The latter technique is called strain compensation. Both of these approaches decrease the

overall strain of the structure and in this way enable high crystalline quality, which is a prerequisite for achieving good laser performance. From the strain compensation point of view, the key difference between the two methods is that addition of nitrogen reduces the maximum strain of the structure [64] but does not necessarily cancel the accumulation of strain, whereas the strain compensation layers cancel strain accumulation but do not reduce the maximum strain experienced in the QW layers [65]. Thus, strain compensation is only useful in structures, which have a QW strain less than the limit of relaxation of the layer (i.e. the QW should not relax during its growth).

This dissertation utilizes the strain compensation method for extending the wavelength coverage of the GaInAs QWs towards longer wavelengths. Furthermore, a reduced QW growth temperature is used for maintaining a high crystalline quality. With the GaInAs/GaAsP/GaAs gain material structures developed in this doctoral study, an output as high as 20 W has been reached at the frequency-doubled wavelength of 588 nm in subsequent studies [48]. This result represents the state-of-the-art performance in terms of power level achieved with an optically pumped VECSEL at the yellow-orange spectral range.

In the regime of passive mode-locking, VECSELs are just in the beginning of extending their operation to the visible part of the spectrum, as seen from the low amount of mode-locked results reported in **Figure 1.1** [62], [63], [P4]. The first demonstration of ultra-short pulses in this wavelength regime was reported by Casel et al. in 2005 [62]. They utilized simultaneous mode locking and intra-cavity frequency doubling of GaInAs/GaAs VECSEL for generating picosecond pulses at the blue part of the spectrum. This demonstration has, so far, remained the only one, among VECSELs, that involves nonlinear frequency conversion. The cause for the lack of reports is easy to understand: namely, the mode-locking element (a saturable absorber) has the lowest losses for high intensity operation, whereas the frequency-doubling element produces the highest losses for the laser at high operation intensities. Thus, the optimal operation point for achieving effective mode locking and frequency doubling are more or less contradicting.

After the first demonstration, the development of visible picosecond VECSELs has been slow or completely stopped for many years. In this doctoral research, the red part of the spectrum is accessed for the first time; i.e. the first passively mode-locked VECSEL emitting directly at red

is demonstrated [P5]. This mode-locked VECSEL is considered as the first step towards the development of compact ultrafast laser sources at the visible part of the spectrum.

1.2 Objectives and motivation

The thesis concentrates on developing VECSELs that are capable of emitting light at the yellow-orange (around 560–590 nm) and at the red wavelength of 675 nm. Yellow-orange light is generated via frequency doubling near-IR radiation emitted by GaInAs/GaAsP/GaAs VECSELs, whereas red light is directly generated from a GaInP/AlGaInP/GaAs VECSEL. Frequency conversion from near-IR to yellow-orange will not be discussed in this thesis; the main focus is to describe the development of the VECSEL emitting at the fundamental wavelength.

The GaInAs/GaAsP/GaAs gain medium has been systematically examined from the design and fabrication point of view since obtaining both high crystalline quality and long emission wavelengths (>1100 nm) is challenging with this material system due to the high lattice strain. The motivation behind developing the GaInAs/GaAsP/GaAs VECSELs is two-fold: the laser is developed to generate high output powers at the yellow-orange and, on the other hand, to obtain stable narrow-linewidth operation both at the fundamental and at the second harmonic (i.e. yellow-orange) spectral range. The high-power laser could be used as a light source in sodium guide star application, and it could enable further frequency doubling to the UV part of the spectrum. The narrow-linewidth laser could be used for detecting and manipulating atoms, ions and molecules in spectroscopic as well as quantum optical applications both at the visible and UV. Furthermore, biomedical application, such as flow cytometry, ophthalmology and stimulated emission depletion microscopy, could benefit from the yellow laser.

As for the GaInP/AlGaInP/GaAs VECSEL, pulsed operation has been demonstrated for the first time at 675 nm wavelength using passive mode locking and a semiconductor saturable absorber mirror (SESAM). The motivation behind developing the mode-locked red VECSEL is to open up the research interest in developing practical picosecond lasers with compact footprint to be used, for example, in life science to image medical samples [66], [67]. At present, the mode-locked laser systems typically rely on fiber, waveguide or bulk solid-state gain medium, which is arranged into a complex laser design [68]. This complex design increases the cost of the

system and thus hinders their widespread use. Exploitation of the semiconductor gain medium and the versatile characteristics of the VECSEL design (bandgap engineering, power scaling, intra-cavity beam manipulation and frequency conversion), however, give promises that the VECSEL could be developed into a cost-effective and compact laser source in the future. The VECSEL is best suited for generating ultrashort pulses at high output power and high repetition rate.

1.3 Thesis outline

This thesis comprises two main parts: the first part contains a summary of the research carried out for the dissertation and the second part is a compilation of the original research articles [P1]–[P5]. The summary part is arranged into 6 chapters. Chapter 2 describes the concepts and fabrication technology of optically-pumped VECSEL, and shortly introduces the principle of passive mode locking. Chapter 3 presents the gain medium development carried out for the GaInAs/GaAsP/GaAs VECSELs, which is reported as well in publications [P1], [P2]. Chapter 4 concentrates on presenting the gain and absorber structures that were utilized in realizing continuous wave operation with the GaInAs/GaAsP/GaAs VECSELs as well as ultra-short pulses with the GaInP/AlGaInP/GaAs VECSEL [P5]. Furthermore, processing of both the GaInAs/GaAsP/GaAs and GaInP/AlGaInP/GaAs gain media is discussed at the end of this chapter. The main laser results achieved with both material systems are reported in Chapter 5. Chapter 6 shortly summarizes the main achievements of the research and points out future research directions.

Chapter 2

Optically-pumped VECSELs

This chapter reviews the main elements of the VECSEL and introduces the principles of ultra-short pulse generation via passive mode locking. The molecular beam epitaxial growth method, which is used to fabricate the VECSEL gain medium and the saturable absorber, is also presented.

The simplest architecture of the VECSEL is sketched in **Figure 2.1**. The device comprises an epitaxially-grown semiconductor gain mirror, an external cavity and a pump source. The output is extracted typically through one of the external mirrors. In order to achieve amplification for the laser signal, the gain region is pumped optically.

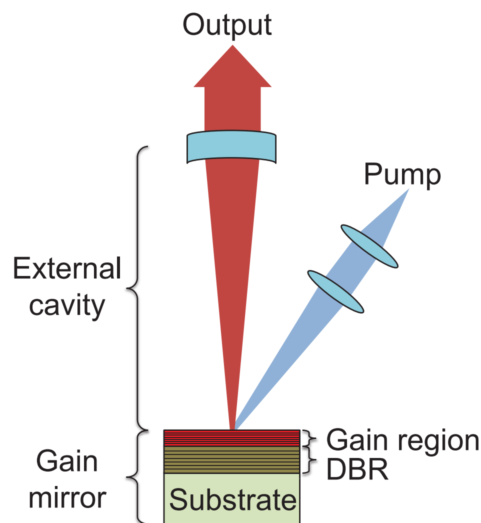

Figure 2.1: *Basic architecture of the VECSEL. The distributed Bragg reflector is denoted as DBR.*

2.1 Gain mirror

The gain mirror is a semiconductor disk structure, which consists of a gain region and a highly reflective (reflectance > 99.9%) semiconductor mirror, i.e. a distributed Bragg reflector (DBR). The gain region and the DBR are both integrated in the same wafer, as schematically shown in **Figure 2.1**. The external cavity is formed between the DBR and one or several external mirrors, and its function is to circulate the laser signal multiple times through the gain region. The gain mirror is mounted on a sample holder that is typically cooled during laser operation.

2.1.1 Design

The DBR is basically a multiple thin-film structure providing high-reflectance. It consists, in its simplest form, of two materials, each having a different index of refraction, layered on top of each other to form a stack. The optical thickness of each material layer is the same, being an odd integer of $\lambda_0/4$, where λ_0 is the design wavelength of the DBR. Typically the lowest integer is chosen, i.e. the consecutive layers are exactly $\lambda_0/4$ thick. Such structure experiences strong reflection at λ_0 due to constructive interference that occurs when the light components reflected from the interfaces superimpose with each other. The reflectance of the DBR depends on the refractive index contrast between the two materials and on the number of layer pairs present in the stack – the higher the index contrast and amount of layer pairs, the higher the reflectance. The maximum reflectance for such a DBR is obtained when the high index layers are placed outermost, i.e. the high index layer being the first and last layer of the stack. For such a layer arrangement, the reflectance R of a DBR that comprises $2N + 1$ quarter-wave thick layers takes the form of [69]

$$R(\lambda_0) = \left(\frac{1-(n_H/n_L)^{2N}(n_H^2/n_s)}{1+(n_H/n_L)^{2N}(n_H^2/n_s)}\right)^2, \tag{2.1}$$

where N is a positive integer, and n_H and n_L are the indexes of refraction of the two materials forming the DBR, the subscript L denoting low and H denoting high. The refractive index of the substrate is marked as n_S.

The DBR forms a high-reflectance band, called as a stop band, on both sides of the design wavelength with a width of $2\Delta g$, where [69]

$$\Delta g = \frac{2}{\pi}\sin^{-1}\left(\frac{n_H - n_L}{n_H + n_L}\right). \tag{2.2}$$

To achieve a sufficiently high reflectance for a VECSEL (R > 99.9%), the amount of layer pairs that form the DBR should be high, which makes the structure several micrometers thick. For a typical VECSEL DBR, composed of AlAs/GaAs, the index contrast is only about 0.7 or less near 1 μm, which means that over 25 DBR pairs are needed. In order to grow the DBR with high quality over large thicknesses, the materials constituting the DBR should be nearly lattice-matched to the substrate, meaning that the lattice constant of the gain mirror layers approximately matches the lattice constant of the substrate. Other requirements set for the materials are that they need to be transparent at the pump and signal wavelength and preferably have low thermal impedances.

The gain medium is located on top of the DBR; typically it consists of QWs or quantum dots (QDs) that are surrounded by the barrier medium. Both of these gain medium geometries exploit the quantum confinement effect to reduce the density of states and thus to achieve population inversion with less excitation power than in the case of bulk semiconductors. The structures developed in this research utilize only GaInAs QWs embedded in GaAs as the gain medium. Normally, the GaInAs/GaAs QWs are compressively strained, which will further reduce the density of states in the valence band of the active medium, resulting in a better laser performance [70], [71]. On the other hand, strain is the limiting factor in extending the emission wavelength.

The charge carriers are generated via optical excitation either only in the QWs (called as in-well pumping) or in most cases also in the barrier/spacer layers from which the carrier thermalize to the QWs (called as barrier pumping). When barrier-pumping is utilized, the energy barrier between the QWs and the barrier layer should be set sufficiently high so that the carriers do not escape from the QWs even at elevated temperatures and thus reduce the gain. The maximum barrier height between the QW and the barrier layer is determined by the pump wavelength: the barriers should have a band gap lower than the pump energy so that the pump can be absorbed to the barrier layers.

The gain region is capped with a window layer and possibly with a separate capping layer. The window layer has a higher band gap than the barrier layers and thus prevents the excited charge

carriers from drifting to the air/semiconductor interface, where they could recombine non-radiatively via surface states. The capping layer protects the gain mirror surface against atmospheric oxidation. The window and capping layers should be transparent at the pump and lasing wavelength, and preferably have a high thermal conductivity.

Highly lattice mismatched QWs, meaning that the lattice constants of the QWs and substrate differ more than 1.8% [72] from each other, are typically stabilized against lattice relaxation by adding so-called strain compensation layers around the QWs [73]. The strain compensation layers have a strain opposite to that of the QWs; thus, they reduce the net strain of the semiconductor structure preventing lattice relaxation and deterioration of the crystalline quality. GaAsP and GaInP are the most commonly used strain compensation materials in the GaInAs/GaAs QW system.

The design of the gain region depends essentially on the application, i.e. what kind of laser performance is expected and how much will the gain mirror heat up during the operation at the desired power level with the applied sample holder and cooling system. One common design principle of the gain region is to position the QWs near the antinodes of the standing-wave electric field of the laser resonator mode. Such an arrangement, called as a resonant periodic gain structure (RPG) [74], maximizes the overlap between the gain medium and the optical standing-wave field and thus increases the effective gain of the QWs. The effective gain may be further enhanced by designing the micro-cavity, which is formed between the DBR and the air/gain mirror interface, to be resonant at the laser resonator mode. In such a resonant design, the micro-cavity has an optical thickness of one or multiple halves of the operation wavelength. The micro-cavity resonance increases the optical field strength inside the gain region and thus enhances the gain, but at the same time narrows the gain bandwidth of the laser and exposes the gain more strongly to temperature effects: The micro-cavity resonance peak and the intrinsic QW gain namely shift along with the gain chip temperature (and thus along with the pump power level) to longer wavelengths. The shift rates are, however, different, which may cause the peaks to walk out of alignment as temperature increases and the peak gain to diminish. Narrowing of the gain bandwidth might be undesirable for some applications, such as for achieving mode locking and large wavelength tuning ranges. Moreover, scattering and other non-radiative losses are higher in the resonant device since the antinode of the resonator mode is positioned at the air/gain medium interface; this configuration enhances nonradiative recombination via surface and defect states.

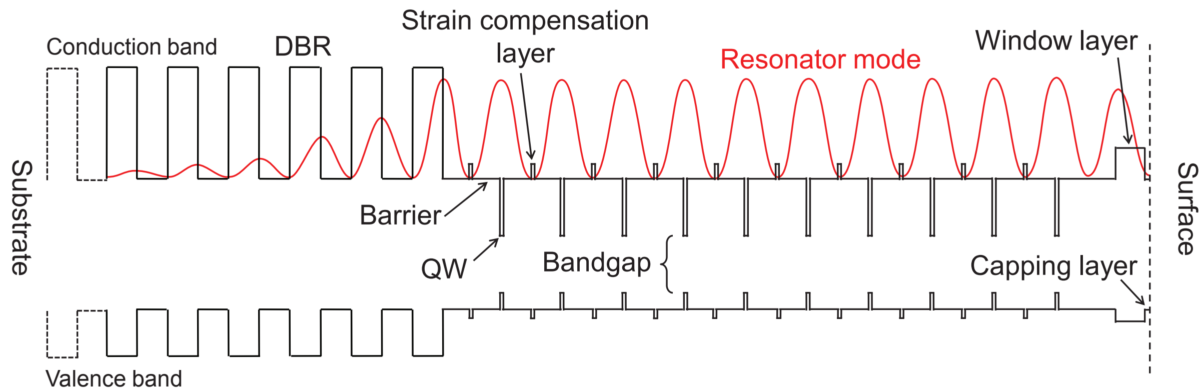

Figure 2.2: *Semiconductor layer structure of an antiresonant gain mirror*.

On the contrary, an "antiresonant design" of the micro-cavity, meaning that the optical thickness of the micro-cavity is an odd integer of quarter operation wavelength, does not limit the gain spectrum; an example of the antiresonant design is illustrated in **Figure 2.2**. The antiresonant microcavity design cannot typically tolerate as high cavity losses as the resonant design and might thus not be used in every VECSEL cavity configuration.

When designing the gain mirror of a VECSEL, one needs to take into account the pump-induced heating of the gain material. This heating affects the gain mirror in many ways: (i) it decreases the bandgap (E_g) of the QWs and their barriers, which lead to an increase in the emission wavelength; (ii) reduces the intrinsic gain due to enhanced nonradiative recombination and thermal carrier escape from the QWs; and (iii) increases the refractive indices of the semiconductor materials and their physical thicknesses causing optical thicknesses to scale up. This latter effect (iii) further causes the center of the DBR stop band (λ_{SB}), the RPG spectral peak, as well as micro-cavity resonance peak shift to longer wavelengths. The shifts rates are generally different; for example, in the GaInAs/GaAs material system, the optical thicknesses shift around 0.1 nm/°C, whereas the peak gain has a shift rate of 0.3 nm/°C [7]. The different shift rates are taken into account by detuning the optical thicknesses of the DBR layers and the micro-cavity accordingly, and by designing the RPG structure to shorter wavelength when it is not pumped. In other words, the gain peak, the stop band center and the RPG peak, and in the case of a resonant design also the micro-cavity resonance peak, should be matched at the desired power level. If the gain mirror is not adequately designed in this respect, there is a risk that the intrinsic gain peak walks out of alignment with the RPG and micro-cavity resonance peaks causing the effective gain to diminish and the laser to switch off.

The number of the QWs used in the structure depends on the laser power and/or threshold requirements. Generally, the more QWs are present, the more gain and output power can be achieved presuming uniform excitation of all the QWs and optimum output coupling. However, the laser threshold will increase along with the number of the QWs. [3] In practice, it is difficult to achieve uniform excitation due to the rapid exponential decay of the pump radiation, unless some special arrangements are utilized, such as placing two or more QWs in the same antinode of the standing-wave or using additional carrier-blocking layers to restrict the amount of pumping volume and thus carriers supplied in the QWs [28], [75]. If the RPG is not properly designed, QWs located deep in the structure might not even reach population inversion since optical excitation is too weak to produce sufficient number of charge carriers in the QW. Moreover, increasing the number of QWs results in a thicker gain region structure, which contains more strained layers. Such a structure is more difficult to grow with high crystalline quality, and it has increased thermal impedance. Thus, an optimum number of QWs should be found depending on the desired laser performance targets, pumping conditions, resonator design, cooling ability and so on.

In this doctoral thesis, the passive optical properties of the gain mirrors developed were designed with the aid of the commercial Essential MacLeod software [76], which is specialized in multilayer thin film simulations. It is based on the transfer matrix method of thin film simulation.

2.1.2 Epitaxial growth

Gain mirrors are grown epitaxially on single-crystal substrates. The two most commonly used techniques are molecular beam epitaxy (MBE) and metalorganic chemical vapor deposition (MOCVD), or alternatively called as metalorganic vapor phase epitaxy (MOVPE). The gain mirrors developed within this work were fabricated with the MBE method utilizing the III/V material system.

In MBE, the semiconductor layers are formed from their elemental constituent materials that are evaporated in a flux of atoms or molecules onto the substrate in an ultra-high vacuum. The atoms or molecules incorporate onto the crystal lattice and form a film that maintains the lattice constant of the substrate. The composition of the semiconductor film is determined by the different elemental material fluxes. The group V materials are typically evaporated in excess in

the growth chamber, whereas the group III fluxes are controlled by the evaporation cell temperature. Thus, the growth rate is determined by the group III fluxes. The substrate is heated and rotated during the growth process to ensure a high crystalline quality and a uniform material distribution. The gain mirrors developed within this research utilized solid source materials; elemental aluminum (Al), gallium (Ga), and indium (In) as group III, and arsenide (As_4) as well as phosphide (P_4) as group V materials. The group V species were cracked to smaller As_2 and P_2 molecules before they were targeted on the substrate.

The growth can be controlled by influencing the substrate temperature and the material fluxes (growth rate). Depending on the materials and growth conditions, essentially three primary growth modes can be distinguished, which are known as Frank van der Merwe (FM), Volmer-Weber (VW) and Stranski-Krastanov (SK) [77]. The FM growth mode generates planar layers with smooth surfaces, whereas the SK and VW are 3-dimensional growth modes, i.e. the growth occur via island formation. In the SK mode the growth begins in a layer-by-layer mode, but after some thickness islands start to form. In the VW mode, the growth already begins via island formation.

Planar growth (i.e. growth in FM mode) can be obtained for lattice-matched and nearly lattice-matched structures; here lattice mismatch f is defined as the difference between the substrate a_s and the overlayer a_o lattice constants as follows:

$$f = \frac{a_o - a_s}{a_s}. \tag{2.3}$$

For high lattice-mismatches (f > 1.8% [72]), the growth mode typically switches from FM to SK.

In order to obtain high crystalline quality QW structures, the growth should occur in FM mode and it should remain pseudomorphic, i.e. the growing layer should accommodate the crystal lattice of the underlying layer/substrate. Thus, the substrate limits the choice of materials that can be applied in the gain mirror.

2.1.3 Thermal management

As part of the optical pumping process, part of the pump energy is converted into heat in the gain medium due to the quantum defect (i.e. energy difference between the pump and laser

photon) and non-radiative recombination of the charge carriers. Heating of the material typically limits the performance of the laser by causing thermal runaway (thermal roll-over), which eventually switches off the laser. During thermal runaway, the quantum efficiency of the laser is reduced to such an extent that increasing the pump power no longer increases the output power of the laser; thus, the pump power is rather converted into heat, which may decrease further the quantum efficiency.

Heating of the material is unavoidable, but proper heat sinking can limit the temperature rise and thus should allow lasing. To extract heat, two cooling techniques are commonly employed: (i) the thin disk approach [6] where the heat is extracted through the DBR or (ii) the intra-cavity heat spreader approach where the heat is dissipated from the topside of the active region [78].

Figure 2.3 shows schematically the implementation of the two cooling approaches and the heat flows within the devices (the heat flow is illustrated with arrows). For both of the cooling techniques the gain mirror needs to be processed, meaning that part of the gain mirror is scribed and cut into gain chips, which are attached to thermally conductive heat spreaders. The heat spreaders are further attached to the actively cooled heat sinks. The gain mirrors are grown in different order for the different cooling techniques: The intra-cavity heat spreader approach utilizes gain mirrors grown in top-emitting configuration, meaning that the DBR is grown first before the active region. For the thin disk device, the growth order is reversed, i.e. the growth starts with the window layer, preceded to the active region and finally ends to the DBR; this growth configuration is called as bottom-emitting. Additional details of the processing steps are described in Section 4.3.

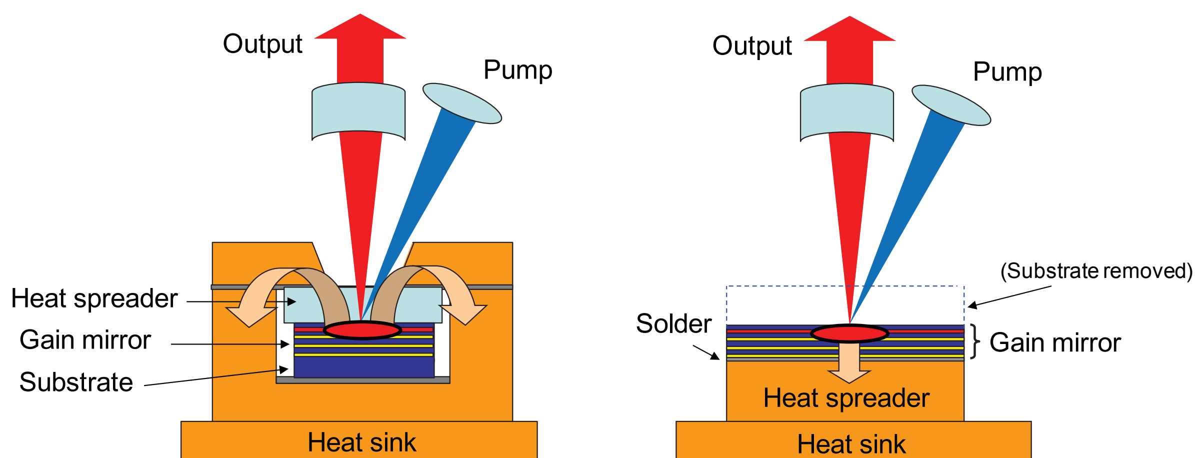

Figure 2.3: *Intra-cavity heat spreader (left) and thin disk (right) approaches utilized for cooling the gain mirror. Reproduced from* [79]*; licensed under CC BY 3.0*.

The intra-cavity heat spreader approach is advantageous over the thin disk approach in two ways: (i) processing of the top-emitting gain mirrors is fairly straightforward, and (ii) the heat conduction path length is very short. Additionally, thermal impedance of the DBR does not play such a critical role in the intra-cavity heat spreader approach than in the thin disk approach. The apparent downside with the intra-cavity heat spreader is that it forms a Fabry–Pérot etalon inside the laser which spectrally filters the laser output [44]. Thus, the intra-cavity heat spreader usually restricts continuous wavelength tuning and mode-locking of the VECSEL. Furthermore, lateral heat flow, which is becoming more pronounced at large pump spots in the heat spreader, might limit the cooling capability of this thermal approach [80]. The etalon effect can, however, be mitigated by using a wedged heat spreader geometry. An antireflective (AR) thin-film coating is typically applied on the heat spreader to reduce additional optical losses induced by the wedge. AR coatings are normally used on intra-cavity heat spreaders and on top of thin disk devices to minimize reflection losses at the air/gain chip -interface. In general, both the intra-cavity heat spreader and the thin disk devices have proven to be able to generate high output powers, especially near the laser wavelength of 1 µm [10], [80]–[83], [P4]. To date, the highest output power from a single chip (over 100 W) has been obtained with the thin disk VECSEL emitting near the wavelength of 1 µm [10].

2.2 Optical cavity

The optical cavity of VECSEL is in its simplest form constructed of two mirrors: the Bragg mirror and a partially-transmissive external mirror. The mirrors are placed in free space and are separated by a suitable distance from each other. Such a cavity is termed as a 2-mirror cavity or an I-cavity, and is schematically sketched in **Figure 2.1**. The simple 2-mirror configuration has traditionally been used for obtaining high output powers [10], [81], [83], [84]. The VECSEL cavity can also be constructed from several external mirrors forming so-called folded V-shaped or Z-shaped architectures. These multi-mirror cavities are particularly useful in application where the laser mode size needs to be adjusted more freely than would be possible with a 2-mirror cavity. In addition to the mirrors, the external cavity may contain various intra-cavity elements, such as etalons, filters, nonlinear crystals and saturable absorbers, which can manipulate the properties of the laser output and thus increase the usefulness of the VECSEL.

The cavity design determines the transverse mode properties of the VECSEL, and is thus a vital part of developing a VECSEL. The optical cavity should be designed to be stable, i.e. the optical elements should be chosen, aligned and placed in such a way that the transversal laser mode will reproduce itself after each roundtrip. Moreover, if fundamental mode operation is desired, the cavity design should give a fundamental mode size that approximately matches with the pump spot size on the gain mirror so that higher order transverse modes experience sufficient additional loss and are thus suppressed. If the pump spot is set larger than the mode size, the laser operates at multiple transverse modes, which are excited by the larger pumped transverse extent. The intra-cavity elements as well as the final laser application might set additional requirements for the cavity design, like, for example, limitations on the mode size at the nonlinear crystal.

The reflectance of the cavity mirrors need to be high since the round-trip gain of a VECSEL is low (few percent) due to the very thin QW layers that provide the gain for the laser. For fundamental wavelength operation, the transmission losses of the external cavity mirror(s) are typically optimized to enable maximum amount of power extraction from the laser. Choosing the adequate output coupling is thus balancing between the amount of losses and gain taking into account also specific operation regime (for example, in the case of intracavity frequency conversion, the entire fundamental radiation is recirculated in the cavity by the external mirror).

Special resonator design tools are typically used to help calculating the evolution of the fundamental transversal mode within a particular cavity; in this research, we utilized the WinLase 2.1 Professional software [85]. It uses the ray transfer matrix analysis to describe the mode properties. The program determines the stability of a particular cavity design as well as the fundamental mode size at various cavity positions.

2.3 Optical pumping

The gain mirror is optically pumped with an external multimode diode laser capable of emitting high output powers (typically from several watts to several tens of watts). Traditionally, the pump is absorbed mainly in the barriers separating the QWs (barrier-pumping) in a single pass, but it is also possible to only pump the QWs (so called in-well pumping [86]–[88]) for reduced quantum defect. The advantages of barrier-pumping over in-well pumping is that it is easier to implement and it sets minimal amount of requirements for the pump laser: the main requirements for the pump laser are that it should be capable of producing uniform pumping over the whole beam spot and emit pump photons that are higher in energy than the bandgap of the barrier material in order to enable absorption. The beam quality of the pump laser is not critical. Consequently, low-cost, low-brightness diode lasers that are readily available can be utilized to pump the gain mirror. In this thesis, we have only utilized barrier pumping.

Optical pumping enables one of the key characteristics of the VECSEL, namely power scaling, which means that the output power of the device can be scaled up without sacrificing the beam quality just by increasing the pump spot and mode sizes adequately. For this to happen, the pump focusing optics and the cavity arrangement need to be modified accordingly in order to match the fundamental resonator mode size with the pump spot size. The laser power can, however, not be scaled to infinitively high levels. Instead, there is an upper limit for the power scaling capability after which other effects, such as thermal runaway or amplified spontaneous emission, limit the power achievable from a single chip. The upper power-scaling limit depends on the applied cooling approach as well as on the materials used in the gain chip.

2.4 Ultra-short pulse generation

VECSELs can emit radiation in continuous-wave or they can be forced to operate in pulsed mode. Mode locking is the established technique to produce ultra-short pulses in the regime from femtoseconds to around 100 picoseconds [89], [90]. In this method, the laser operates in multiple longitudinal modes that are in phase with each other. Due to this constant phase relation, the intensities of each mode add up to form a repetitive optical pulse train. The locking of the phase of the modes is initiated and maintained either via active or passive means. The active methods can involve an electro-optic modulator, which is driven by an external source, to modulate the optical resonator losses, gain or round-trip phase change, whereas the passive method utilizes a saturable absorber for achieving corresponding modulation [90]. In this doctoral work, a semiconductor saturable absorber mirror (SESAM [91]), which is widely used in a variety of ultrafast lasers [68], [91], was used in achieving passive mode locking. Passive mode locking is beneficial over active mode locking, since the pulses can be modulated much faster resulting in shorter pulse durations.

A SESAM is a thin film semiconductor structure that is placed as one of the VECSEL cavity mirrors. It comprises a thin absorber region which is integrated on top of a DBR. A cap layer may be applied on top of the structure. The absorber region typically consists of QWs or QDs that are surrounded by barrier material. As in the case of the gain mirror, the QWs or QDs are usually placed at the antinode of the standing-wave electric field at the operation wavelength. Moreover, the electric field strength inside the device can be enhanced by designing the micro-cavity resonant at the operation wavelength. The reflectivity of the SESAM and thus the resonator losses are modulated by absorption of the active region: at low fluences, the absorption is more pronounced and the losses are higher than for higher fluences, in which case the absorber is saturated and thus the absorption losses are lower. The maximum difference of the nonlinear reflectance as well as the pulse fluence needed to saturate the absorber can be tailored through the SESAM design and the materials used. The SESAMs are fabricated via an epitaxial process on single-crystal substrates.

During mode-locked operation, usually a single pulse is circulating inside the cavity (fundamental mode locking). Every time the pulse hits the SESAM, the SESAM is temporarily saturated causing the excited charge carriers to fill up the available states in the valence and

conduction band of the absorber. Consequently, the resonator losses experienced by the pulse are minimized causing a net gain window to open up for a short period of time. At other times, the SESAM is not saturated which causes the resonator losses to remain higher than the gain. Thus, the SESAM makes the VECSEL to favor pulsed operation over continuous wave. Moreover, the SESAM effectively suppresses any other intensity fluctuations induced by the laser and thus stabilizes the mode locked operation. After the SESAM is bleached with a short optical pulse, the absorption needs to recover, i.e. the excited charge carriers need to recover back to their original states via thermal relaxation and recombination. The time it takes for the SESAM to recover is called the recovery time and it determines the minimum pulse duration achievable with the device [68]. To enhance the recovery time, defects can be incorporated in to the absorber region by low-temperature growth or ion implantation [92]. These defects induce trap states inside the bandgap through which the charge carriers can recombine more quickly (intraband transition).

The length of the laser cavity determines the pulse repetition rate of the mode-locked VECSEL: the pulse repetition rate is the inverse of the pulse round-trip time, $f_{REP} = 1/t_r$. Theoretical limit for the pulse duration is determined by the spectral width of the laser (in frequency space); a pulse that approaches this theoretical limit is said to be transform-limited.

Chapter 3

Highly strained GaInAs/GaAsP/GaAs QW structures

This chapter reviews the structural analysis that was carried out with the GaInAs/GaAsP/GaAs material. The target of the study was to find adequate structural and epitaxial growth parameters, which would enable the growth of GaInAs/GaAsP/GaAs VECSEL gain mirrors with high crystalline quality at emission wavelengths beyond 1100 nm. The main challenge associated with the growth of GaInAs/GaAs on (001) GaAs substrates for such long emission wavelengths is the high lattice mismatch of the two materials: namely, to achieve emission wavelengths over 1100 nm using GaInAs/GaAs QWs, the amount of indium needs to be higher than 25% [93]–[95] corresponding to a lattice misfit of 1.8%; the exact amount of indium required depends on the growth conditions and QW thickness. Such a high lattice strain may already break down the pseudomorphic growth unless proper optimization of the growth condition and layer structure is applied.

In this dissertation, the challenge associated with the growth of high-quality GaInAs/GaAs has been addressed in two ways: The growth temperature of the GaInAs QWs has been lowered from the value typically used for low or moderately strained GaInAs in order to hinder relaxation of the single QWs. Furthermore, the net strain induced by the compressively-strained QWs has been compensated with tensile-strained GaAsP layers in order to avoid relaxation of the whole gain structure. The low growth temperature and the use of strain compensation have shown to be effective methods in obtaining high quality gain mirrors.

The chapter begins with a brief description of the relaxation processes obtained in highly strained single and multiple GaInAs/GaAs QW layers. The description is followed by the experimental work carried out on the optimization of single QW growth temperature and on the analysis of strain compensation.

3.1 Strain relaxation

The high lattice strain present in GaInAs/GaAs structures may partially relax by inducing a change in the growth mode from the planar FM to quantum-dot like SK growth, and/or by generating misfit dislocations in the crystal structure. Both of these strain-induced modifications are unwanted in the growth of QW devices: The SK growth mode generates a wavy growth front, which roughens the interfaces of the strained layer and generates thickness as well as strain field undulations. Plastic relaxation, on the other hand, forms defects and dislocations in the structures, which have been observed to act as a nonradiative recombination centers [96]–[98]. Consequently, these crystalline imperfections reduce the efficiency, life time, and reliability of the devices [99].

Plastic strain relaxation

Misfit dislocations typically appear at the hetero-interfaces when the crystal can no longer elastically sustain the misfit strain. This happens when the layer thickness exceeds the critical layer thickness, a term developed to describe the onset of relaxation in theoretical calculations. The strained layer may have several critical layer thicknesses depending on the different strain relaxation mechanisms involved [65], [97]. The most widely used model for determining the critical layer thickness is the equilibrium model of Matthews and Blakeslee [100]. This model assumes that the first misfit dislocations are generated in the bending of the threading dislocations already existing in the substrate. According to the model, the critical thickness h_c can be given as

$$h_c = \frac{|\boldsymbol{b}|(1-\nu cos^2\alpha)[\ln(h_c/|\boldsymbol{b}|)+1]}{2\pi|f|(1+\nu)\cos\beta}, \tag{3.1}$$

where **b** is Burgers vector for the threading dislocation, ν is Poisson ratio, f is lattice mismatch, and angles α and β are related to the geometry of the dislocation.

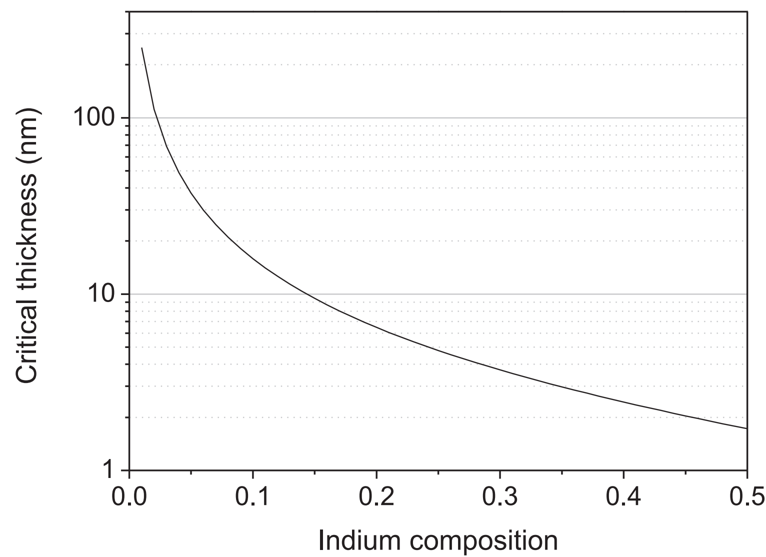

Figure 3.1: *Critical thickness of GaInAs as a function of indium composition calculated by the Matthews and Blakeslee equilibrium model.*

Figure 3.1 shows the calculated critical layer thickness for a single GaInAs layer grown on (001) GaAs as a function of the misfit strain. From **Figure 3.1**, the critical layer thickness can be seen to decrease as the strain, i.e. indium composition, is increased. Another way to control the onset of plastic relaxation, in addition to affecting the lattice misfit, is to kinetically limit the nucleation and formation of dislocations. Thus, by decreasing the substrate temperature [101], [102], defect-free layers can be grown at thicknesses exceeding the predictions given by the equilibrium models. As a result, metastable layers are formed [72]. For the optoelectronic device designer, the critical layer thickness given by the Matthews and Blakeslee model can be regarded as kind of safety limit – if the layer is kept thinner than the predicted critical layer thickness, the crystal will most probably be free from misfit dislocations.

Elastic strain relaxation

Highly mismatched (misfit >1.8%) heteroepitaxial structures, such as GaInAs on (001) GaAs, tend to epitaxially grow in a SK growth mode, where the growth begins in a layer-by-layer fashion, but after a critical threshold coverage switches to three-dimensional (3D) island growth. The two-to-three-dimensional (2D-to-3D) growth transition enables partial relief of the accumulated strain energy and is thus energetically favored by the structure. The strain is relieved elastically, i.e. the in-plane lattice parameter continuously relaxes along the growth

direction without formation of misfit dislocations in the heterointerfaces. Thus, the threshold thickness for 2D-to-3D growth transition generally deviates from the critical layer thickness described above. However, dislocated 3D islands can as well be formed when the growth is continued beyond the threshold coverage thickness [103]. The critical threshold coverage depends on the lattice misfit as well as on the growth conditions. High lattice misfits result in low threshold coverages [104], [105], whereas the growth parameters have generally a more complex influence on the epitaxial growth. The 2D-to-3D transition can be kinetically controlled and thus shifted to higher thicknesses by reducing the surface diffusivity for adatoms, for example by lowering the substrate temperature [106]–[108] or increasing the V/III ratio [109], [110], or by increasing the growth rate [111]. Furthermore, surfactants may also decrease the tendency for 3D island formation [112]–[114].

Relaxation in multi-QW structures

Optoelectronic structures, such as the gain mirror of a VECSEL, typically comprise not only a single, but instead a stack of QWs. In such situation, the strain arising from each QW is accumulated during the growth resulting in a net strain to be induced in the structure. Consequently, this net strain affects the growth of the subsequent layers, and may cause the structure to relax even though the thickness of each individual QW is kept below their relaxation threshold. Therefore, a critical layer thickness (or correspondingly threshold coverage thickness) can be defined for the whole multilayer structure as well, which generally differs from the critical thicknesses (threshold coverage thicknesses) determined for the individual strained layers [73], [97]. To obtain pseudomorphic growth in a stack of QWs, each individual layer as well as the entire multi-QW stack needs to be grown below its critical thickness [65], [72], [97], [115], [116] so that plastic strain relaxation does not occur, and the 2D-to-3D growth transition should be avoided by keeping the strained layers thicknesses below the corresponding threshold coverage thicknesses.

3.2 Single QW growth temperature optimization

The effect of growth temperature on the optical quality of QW was assessed by room-temperature photoluminescence (PL). For this test, single QW calibration samples were grown at different temperatures. The structure of the samples is shown in **Figure 3.2**. The QW was 10 nm thick and was targeted for emission near 1120 nm corresponding to an indium composition of 31% (misfit strain -2.2%). Such a QW exceed the critical thickness calculated by the Matthews and Blakeslee model (see **Figure 3.1**), and might thus be vulnerable to plastic relaxation.

The growth was performed on quarter pieces cut from the whole substrate wafers. The measured PL signal are shown in **Figure 3.3**. Temperatures given are thermocouple readings obtained from the sample holder, since the infrared pyrometer, which was typically used for determining the growth temperatures, could not reliably measure temperatures below 500 °C. A thermocouple reading of 545 °C corresponds to a pyrometer temperature of 500 °C for these experiment. Low or moderately strained GaInAs are normally grown at 560-565°C (thermocouple reading). The growth rate of the QWs was 1 µm/h, and indium compositions varied between 30.8–31.4% as determined from (004) ω-2θ x-ray diffraction profiles (see Section 4.1 'Wafer characterization' for the x-ray diffraction analysis). In addition to the samples shown in **Figure 3.3**, two calibration samples were grown also at 565 °C and 370°C. However, these samples did not give any PL signal and are therefore excluded from **Figure 3.3**.

Layer	Thickness
GaAs cap	10 nm
AlAs cladding	20 nm
GaAs barrier	50 nm
$Ga_{0.769}In_{0.31}As$ QW	10 nm
GaAs barrier	50 nm
AlAs cladding	200 nm
GaAs buffer	150 nm
(001) *n*-GaAs substrate	350 um

Figure 3.2: *Structure of the QW calibration sample.*

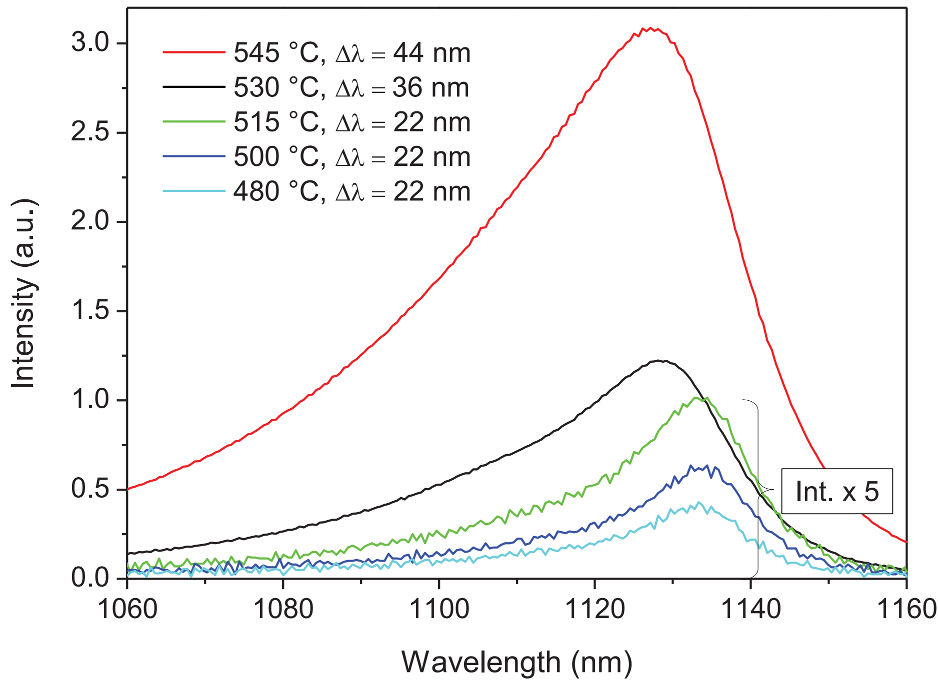

Figure 3.3: *PL spectra measured at different growth temperatures. The PL signals obtained at 515 °C, 500 °C and 480 °C were multiplied by a factor of 5 for illustrative purposes.*

As shown in **Figure 3.3**, the optimal temperature for the GaInAs QW growth seems to be 545 °C, because it yields the highest quantum efficiency, although the emission is broadened to a FWHM linewidth of 44 nm. Broadening of the peak might indicate beginning of 3D growth and thus elastic relaxation. Probably misfit dislocations are not yet formed, since the PL intensity is still high at this temperature. Vanishing of the luminescent signal as the growth temperature is increased from 545 °C to 565 °C is probably a result of plastic relaxation, whereas incorporation of other defect, such as arsenic antisites and gallium vacancies [117], probably explain the disappearance of the PL signal at 370 °C.

3.3 Strain compensation analysis

Strain compensation [65], [73] is a technique that can be used to reduce the accumulation of net strain in multi-QW structures. In this technique, the compressive strain caused by a strained layer, for example QW, is compensated with another layer, which has a strain opposite to the formerly mentioned layer. By stacking such layers one after another, one can increase the critical layer thickness of the multi-QW stack [70], [100] and thus increase the number of QW

periods that can be grown before relaxation occurs. When the compressive and tensile strain is evenly balanced in the structure, it should, in theory, be possible to stack an infinite amount of periods. However, ideal balancing of tensile and compressive strains has shown to be unnecessary, since partial balancing can already result in high-quality multi-QW structures. [65], [118]

This section describes the structures, epitaxial growth processes and characterization techniques used to analyze relaxation, net strain as well as thermal stability of the structures. Out of the techniques used, dark defect imaging was found to be the most sensitive method for detecting relaxation of the crystal, whereas strain-induced bending was shown to give information on the net strain present in the structures. Thermal stability was examined with post-growth annealing tests. Strain compensation was shown to decrease the net strain of the samples and hinder plastic relaxation.

Structure of the samples

The effect of strain compensation on the crystalline quality and on the net strain of the structure was examined for the active region and gain mirror samples designed for emission near 1120 nm. The layer structures of the samples are shown in **Figure 3.4**. The active region samples comprise only the gain region part and the window layer of the gain mirror structures. The samples utilized bottom-emitting geometry as shown in **Figure 3.4**. Both samples with and without GaAsP strain compensation layers were grown, the former were called as strain-compensated and the latter as uncompensated structures; GaAsP layers were replaced with GaAs material in the uncompensated samples in such a way that the optical thickness remained unchanged.

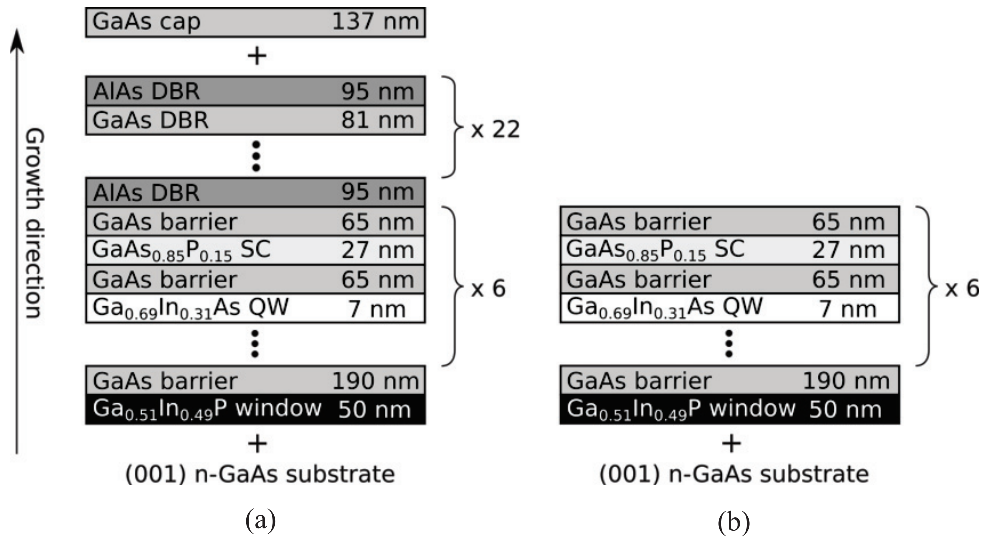

Figure 3.4: *Layer structure of (a) the gain mirror and (b) the active region sample; SC stands for strain compensation.*

The QWs were 7 nm thick and comprised around 31% of indium, which induced a misfit strain of -2.2%. The QWs were arranged to coincide with the standing wave electric field (**E**) antinodes of the cavity mode in the gain mirror structure, as schematically illustrated in **Figure 3.5**. Each QW was positioned to separate standing wave antinode by adjusting the GaAs barrier thicknesses. The $Ga_{0.51}In_{0.49}P$ layer served as a window and protection layer preventing oxidation of the gain material.

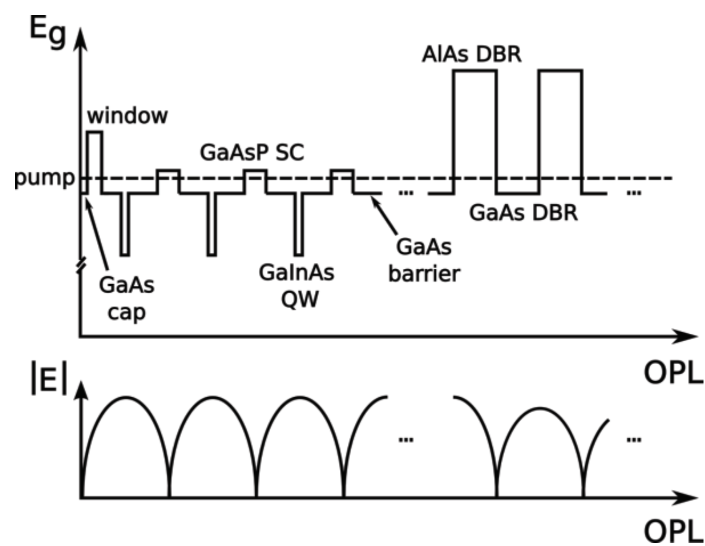

Figure 3.5: *Bandgap profile and distribution of the electric field intensity inside the gain mirror structures. The illustrated design is antiresonant for the cavity mode. OPL stands for optical path length.*

The GaAsP strain compensation layers were chosen to have around 15% of phosphorus content, and they were located evenly in between the QWs, near the nodes of the standing wave, as shown in **Figure 3.5**. Thus, the structures had an equal amount of QWs and GaAsP layers. Thickness of each GaAsP layer was chosen to be around 27 nm, which is still below the critical layer thickness calculated with the model of Matthews and Blakeslee (see **Figure 3.1**). The amount of net strain ε_{net} induced in the gain region part of the structures was estimated using the thickness weighted method described in [73], with the exception that equal compensation was not aimed for. In this method the strain-thickness product calculated for each strained layer is summed up as follows

$$\left(N_{QW}t_{QW} + N_{SC}t_{SC}\right)\epsilon_{net} = N_{QW}t_{QW}\epsilon_{QW} + N_{SC}t_{SC}\epsilon_{SC}, \tag{3.2}$$

where t_{QW} and t_{SC} are thicknesses; ε_{QW} and ε_{SC} are misfit strains; and N_{QW} and N_{SC} represents the number of layers for the QW and GaAsP strain compensation layer, respectively. The net strain corresponding to N_{QW} = 6, N_{SC} = 6, t_{QW} = 7 nm, t_{SC} =27 nm, ε_{QW} = -2.2%, and ε_{SC}= 0.54% was calculated to be around -0.03% (strain-thickness product around -6.1 %nm). Thus, the gain region parts of the structures were slightly compressive. Full compensation would have required the use of GaAsP layers with thicknesses near or exceeding the critical layer thickness given by Matthews and Blakeslee (Equation (3.1)) model resulting in layers that would have been susceptible to strain relaxation.

Epitaxial growth

All the structures were grown with MBE on whole GaAs (001) substrates having a diameter of 2 inch, or on a quarter pieces scribed and cut from the whole wafer. The growth order of the layers is pointed out with an arrow in **Figure 3.4**. Typical growth conditions were used in the epitaxial growth of the samples, except for the QWs, which were grown at a lower temperature of 545 °C (thermocouple reading) in order to hinder relaxation. Moreover, a reduced phosphorus cracker temperature was utilized in the growth of GaAsP and $Ga_{0.51}In_{0.49}P$ layers since the quality of the phosphorus material was suspected to be low [119]–[121].

The growth was interrupted for adjusting the growth temperature as well as the As and P fluxes. The temperature adjustments were executed during 7 minutes long interruptions before and after each QW resulting in a temperature ramping rate of 18 °C/min. A 10 nm thick GaAs layer was grown on both sides of the QWs before the growth was interrupted so that defects and other

impurities that could possibly be incorporated in the crystal during growth interruptions would not affect the optical quality of the QWs. A 4-minute-long growth interruption was used in adjusting the growth temperature for the $Ga_{0.51}In_{0.49}P$ window layer, which corresponds to a temperature ramping rate of 28 °C/min. The As and P flux adjustments were performed at 30 seconds long interruptions before and after each GaAsP strain compensation layer.

Prior to the gain mirror growths, several calibration structures were grown. First, 2-period GaAsP/GaAs superlattice structures were grown and used to obtain the desired As and P fluxes for the GaAsP layer. The composition of the material was deduced from ω-2θ x-ray diffraction measurements performed at (004) and the composition was iteratively adjusted. In other words, several superlattice samples with slightly different As and P fluxes were grown and characterized with x-ray diffraction, and this procedure was repeated until the proper fluxes were found with which the measured composition matched the desires value. Second, the emission of the QWs was calibrated with single- or two-QW PL samples, which comprised a similar structure as shown in **Figure 3.2**. Based on the room-temperature PL measurements, the indium composition of the QWs could be adequately adjusted in order to reach the desired wavelength. Finally, the growth rates were calibrated with special cavity samples, which comprised a half-wave thick GaAs layer in between two quarter-wave thick AlAs/GaAs DBR stacks, in a similar method as described in [122].

3.3.1 Structural quality

Two x-ray diffraction based methods were used in the research to examine the structural quality of the samples: reciprocal space mapping and strain-induced bending measurements. Reciprocal space mapping is a technique used in connection with a high-resolution diffractometer to gain information about the composition and strain of the epilayer structure simultaneously, whereas strain-induced bending measurement give only information about the net strain present in the crystal. The analyses carried out with both methods are described in more detail below.

Reciprocal space mapping

In the reciprocal space mapping measurement, a set of ω-2θ scans are typically recorded around the Bragg angle of the examined crystal plane. The obtained scans are then combined together to form an intensity profile map. Here, ω is denoted as the incidence angle and 2θ as the

detector angle of the x-ray beam in respect to the surface of the crystal. The angular coordinates of the map can be transformed into reciprocal space units (Q_x, Q_y, Q_z) in which case the map is called as a reciprocal space map. The transformation of the coordinates is described, for example, in [123]. The real lattice parameters of the crystal can be related to the reciprocal space vectors and thus also to the measured angular coordinates.

In this research, reciprocal space maps were measured from the uncompensated and strain compensated active region and gain mirror samples around (004) and (113) reciprocal space points in direction [011] and [01-1]. The measurements were performed on 3×3 mm^2 sized samples in triple-axis geometry. The (113) reciprocal space maps were measured in the grazing exit configuration.

The measurements indicated that the active region samples were strained and of high quality (see **Figure 3.6**), whereas the gain mirrors could not be analyzed properly since the measurements performed near (113) reciprocal space point suffered from low intensity. The (004) maps could not give valuable information by themselves on the gain mirror structures since strain and compositional changes cannot be distinguished from a symmetrical scan. The result obtained with the active region samples was, however, shown to be misleading in subsequent studies: namely, the uncompensated active region sample was shown to comprise dislocations which could be revealed by the dark defect imaging method described in Section 3.3.2. Thus, we concluded that the degree of relaxation was below the limit detectable with the reciprocal space mapping measurement.

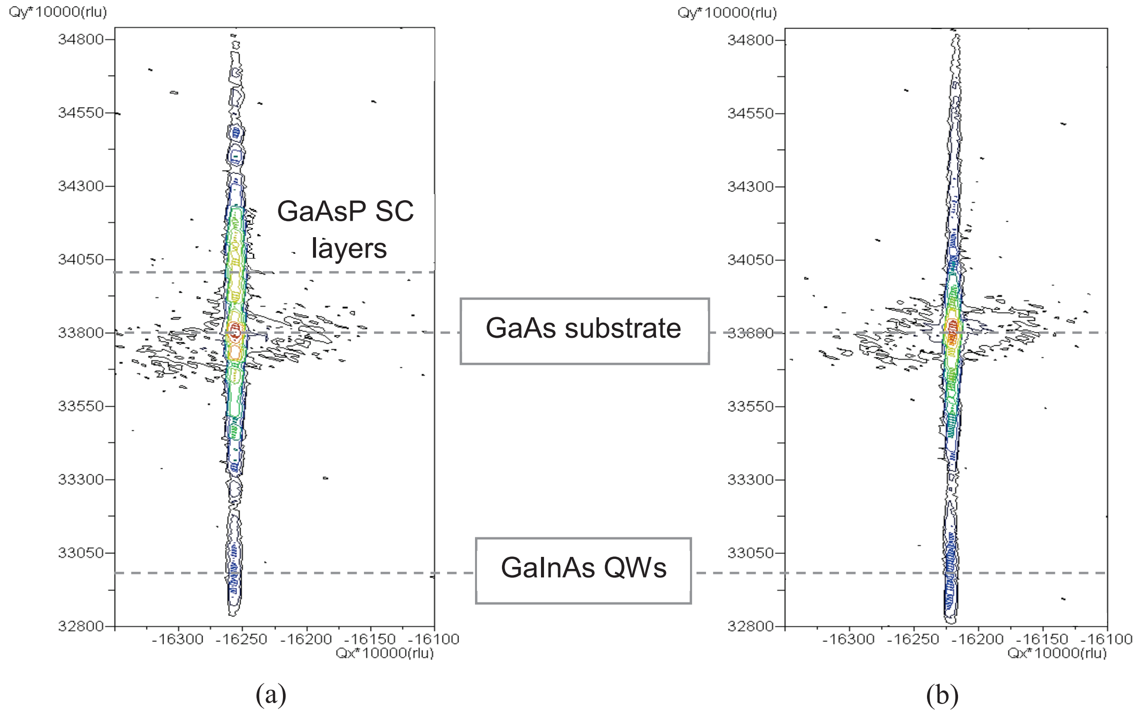

Figure 3.6: *Reciprocal space maps measured from (a) strain compensated and (b) uncompensated active regions around the (113) reflection in [01-1] direction as a function of reciprocal space vectors Q_x and Q_y. The vector Q_x is related to the in-plane lattice parameter, in this case in [01-1] direction, and the vector Q_y is related to the out-of-plane lattice parameter* [123]. *The GaInAs QWs and the GaAsP strain compensation layers are aligned at the same vertical line with the GaAs substrate, i.e. the in-plane lattice parameter of GaInAs and GaAsP coincide with the lattice parameter of GaAs indicating that the structures are strained. Furthermore, the peaks are narrow and the Pendellösung oscillations are present which show that the structures are essentially free from defects. The diffraction peaks related to GaAsP, GaAs and GaInAs are indicated with horizontal dashed lines in the figures.*

Strain-induced bending

Pseudomorphic layers grown on top of a substrate induce strain in the wafer that causes bending of the crystal planes. The radius of curvature (RoC) caused by this bending can be measured with x-ray diffraction and can be theoretically calculated with a model introduced by Dieing and Usher [124]. Thus, the RoC of the wafer can be used to approximate the amount of net strain present in the crystal. In this research, the strain induced bending was measured from both gain and active region samples as well as from an AlAs/GaAs DBR.

The x-ray diffraction measurements were performed either for a whole wafer or for a quarter piece scribed and cut from the whole wafer. All the substrates were nominally 350 ± 25 μm thick. The samples were attached with two-sided tape to the sample holder. As little tape as possible was used in the attachment process and the measurements were performed only after 2 hours waiting time in order to be sure that the tape would not affect the measurement; namely, the mounting process induce mechanical stress in the wafers which could influence the measurement unless an appropriate time is given for the mounting-induced stress to relax.

The measurements were performed with a high-resolution x-ray diffractometer. The diffraction peak caused by the substrate was measured as a function of the sample angle ω at different positions of the wafer, and the detector angle 2θ was kept fixed. The measurements were performed in 2 mm steps in both [011] and [01-1] directions at 5 or 17 different spots depending on the size of the sample. In other word, the quarter-sized wafers were measured at 5 positions, whereas the full wafers had 17 measurement spots. **Figure 3.7** shows the measurement directions and the sample dimensions. Since the crystal planes are bent, the diffraction peak position is shifted as the wafer position is changed. From this peak shift the RoC of the bent crystal planes can be determined when the displacement of the sample is known [124].

Measured values of RoC obtained from active region samples and 1120 nm bottom-emitting gain mirror are listed in **Table 3.1**. Both active region samples with and without strain compensation were measured. The gain mirror was strain compensated. As a reference, the RoC was measured also from a plain substrate and an AlAs/GaAs DBR sample that was similar to the DBR utilized in the gain mirror, but contained only 21 layers pairs instead of 22.5 pairs typically used in gain mirror samples (see **Figure 3.4**).

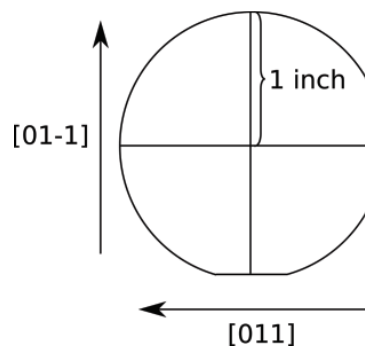

Figure 3.7: *Measurement direction of the samples grown on (001) GaAs substrate*.

Table 3.1: *Measured radius of curvatures (RoC) in [011] and [01-1] directions. Active region samples are denoted with acronym AcR.*

Sample	Strain-thickness product (% nm)	Measurement points	RoC [011] ($\times10^{-2}$ m^{-1})	RoC [011] (m)	RoC [01-1] ($\times10^{-2}$ m^{-1})	RoC [01-1] (m)
GaAs (001)	-	17	0.25 ± 0.011	390	0.78 ± 0.041	130
AcR with SC	-30	17	2.0 ± 0.013	50	1.5 ± 0.012	66
AcR without SC	-94	17	4.5 ± 0.027	22	3.5 ± 0.018	29
AlAs/GaAs DBR	-280	5	12 ± 0.025	8.0	12 ± 0.11	8.3
Gain mirror with SC	-310	5	14 ± 0.16	7.3	14 ± 0.25	7.3

As can be seen in **Table 3.1**, the DBR layers induce most of the bending of the gain mirrors. Thus, expanding strain compensation to include also the DBR layers could be an interesting test for future studies. When only the active region samples are compared, the RoC (m) of the uncompensated active region is seen to be over two times smaller than the RoC (m) of the strain compensated active region. This indicates that the strain compensation has substantially decreased the bending of the crystal planes and thus the net strain. Moreover, the wafer bending measurements show that the strain compensated active region sample has a net compressive strain, as designed.

The RoC values were theoretically calculated for the active region samples similarly as in [124]. Theoretical RoC for the strain compensated and uncompensated active region samples were calculated to be 1.4 and 3.9 $\times10^{-2}$ m^{-1}, respectively. These values are within the measured RoC range.

3.3.2 Optical quality

During the research, dark defect imaging was utilized to assess the optical quality of the samples. Dark defect imaging is a non-destructive technique that similarly to photoluminescence microscopy [125]–[127] or any other luminescence imaging technique [128] utilizes optical excitation to detect nonradiative defects, such as misfit dislocations, from the semiconductor wafers. In dark defect imaging, the wafer is illuminated optically from a large

area and a camera is use to detect the integrated PL signal. Electronically active defects are seen as dark regions in the image since nonradiative recombination rate is enhanced near the defects [96], [97]. In this research, dark defect measurement was used to detect misfit dislocations, which are shown as dark lines in the dark defect images, from the grown samples and thus to indicate whether the grown wafers are strained or partially relaxed.

Setup

Figure 3.8 shows the dark defect imaging setup. The wafers were illuminated with an 808 nm laser radiation produced from a fiber-coupled pump laser. The pump radiation was focused off from the wafer in order to spread the pump spot to a large area and to keep the pump intensity low so that the wafers would not be thermally damaged. The camera could image an area of size 1.2 × 0.9 mm^2; thus, the pump spot was adjusted such that it could barely illuminate this area. The wafer was placed on a stage that could be moved in all three axes. The wafer was not actively cooled. An 850 nm high pass filter was placed in front of the camera to filter out the pump radiation. To reduce the effect of speckle, from which the imaging setup suffered, a vibration source was attached on the pump laser fiber so that the standing wave modes of the pump laser would be spatially mixed and thus the intensity over the wafer would average out.

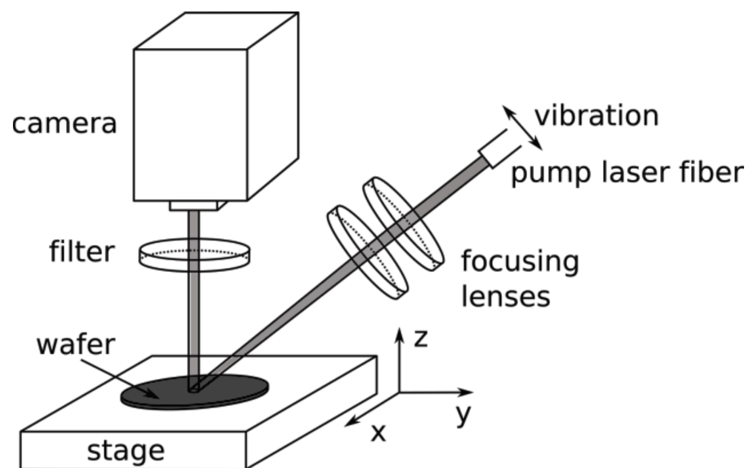

Figure 3.8: *Dark defect imaging setup*.

Figure 3.9 demonstrates typical dark defect images measured from a sample that has high optical quality and from another sample that exhibits deterioration of its crystalline quality. As can be seen in **Figure 3.9**, the imaging setup still suffered from speckle, which appears as a wavy intensity profile on the captured images. To better resolve the defects, the images were processed: the speckle pattern was spatially filtered away by using gaussian filtering in fourier space, i.e. high and low spatial frequencies were removed from the image with a bandpass filter; and the contrast as well as brightness of the images were enhanced. Large structures were filtered down to 6 pixels (corresponds to ~5.6 µm), and small structures up to 2 pixels (corresponds to ~1.9 µm). The processed images can be seen below the original ones in **Figure 3.9**. The dark lines seen in **Figure 3.9** correspond to misfit dislocations present in the structures [99]. The dark spots may originate from threading dislocations, or from other defects (such as oval defects) that act as nonradiative recombination centers.

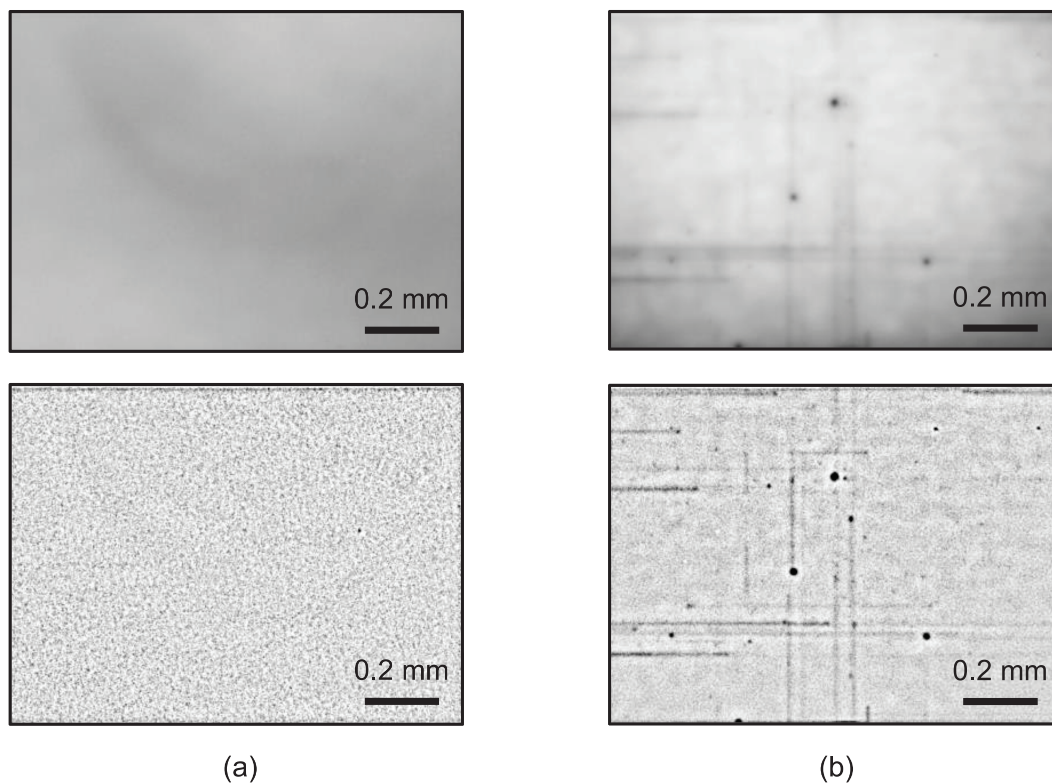

Figure 3.9: *Dark defect images (1280 px × 960 px) captured from (a) high-quality sample and (b) deteriorated sample. The original images are shown above; the processed images are situated below.*

Strain compensation analysis

The effect of strain compensation on the optical quality of the gain and active region sample was examined by taking dark defect images from the surface of the samples. **Figure 3.10** shows typical images taken from the active region as well as gain mirror samples when strain compensation was either utilized or not. All of the samples show a high crystalline quality; only a small amount of dark figures are present in the images. Furthermore, the number of dark lines can be seen to reduce with the use of strain compensation. Thus, strain compensation seems to hinder plastic relaxation.

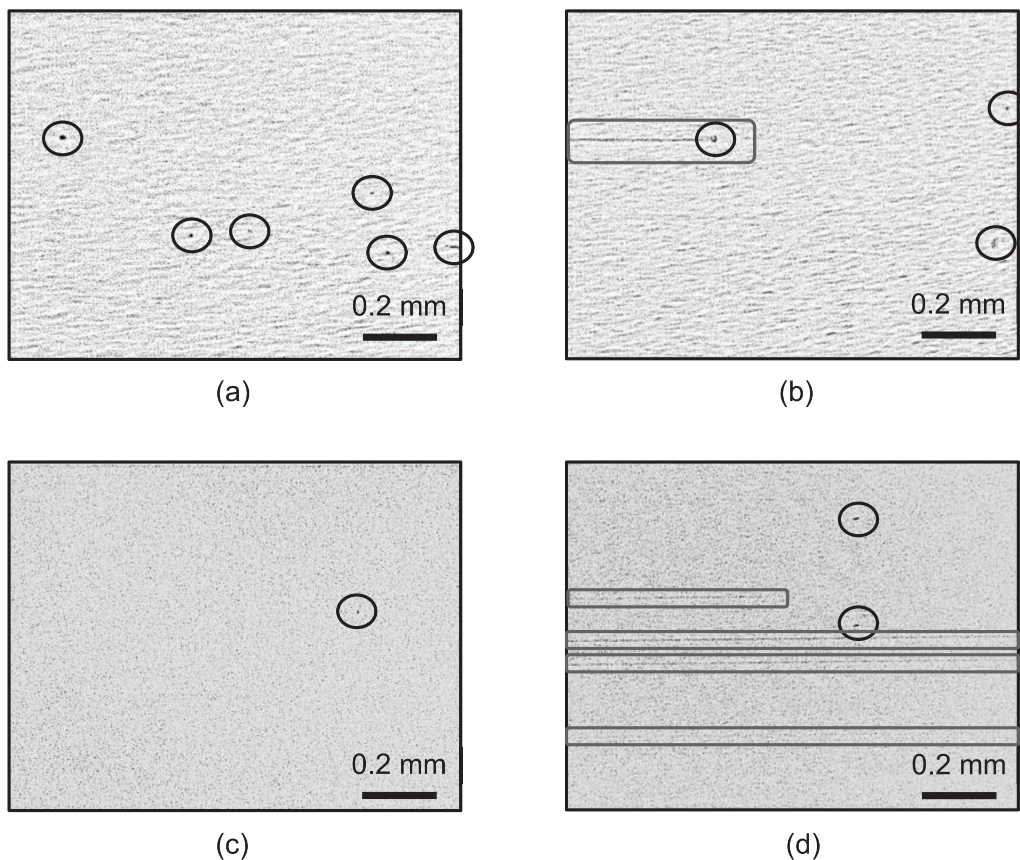

Figure 3.10: *Dark defect images taken from (a) strain-compensated active region sample, (b) uncompensated active region sample, (c) strain-compensated gain mirror, and (d) uncompensated gain mirror. Dark spot defects are highlighted from the figure with circles and dark line defects with rectangles.*

3.3.3 Thermal stability

Structural stability of the gain mirrors and active region samples against thermal stress was examined with rapid thermal annealing (RTA) test that were performed after the epitaxial growth [129]. RTA treatment has shown to initiate plastic relaxation in the semiconductor wafers, and this relaxation seems to be dependent on the amount of net strain [130], [131]; namely, structures that have a higher net strain, relax at lower energy treatments, i.e. at lower temperatures and/or shorter treatment times. Since strain compensation reduces the net strain present in the structure, strain compensated samples are expected to be structurally more stable against thermal stress than uncompensated samples.

In the RTA study, samples of 3 x 3 mm^2 sizes were annealed for 1 min, 2 min, 4 min and 8 min at 700°C, 750°C and 800°C in a separate furnace under vacuum. The samples were capped with 5 × 5 mm^2 GaAs pieces to prevent arsenic outdiffusion. Dark defect imaging was used to assess the quality of the samples before and after thermal treatment.

Figure 3.11 presents a series of dark defect images taken from uncompensated and strain compensated gain mirrors before and after thermal treatment. As seen in **Figure 3.11**, annealing even as long as 8 min at 700 °C did not affect the strain compensated gain mirror, whereas the same treatment already slightly degraded the crystalline quality of the uncompensated gain mirror. However, a sufficiently high and long RTA treatment (4 min at 800 °C) caused dark line defects to appear in the strain compensated gain mirror as well. Thus, the tests showed that the strain compensated gain mirror could resist more effectively thermal stress than the uncompensated gain mirror.

In contrary to the gain mirror samples, active region samples did not show any degradation in their crystalline quality even after the harshest thermal treatment (8 min at 800 °C), possibly because these structures initially contained only a very small amount of dark defects.

To conclude, according to the performed RTA test, the gain mirror structures should be thermally stable and thus endure subsequent processing and be use as VECSEL gain chips.

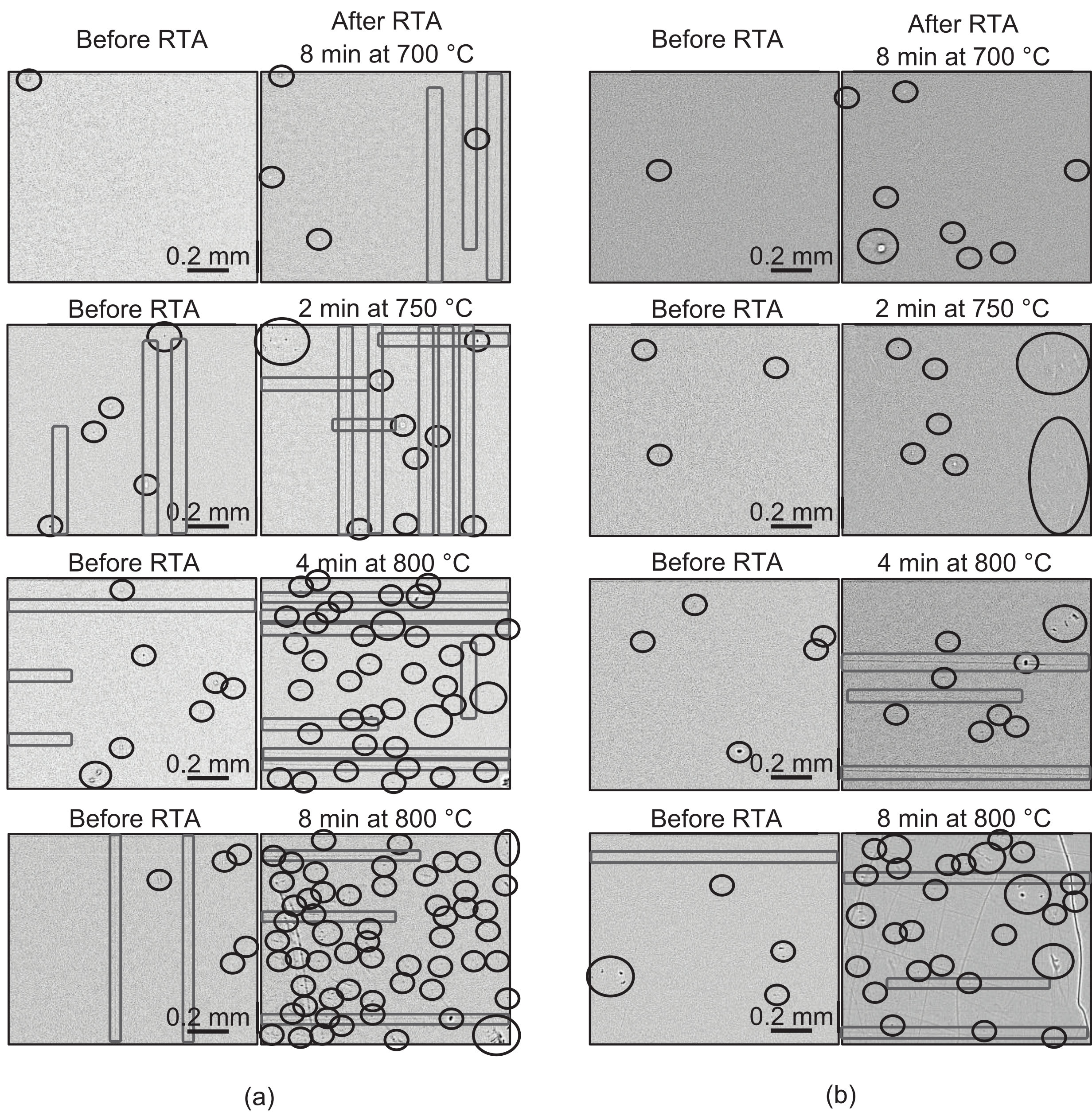

Figure 3.11: *Dark defect images measured from (a) uncompensated and (b) strain compensated gain mirrors before and after thermal treatments. Dark spots and other point defects are highlighted from the figures with circles and dark line defects with rectangles.*

Chapter 4

Gain and absorber structures for near IR and red emission

This chapter reports the design and growth procedures utilized to obtain high-quality GaInAs/GaAsP/GaAs and GaInP/AlGaInP/GaAs gain structures for emission in the near IR (1100–1200 nm) and in the red (around 675 nm), respectively. The last section of the chapter is focused on describing the fabrication steps needed, as well as materials and cooling approaches utilized, to transform the epitaxially grown gain mirror wafers into thermally conductive gain chips.

4.1 GaInAs/GaAsP/GaAs gain mirrors for continuous wave near IR emission

This section describes briefly the strain-compensated GaInAs/GaAsP/GaAs gain mirror structures and the epitaxial growth parameters that were used in obtaining high crystalline quality. Characterization results obtained from the grown gain mirror structures are shown at the end of the section.

Gain mirror structures

Three gain mirror structures were developed: two gain mirrors for emission near 1120 nm and one for emission around 1178 nm. The 1120 nm gain mirrors utilized both bottom- and top-emitting geometries, whereas the 1178 nm gain mirror used only a top-emitting design. The

bottom-emitting design was used for material optimization and characterization studies (see Chapter 3), while most of the laser characteristics (see Chapter 5) were obtained with the top-emitting design. **Figure 4.1** shows the layer structures of the top-emitting gain mirrors. The bottom-emitting gain mirror design was already shown in **Figure 3.4** (a).

The gain regions of the top-emitting gain mirrors were designed similarly as for the bottom-emitting gain mirror case: The QWs were positioned at separate standing wave antinodes of the cavity mode (see **Figure 3.5**), and GaAsP strain compensation layers were utilized to compensate the QW strain; The strain compensation layers were located between each QW at the standing wave nodes of the cavity mode. The only major difference between the bottom- and top-emitting gain mirrors lied in the number of QWs and strain compensation layers. Namely, the number of these layers was increased to 10 for the top-emitting gain mirror. The higher amount of QWs should ensure sufficient gain and maximize the output power [7].

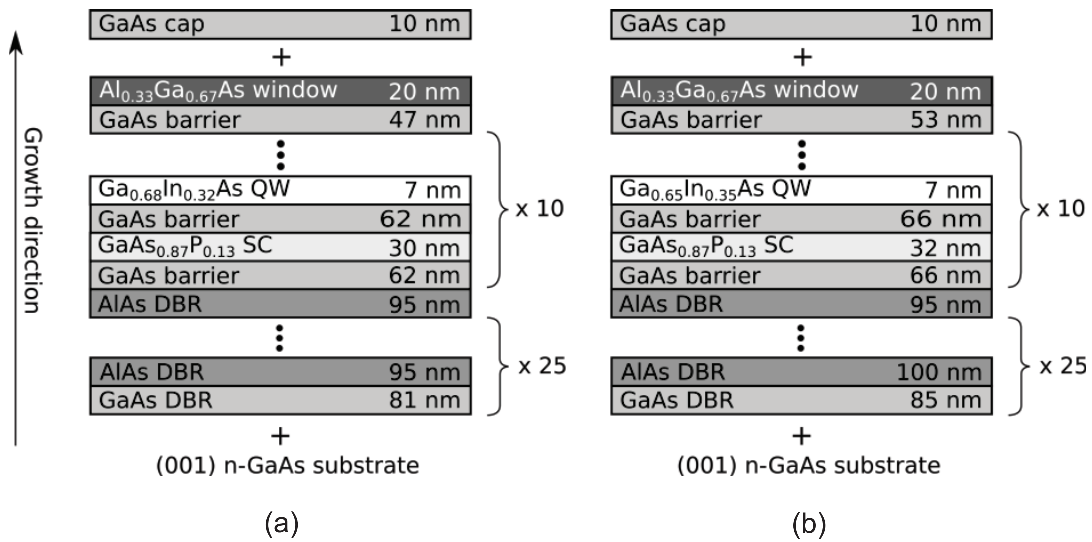

Figure 4.1: *Layer structure of the (a) 1120 nm and (b) 1178 nm top-emitting gain mirror; SC stands for strain compensation. The nominal compositions are given for all the layers, except for the QWs, whose compositions were estimated from the ω-2θ x-ray diffraction measurements performed near (004) with the aid of dynamical simulations (for example* [97]*). The x-ray diffraction analysis is described in more detail in Chapter 4, in Section 'Wafer characterization'.*

Table 4.1: *Calculated net strain and strain-thickness product of the gain mirrors' active regions. Compressive strain is indicated with negative and tensile strain with positive values.*

λ(nm)	$N_{QW,SC}$	t_{QW} (nm)	t_{SC} (nm)	ε_{QW} (%)	ε_{SC} (%)	ε_{net} (%)	Strain-thickness product (% nm)
1120	6	7	27	-2.2	0.54	-0.03	-6.1
1120	10	7	30	-2.3	0.47	-0.06	-21
1180	10	7	32	-2.5	0.47	-0.07	-26

The QWs were 7 nm thick and comprised around 31–35% of indium, which induced a misfit strain of -2.2% to -2.5%. The GaAsP strain compensation layers had a phosphorus content of 15–17%, and their thickness was kept below or near the critical layer thickness calculated by the model of Matthews and Blakeslee (see **Figure 3.1**). The amount of compressive and tensile strain exhibited by each gain mirror, as well as the targeted net strain, is presented in **Table 4.1**. The calculation was based on Equation (3.2).

The top-emitting gain mirrors utilized both antiresonant and resonant configurations. $Al_{0.33}Ga_{0.67}As$ was used as the window layer and a GaAs capping layer was used to protect the gain mirror against oxidation.

The DBR of the gain mirrors consisted of alternating quarter-wave thick AlAs and GaAs layers. These materials were chosen because they have desirable properties for the application's point of view, such as high refractive index contrast and sufficiently high thermal conductivities. Furthermore, AlAs has a close lattice match to GaAs, (misfit 0.14%) which provides the opportunity to grow high number of layer pairs without degrading the crystalline quality. The number of layer pairs embedded in the DBR is dependent on the gain mirror configuration, i.e. whether the gain mirror utilizes a top- or bottom-emitting geometry. For top-emitting device, the number of layers was determined such that over 99.9% reflectance was achieved at the desired wavelength at room temperature. This reflectance was achieved with a 25.5 pair AlAs/GaAs DBR. For the bottom-emitting device, a compromise needed to be made between the thermal conductivity of the DBR and the achievable reflectance. Consequently, 22.5 DBR layer pairs were chosen for the bottom-emitting gain mirror. Such a number of layer pair could provide a maximum reflectance of 99.74% at 1115 nm. **Figure 4.2 (a)** shows the simulated

reflectance of a 22.5 pair AlAs/GaAs DBR designed for room temperature operation at 1115 nm. The reflectance corresponding to a 25.5 pair AlAs/GaAs DBR designed for room temperature operation at 1174 nm, is shown in **Figure 4.2 (b)**. Both DBR structures were designed for slightly shorter operation wavelengths in order to take into account the optical thickness shifts induced by heating of the gain mirrors during pumping. The compressive strain caused by the AlAs DBR layers was left uncompensated.

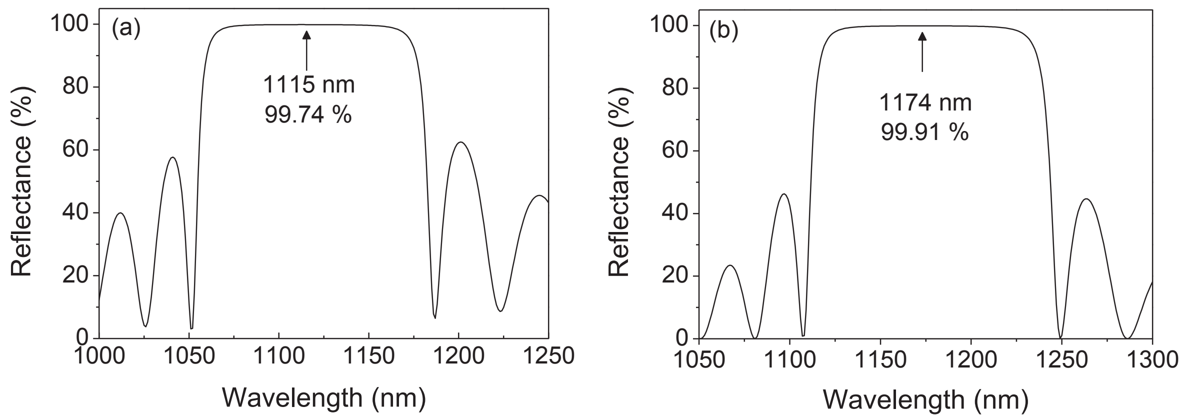

Figure 4.2: *Simulated reflectance of (a) 22.5- and (b) 25.5-pair quarter-wave AlAs/GaAs DBR structures designed for room-temperature operation at 1115 nm and 1174 nm, respectively*.

Epitaxial growth

All the gain mirrors were grown by MBE on GaAs (001) substrates that had a diameter of 2 inch. The growth order of the layers is pointed out with an arrow in **Figure 4.1** for the top-emitting gain mirror and in **Figure 3.4 (a)** for the bottom-emitting gain mirror structure. The growth parameters used are listed in **Table 4.2**. The growth temperatures were measured with a pyrometer, except for GaInAs, which was grown below the measurement range of the sensor. Thus, temperature of the sample holder's thermocouple is given instead as an estimate for the QW growth temperature. A reduced phosphorus cracker temperature was utilized in the growth of GaAsP and $Ga_{0.51}In_{0.49}P$ layers.

Table 4.2: *Growth parameters of the gain mirrors. Growth temperatures were measured with a pyrometer except for GaInAs, for which the sample holder's temperature is given. The V/III beam equivalent pressure (BEP) was not measured for $Ga_{0.51}In_{0.49}P$; the growth was performed in high phosphorus overpressure.*

Material	V/III BEP	Growth rate (µm/h)	Temperature (°C)	Temperature sensor
GaAs	30	1	580–590	pyrometer
AlAs	50	0.83	580–600	pyrometer
$Al_{0.33}Ga_{0.67}As$	65	0.57	580–600	pyrometer
$Ga_{0.69}In_{0.31}As$	25	1.1	545	thermocouple
$Ga_{0.69}In_{0.32}As$	25	1.1	545	thermocouple
$Ga_{0.69}In_{0.35}As$	25	1.0	460	thermocouple
GaAsP	27	1.0	580–590	pyrometer
$Ga_{0.51}In_{0.49}P$	-	1.3	500	pyrometer

The QW growth temperature was adjusted prior to the gain mirror growths with single QW calibration samples (structure shown in **Figure 3.2**) and fine-tuned by growing several active region samples (structure shown in **Figure 3.4 (b)**). Single QW samples were used to examine possible relaxation of a single QW, while the active region samples were used to assess the relaxation in the entire gain region scale. The crystalline quality of the active region samples was examined with dark defect imaging (see Section 3.3.2). Single QW samples were not systematically measured with the method since the crystalline quality of these samples was typically already high. On the contrary, the active region samples were more vulnerable to experience relaxation than the single QW samples. If defects were observed, a new active region sample was grown at a lower QW growth temperature and examined with the dark defect measurement. With this iterative method, the 545 °C and 460 °C QW growth temperatures were found optimal for the 1120 nm and 1178 nm gain mirrors, respectively. The QW growth temperature needed to be lowered to 460 °C in the 1178 nm gain mirror case probably due to the higher strain present in the structure.

Growth interruptions were used during the growth of both top-emitting and bottom-emitting gain mirrors (see Section 3.3 'Epitaxial growth'). The temperature adjustments were executed during 7 and 9 minutes long interruptions which resulted to a corresponding ramp rate of

18 °C/min and 24 °C/min for the 1120 nm and 1178 nm gain mirror, respectively. The growth rates, emission wavelength and the As/P flux ratio were optimized prior to the gain mirror growths following the same procedure as for the bottom-emitting gain mirror structure (see Section 3.3 'Epitaxial growth').

Wafer characterization

After the epitaxial growth, the gain mirror wafers were characterized in terms of room-temperature PL, reflectance and x-ray diffraction. The purpose of this characterization was to assess the device properties of the gain mirrors, such as the emission wavelength of the QWs and the reflectance band of the DBR, and to verify that the gain mirrors were grown with high crystalline quality.

PL measurements were performed either normal to the epitaxial surface (surface PL) or from the edge of the wafers (edge PL). Surface PL measurements could be performed only for the top-emitting gain mirrors, since the thick DBR located at the surface of the bottom-emitting structure absorbed the 532 nm pump wavelength of the PL system, thus preventing the pump to reach the QWs. Edge PL measurements were used to detect the inherent emission of the QWs, whereas the surface PL measurements gave information mainly about the resonance of the micro-cavity formed between the semiconductor/air and the DBR interfaces. The reflectance spectrum was measured normal to the epitaxial surface of the wafers, and it revealed the DBR reflectivity band, as well as the QW absorption edge and cavity resonances of the top-emitting gain mirror. Dark defect measurements were utilized to detect the existence of possible nonradiative defects using similar configuration as described in Section 3.3.2. ω-2θ x-ray diffraction measurements performed around (004) gave information about the structural quality of the gain mirrors and dynamic x-ray simulations were used to assess the layer structure of the grown wafers.

Figure 4.3 shows the measured room-temperature PL and reflectance spectra. The center wavelength of the DBR's reflectance band and the wavelength corresponding to the maximum QW emission were tuned away from the desired operation wavelengths (1120 nm and 1178 nm) in order to take into account the gain and optical thickness shifts induced by heating of the gain chip during optical pumping. Thus, the gain mirrors were targeted to reach the optimal performance at high pump powers. Because the QW gain shifts more strongly than the optical thicknesses, the center wavelength of the reflectance band was detuned less than the QW peak

gain from the operation wavelength. For the 1120 nm gain mirror structures, the QW gain was aimed at 1105 nm and the center wavelength of the DBR stop band at 1115 nm. The corresponding values were 1160 nm and 1174 nm for the 1178 nm gain mirror, respectively. The amount of detuning was estimated by assuming the wavelength shift rates of around 0.1 nm/°C and 0.3 nm/°C [7] for the optical layer thickness and peak gain, respectively, and an active layer temperature rise around 50 °C during laser operation.

As shown in **Figure 4.3**, the measured parameters mainly comply with the targeted values. Only few deviations were found: the emission of the 1120 nm top-emitting gain mirrors was observed to be 15 nm longer [**Figure 4.3 (a)** and **(b)**] and the stop band of the DBR of the antiresonant 1120 nm structure [**Figure 4.3 (b)**] was centered 8 nm longer than was aimed at.

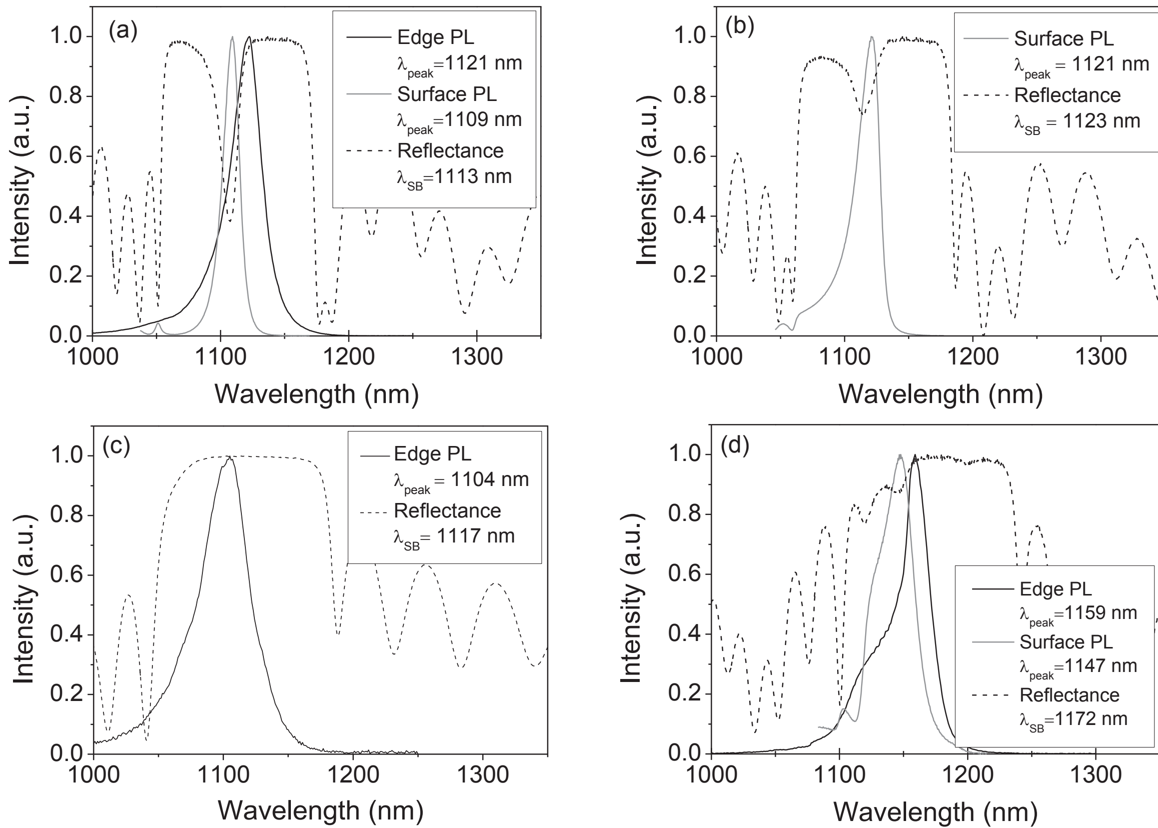

Figure 4.3: *PL and reflectance spectra of (a) 1120 nm top-emitting resonant gain mirror, (b) 1120 nm top-emitting antiresonant gain mirror, (c) 1120 nm bottom-emitting antiresonant gain mirror and (d) 1178 nm top-emitting antiresonant gain mirror.*

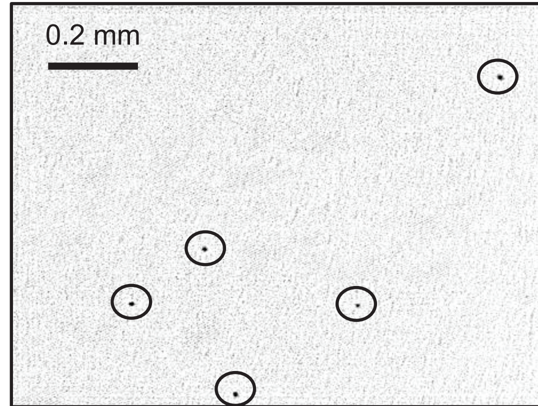

Figure 4.4: *Dark defect image taken from the 1120 nm top-emitting resonant gain mirror. Dark spot defects are highlighted from the figure with circles.*

An example of a typical dark defect image taken from the surface of one of the gain mirror is shown in **Figure 4.4**. The measurement did not reveal any misfit dislocations in any of the gain mirrors, but an increased amount of dark spot defects were observed. As describe in Section 3.3.2, the dark lines are typically induced by strain, whereas the dark spots may originate from different kind of defects that act as nonradiative recombination centers. Based on the PL images, the gain mirror structures can be said to be free of misfit dislocation, which indicates that plastic relaxation has not been occurred.

Since the gain mirrors were not plastically relaxed, a single ω-2θ x-ray diffraction scan performed around the (004) reciprocal space point could be utilized to analyze the gain mirror structures with the aid of dynamical simulations [97]. The x-ray diffraction analysis began by deducing the diffraction profile of the nominal structure, and preceded by comparing the obtained diffraction profile to the measured one. The model of the nominal structure was subsequently refined to fit the experimental diffraction profile so that an agreement between the simulated and experimental profiles could be achieved in the end. The simulated structure was assumed to closely represent the physical sample. Thus, the simulated structure could directly reveal the compositions and thicknesses of the grown layers. The indium compositions given for the QWs in **Figure 4.1** were deduced with such a procedure.

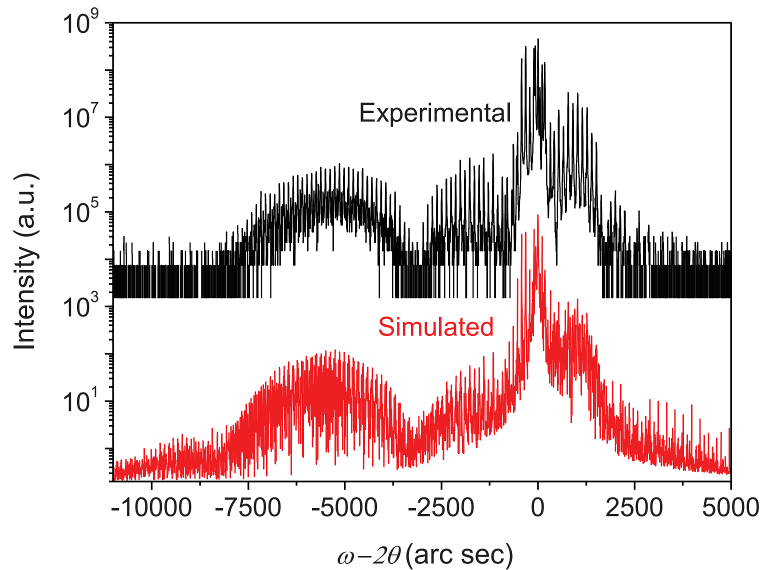

Figure 4.5: *Experimental and simulated x-ray diffraction profiles measured around the (004) reciprocal space point for the strain compensated 1120 nm antiresonant gain mirrror. The experimental curve has been offset relative to y-axis for illustrative purposes.*

Figure 4.5 shows, as an example, the ω-2θ x-ray diffraction curve measured from the 1120 nm top-emitting antiresonant gain mirror and the corresponding simulated curve that gives the best fit to the measured data. As seen in **Figure 4.5**, the simulation has a good agreement with the measurement and thus should give a reliable prediction of the grown gain mirror structure. Moreover, the fine structure pattern and the narrow diffraction peaks seen in **Figure 4.5** indicate that the gain mirror has a high crystalline quality, i.e. the interfaces are sharp and smooth; the fine-structure pattern would otherwise vanish from the x-ray diffraction profile. In general, all the gain mirrors were observed to have a high crystalline quality and to agree well with the nominal structures.

4.2 GaInP/AlGaInP/GaAs gain mirror and SESAM structures for red mode-locked emission

Direct red emission (630–690 nm) can be generated using GaInP/AlGaInP/GaAs QW material, which is the only III-V material capable to emit directly at this spectral range without resorting to higher quantum confinement such as quantum dots or quantum wires. Emission is restricted to 630 nm below which laser operation is hindered due to the low conduction band offset between the GaInP QW and AlGaInP barrier material. This carrier confinement decreases along with the emission wavelength. Thus, the achievable output power is lower compared to operation of GaInAs QWs at 1 μm. A maximum power of about 2 W has been demonstrated around 670 nm with the edge-emitting laser diodes [132], while in the VECSEL geometry, a maximum power of 1.2 W has been reached in the same wavelength range [27]. These output powers obtained are, however, sufficient for most applications linked to life-science.

In this research GaInP/AlGaInP/GaAs QW material has been used both as gain material for obtaining laser emission at red and as absorber medium for the red SESAM structure. This section is concerned with the gain mirror and SESAM structures designed for operation near 670 nm.

Design limitations

In order to achieve as good as possible laser performance from the GaInP/AlGaInP QW material, the conduction band offset between the QW and barrier needs to be maximized. Since the band gap of the QW material is limited by the desired emission wavelength, the only way to increase the offset is to increase the band gap energy of the AlGaInP barrier material. It has been shown, that for maximizing the conduction band offset, lattice-matched $(Al_{0.6}Ga_{0.4})_{0.51}In_{0.49}P$ barriers should be used [133]. This composition gives a band gap value of around 2.25 eV [134], which is near the direct-to-indirect transition. Lattice matching is desirable since it allows the growth of thick layers without the risk of forming strain-induced dislocation and defects.

When designing the laser structure for red emission, one should note that GaAs cannot be utilized as part of the intra-cavity elements since it absorbs red light. Thus, the GaAs DBR

layers, typically used in the VECSELs emitting near 1 μm, need to be replaced with some other material, which has a close lattice-match to GaAs and is transparent for the red emission. For the emission wavelength of 670 nm $Al_{0.45}Ga_{0.55}As$ seems to be the best choice since it has a close lattice-match to GaAs, it is transparent, and it has a fairly high refractive index contrast to AlAs (about 0.36 [135]). This index contrast is, however, still only about half the value achieved with an AlAs/GaAs DBR (0.71 at 670 nm [135]). Therefore the number of layer pairs needs to be increased in the $AlAs/Al_{0.45}Ga_{0.55}As$ DBR in order to achieve the same reflectance as with the AlAs/GaAs DBR. For example, in order to achieve a theoretical reflectivity of 99.9% at 670 nm, one would need only 17 pairs of AlAs/GaAs instead of 32 pairs of $AlAs/Al_{0.45}Ga_{0.55}As$. The lower index contrast of the $AlAs/Al_{0.45}Ga_{0.55}As$ DBR also narrows the width of the stop band. Other disadvantages of the $AlAs/Al_{0.45}Ga_{0.55}As$ DBR include the lower thermal conductivity of bulk AlGaAs compared to bulk GaAs [136] which combined with the high number of layer pairs decreases the total thermal conductivity of the mirror even further.

Gain mirror and SESAM structures

The design of the red gain mirror and SESAM are shown in detail in **Figure 4.6** and **Figure 4.7**. The gain mirror utilized a top-emitting structure, and comprised 20 $Ga_{0.46}In_{0.54}P$ QWs which were designed for emission at 670 nm; such a high amount of QWs were chosen in order to achieve a sufficiently high gain. The SESAM structure contained only a single $Ga_{0.4}In_{0.6}P$ QW capable to absorb the 670 nm emission; a single QW can, namely, provide low nonsaturable losses and a low saturation fluence, both of which are beneficial for obtaining stable mode-locking, especially at high pulse repetition rates. The QWs were embedded in lattice-matched $(Al_{0.6}Ga_{0.4})_{0.51}In_{0.49}P$ barriers. In the future, the carrier confinement could be possibly enhanced by utilizing a separate confinement heterostructure arrangement similar to [27].

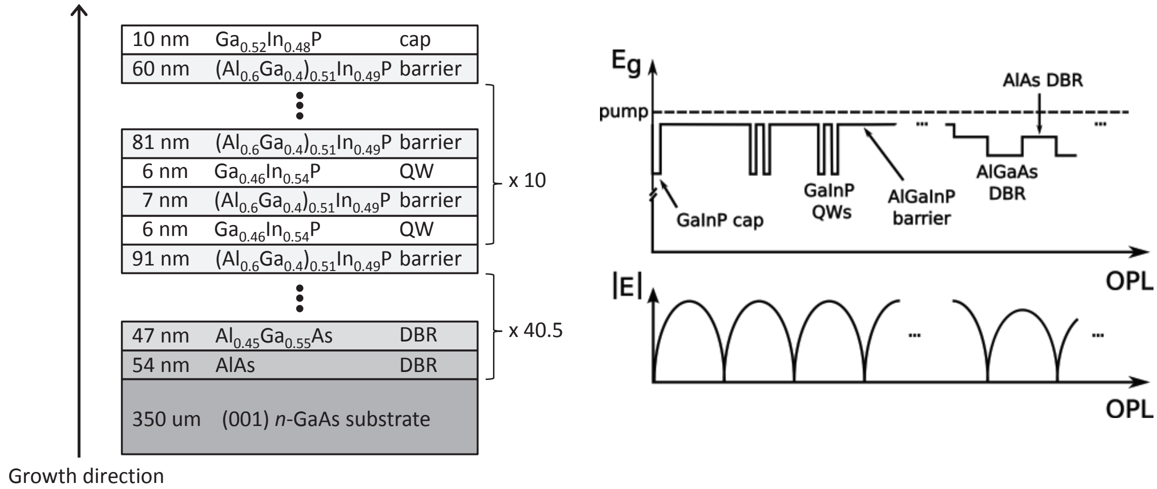

Figure 4.6: *Layer structure (left), and bandgap profile as well as standing wave intensity distribution (right) inside the gain mirror.*

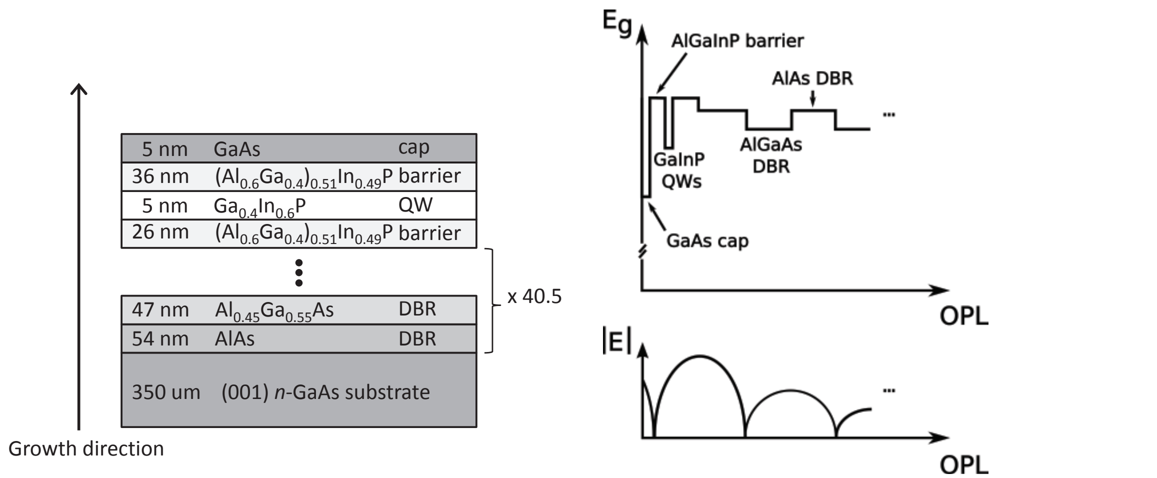

Figure 4.7: *Layer structure (left), and energy gap profile as well as standing wave electric field intensity distribution (right) inside the SESAM structure.*

For the gain mirror, the QWs were arranged to coincide with the standing wave electric field antinodes of the cavity mode, whereas the QW of the SESAM was located between the node and antinode of the same field. The gain mirror and SESAM structures were capped with $Ga_{0.52}In_{0.48}P$ and GaAs layers, respectively. These layers protect the surface against oxidization which readily occurs in aluminum containing layers. No suitable aluminum-free material exists that could be used to prevent nonradiative recombination via surface states at this wavelength range. Since the GaAs capping layer was only 5 nm thick, absorption occurring in this layer was

considered to be insignificant. Besides, part of the GaAs layer is oxidized upon exposure to atmosphere, and the Ga/As oxides formed do not absorb the laser light.

The DBR consisted of 40.5 pairs of quarter-wave thick AlAs/$Al_{0.45}Ga_{0.55}As$ layers. The corresponding simulated reflection at 670 nm was 99.96% (see **Figure 4.8**), while the width of the stop band was around 45 nm. The gain mirror was designed to be antiresonant and the SESAM structure was designed to be nearly antiresonant for the cavity mode. The misfit strain of the QWs and DBR layers were not compensated.

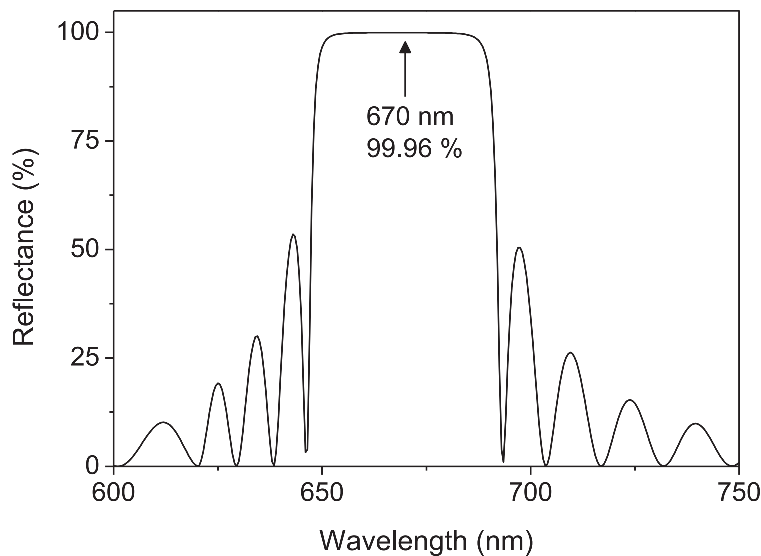

Figure 4.8: *Simulated reflectance of the quarter-wave AlAs/$Al_{0.45}Ga_{0.55}As$ DBR.*

Fabrication details

The gain mirror and SESAM structures were grown by MBE on GaAs (001) substrates that had a diameter of 2 inch. The growth order of the layers is pointed out with an arrow in **Figure 4.6** and **Figure 4.7**. Typical growth conditions were used; the growth parameters are listed in **Table 4.3** for each material. The growth was performed at As and P overpressures, but the V/III BEP ratios were not measured. Growth temperatures were measured by a pyrometer. The growth was interrupted after the DBR layers for 3 minutes for adjusting the growth temperature and changing the group V component from As to P. Changing of the group V fluxes was performed at the end of the interruption in order to minimize the incorporation of P to the grown AlAs layer.

Table 4.3: *Parameters utilized in the growth of the gain mirror and SESAM structures.*

Material	**Gain mirror**		**SESAM**	
	Growth rate (μm/h)	Temperature (°C)	Growth rate (μm/h)	Temperature (°C)
AlAs	1.4	580–590	1.3	580–590
$Al_{0.33}Ga_{0.67}As$	1.7	580–590	1.8	580–590
GaInP QW	1.1	480	0.8	480
$(Al_{0.6}Ga_{0.4})_{0.51}In_{0.49}P$	2.2	480	1.6	480
GaAs cap	-	-	1.0	480
$Ga_{0.52}In_{0.48}P$ cap	1.0	480	-	-

After epitaxial growth, the SESAM structure was irradiated with ions in order to incorporate defects in the absorber region. These defects introduce trap states inside the bandgap through which the charge carriers can recombine more quickly. Thus, the absorption recovery time should be reduced. The recovery time is estimated to be in the sub-10 ps range similarly to typically used GaAs-based samples [92]. Due to lack of suitable pump laser, the nonlinear optical and temporal characteristics of the SESAM could not be determined.

Prior to the gain mirror growth, the growth rates of the layers were calibrated similarly as in the case of GaInAs/GaAsP/GaAs gain mirrors (see Section 3.3 'Epitaxial growth'). Only this time the calibration sample comprised two $Ga_{0.46}In_{0.54}P$ QWs that were separated by $(Al_{0.6}Ga_{0.4})_{0.51}In_{0.49}P$ barriers, and the cavity was placed between AlAs/$Al_{0.45}Ga_{0.55}As$ DBR stacks. The SESAM structure utilized only a single quarter-wave AlAs/$Al_{0.45}Ga_{0.55}As$ DBR stack for the corresponding calibrations. Emission of the QWs was calibrated to the desired wavelength by PL calibration samples grown prior to the growth of the gain mirror and SESAM structure. Similar calibration procedures were used as in the case of GaInAs/GaAsP/GaAs gain mirrors.

Wafer characterization

After epitaxial growth, the gain mirror and SESAM structure were characterized by PL and reflectance, both measured normal to the surface of the wafers. Edge PL measurement were not performed for the structures. **Figure 4.9** shows the results of these measurements.

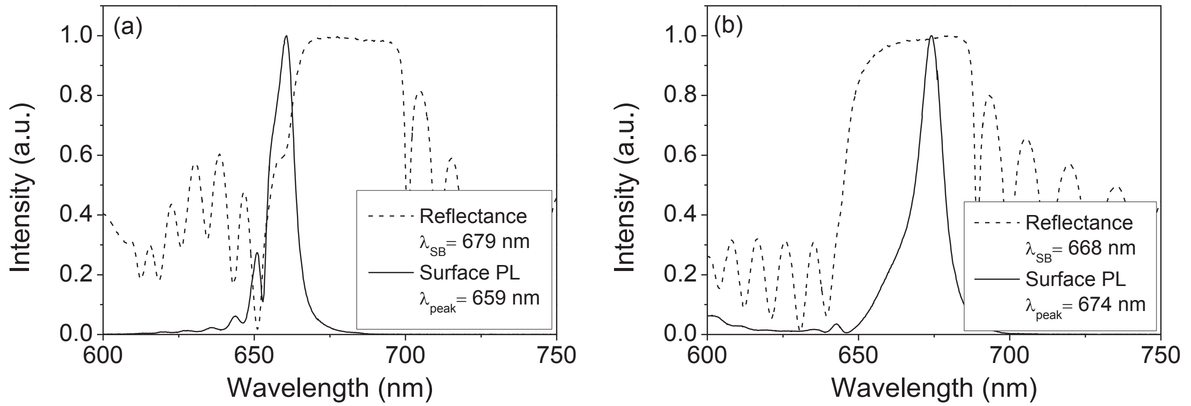

Figure 4.9: *Surface PL and reflectance measured from (a) gain mirror and (b) SESAM structures*.

The stop band of the DBR was centered to 670 nm for both structures. However, the QW emission wavelength of the gain mirror was set to 660 nm in order to take into account the gain peak shift resulting from heating of the gain chip. Heating was assumed to increase the optical thicknesses only slightly at this spectral range; therefore the center wavelength of the DBR reflectance band was not tuned away from the operation wavelength.

As seen in **Figure 4.9 (a)**, the measured PL emission peak for the gain structure is near the desired 660 nm wavelength, but the stop band is shifted to longer wavelengths than targeted (λ_{SB} = 679 nm). Cavity resonance of the etalon, which is formed between the semiconductor/air and the DBR interfaces, is located near 656 nm as revealed by simulations performed with the Essential Macleod software for the gain mirror structure. Thus, the resonance peak is positioned near the absorption wavelength of the QWs (659 nm); both the cavity resonance and the QW absorption cause the deep decrease in reflectance at the lower wavelength side of the reflectance band.

The grown SESAM structure meet the given design targets: the stop band of the DBR is centered at 668 nm, which is near the 670 nm target; and the QW emits at 671 nm, defined by the PL calibration sample grown prior to the SESAM structure.

4.3 Gain mirror processing

Both top- and bottom-emitting gain mirrors were developed. The top-emitting gain mirrors dissipated heat via the intra-cavity heat spreader, whereas the bottom-emitting gain mirror

utilized the thin disk approach, meaning that the substrate was etched away and the heat was dissipated through the DBR. The main processing steps utilized for the top- and bottom-emitting gain mirrors are shown in **Figure 4.10**. The ultimate target for both the process was to obtain good thermal conductivity between different materials without introducing damage or optical loss to the gain chip.

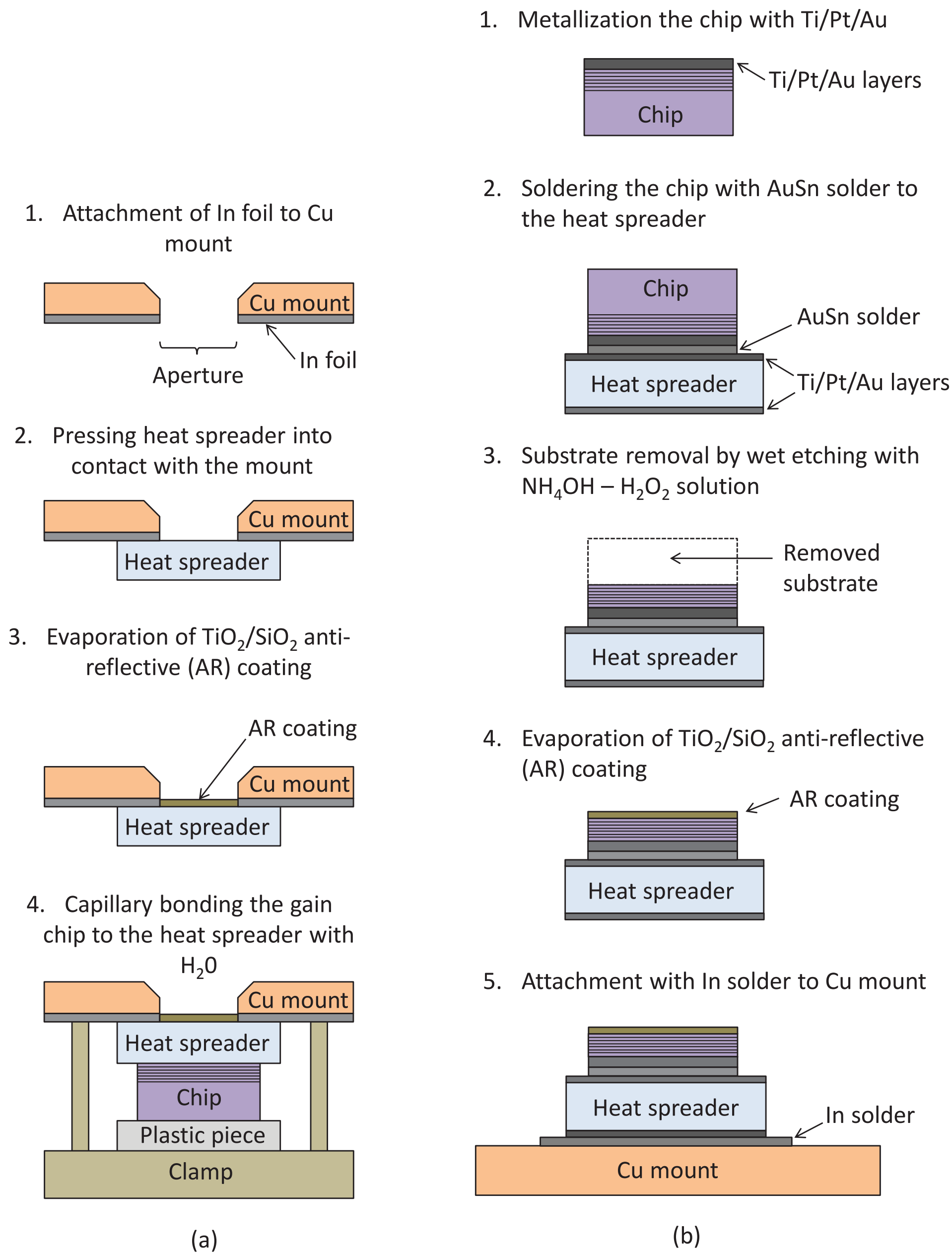

Figure 4.10: *(a) top-emitting and (b) bottom-emitting gain mirror processes viewed from the side of the device. The gain chips were scribed off from the gain mirror wafer before the presented processing steps took place. The Ti/Pt/Au layers and the AuSn solder were pre-deposited on the heat spreader by the manufacturer.*

Table 4.4: *Gain chip and heat spreader details*.

	Bottom-emitting gain mirror	Top-emitting gain mirror
Thermal management approach	Thin disk	Intra-cavity
Heat spreader geometry	Flat	Flat or slightly wedged (2°)
Heat spreader material	Silicon-diamond composite	Synthetic diamond
Heat spreader size	1.9 × 1.9 × 0.3 mm^3	3 × 3 × 0.3 mm^3
Gain chip size	1.5 × 1.5 mm^2	2.5 × 2.5 mm^2

The most vital part in the top-emitting gain mirror process is the gain chip/heat spreader interface [137]. It is important that the surfaces of the gain chip and heat spreader are clean and smooth so that capillary bonding [138] can be realized with good quality and losses could be minimized. In this research, the surfaces were wiped clean with dust-free paper or cotton bud, which was saturated with a solvent, typically ethanol or isopropanol. Deionized water was utilized in capillary bonding. To secure the bond and speed up the bonding, the heat spreader was clamped to the gain chip. A thin plastic piece was placed between the clamp and the chip in order to have an equal pressure over the chip and to prevent damaging the chip.

Table 4.4 shows a summary of the gain chip and heat spreader sizes as well as heat spreader materials utilized to extract heat from the gain chip. Some of the top-emitting gain mirrors were attached to wedged heat spreaders in order to alleviate the Fabry-Pérot etalon effect of the heat spreader. Silicon-diamond composite was used as the heat spreader material in the first VECSEL demonstrations since this material could provide moderate thermal conductivity at cheap price. However, after the gain material quality was developed to a high level, which was the target for the first VECSEL demonstrations, the heat spreader material was changed to less thermally resistive synthetic diamond.

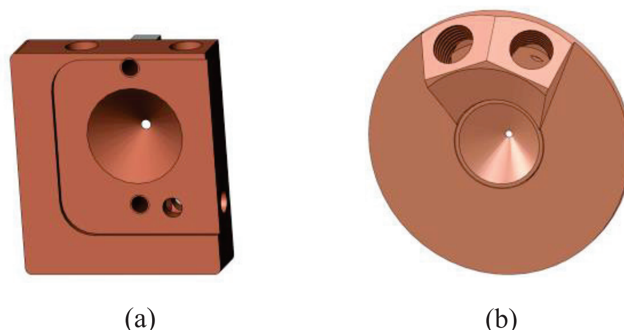

(a) (b)

Figure 4.11: *Laser mount designs utilized to cool the top-emitting gain mirrors. The mounts are aligned in the VECSEL cavity in such a way that the front side of the mounts, which are shown here, point towards the cavity.*

The gain chips were attached to sample holders machined from copper, which served as heat sinks. **Figure 4.11** presents the two mount designs used in the research to cool the top-emitting gain mirrors. The mounts had a circular aperture (diameter ~1.5 mm), as shown in **Figure 4.11**, through which the pump signal could enter the gain region and allowed the laser signal to travel inside the laser cavity. The bottom-emitting gain mirrors were attached to a plain copper plate sized 50 × 20 × 5 mm^3. A thin Ni/Au layer was applied on top of all the mounts to prevent oxidization of the copper, which would weaken the heat flow between the chip and the mount.

Most of the top-emitting gain chips were coated with a two-layer TiO_2/SiO_2 stack, which was designed to minimize intra-cavity reflection losses at the lasing wavelength arising from the use of wedged heat spreader. The coating also reduced reflection losses at the pump wavelength. A similar anti-reflective coating was usually applied also on the bottom-emitting structures to reduce pump reflection and to passivate the semiconductor surface. **Figure 4.12** shows, as an example, the measured reflectance of a TiO_2/SiO_2 stack that was designed to have minimum reflection near 1180 nm. The reflectance was measured at normal incidence, i.e. perpendicularly to the surface of the sample. Although the reflectance curve has shifted around 40 nm to higher wavelengths probably due to growth instabilities (drifting of the material fluxes), the reflectivity is still < 0.5% at the desired 1180 nm wavelength, and < 4% at 808 nm pump wavelength.

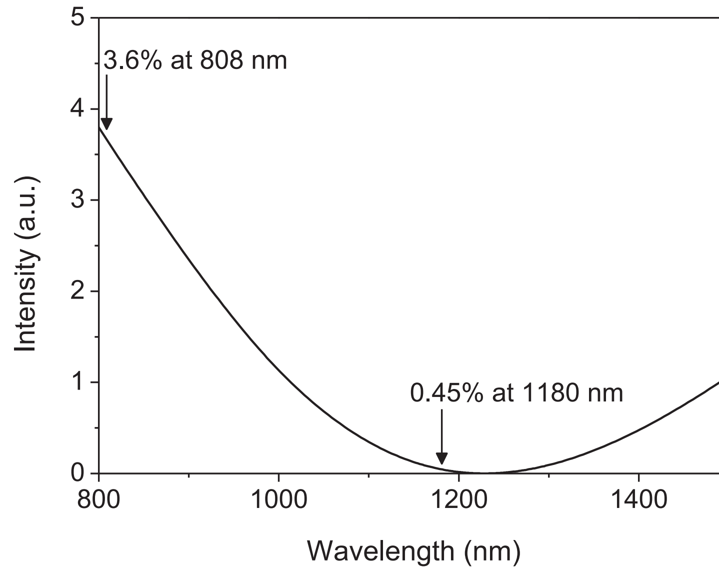

Figure 4.12: *Measured reflectance (at normal incidence) of a TiO_2 (85 nm)/SiO_2 (190 nm) stack. The layer thicknesses were deduced by fitting a simulated reflectance curve to the measured reflectance in the Essential Macleod software* [76].

Chapter 5

Characterization of VECSELs

This chapter concentrates on reporting the main lasing characteristics obtained with the gain chips. The continuous wave results recorded for the GaInAs/GaAs chips are separated from the mode locked results obtained for the GaInP/AlGaInP/GaAs gain chip.

5.1 Near IR continuous wave characteristics

The GaInAs/GaAs gain chips were characterized with two objectives in mind. One concentrated on testing the maximum output power and wavelength tuning range achievable at the fundamental lasing frequency. The other focused on demonstrating stable narrow-linewidth operation at the fundamental as well as at the second harmonic frequency. The author has been mainly involved in the first objective, i.e. obtaining high-power wavelength-tunable operation, and only provided the gain mirrors for the narrow-linewidth measurements. The high-power results are reported in the appended publication of [P4], and the results obtained when the laser was operated at narrow-linewidth are shown in [P2], [P3]. The scope of this research was to examine the fundamental laser characteristics; therefore, second harmonic generation has only been demonstrated within [P2], [P3]. The preliminary frequency-doubled results are briefly mentioned in Chapter 6 along with the future research directions. The main laser results were obtained with the top-emitting gain mirrors, although the first VECSEL characterization studies presented in [P1] were conducted with the bottom-emitting gain mirrors.

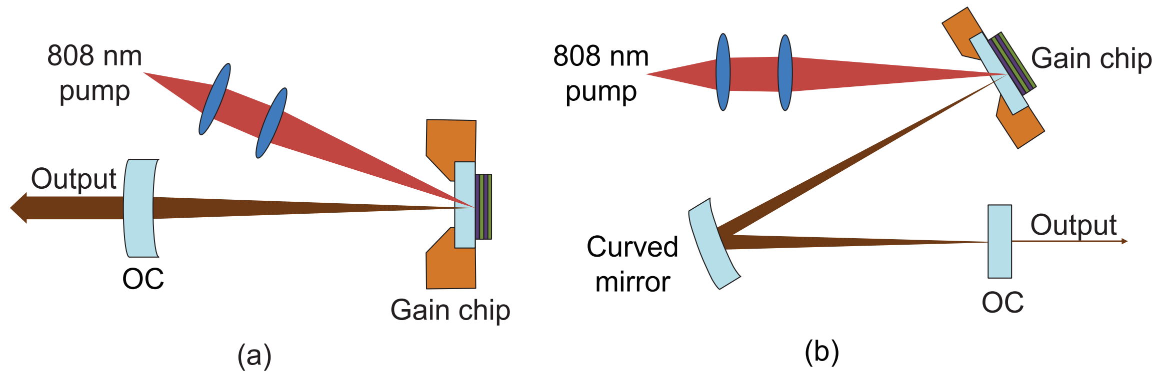

Figure 5.1: *(a) 2-mirror and (b) 3-mirror cavities utilized in obtaining continuous wave operation near 1120 nm and 1178 nm. OC stands for output coupler.*

The basic cavity configurations utilized to characterize the performance of the gain mirrors are shown in **Figure 5.1**. The cavities comprise either two or three mirrors. Fiber coupled 808 nm diode laser modules were used as pump sources. Depending on the laser characteristic of interest, either bare laser cavities or cavities containing additional intra-cavity optics were utilized. The 2-mirror cavity was utilized to obtain maximal output powers, and the 3-mirror cavity was used for obtaining stable narrow-linewidth operation at the primary and at the second harmonic frequency.

5.1.1 Stable narrow-linewidth operation

The output of a free-running VECSEL consists typically of multiple transverse and/or longitudinal modes, each fluctuating both in amplitude and frequency, which results in a broad spectral linewidth. To narrow the linewidth, the laser should be forced to operate in a single transverse as well as longitudinal mode, and the laser cavity should be stabilized against any perturbations that might cause frequency fluctuations. These fluctuations are mostly due to variations in the cavity length induced by temperature and air pressure alterations as well as mechanical vibrations.

Narrow-linewidth operation was achieved within this doctoral research by employing only passive frequency stabilization methods, meaning that the cavity was designed, constructed and protected in such a way that the effective cavity length was perturbed as little as possible by the surroundings. Single transverse mode operation was ensured with gain aperturing, i.e. providing optical pumping for such a small gain mirror area that only the TEM_{00} cavity mode was

supported. A single longitudinal mode could be selected with a 1 mm thick yttrium aluminum garnet (YAG) etalon and a 3 mm thick quarz birefringent filter (BRF) that were placed inside the cavity. These filters induced losses and eliminated lasing of the unwanted modes. Both the etalon and the BRF were needed to ensure single longitudinal mode operation; namely, without the etalon, i.e. having only the BRF inside the cavity, the laser operated still occasionally in a couple of longitudinal modes. Active frequency stabilization was used to narrow the laser linewidth even further. This stabilization was performed by locking the laser to the side of a transmission maximum of a reference Fabry–Pérot cavity. Locking was realized with an electronic feedback circuit (a commercial 'lockbox'), which controlled the cavity length via a piezo-electric transducer (PZT) to which one of the cavity mirrors was mounted. **Figure 5.2** illustrates schematically the measurement setup. The VECSEL comprised either 2 or 3 cavity mirrors. A 2-mirror VECSEL configuration is shown as an example in **Figure 5.2**.

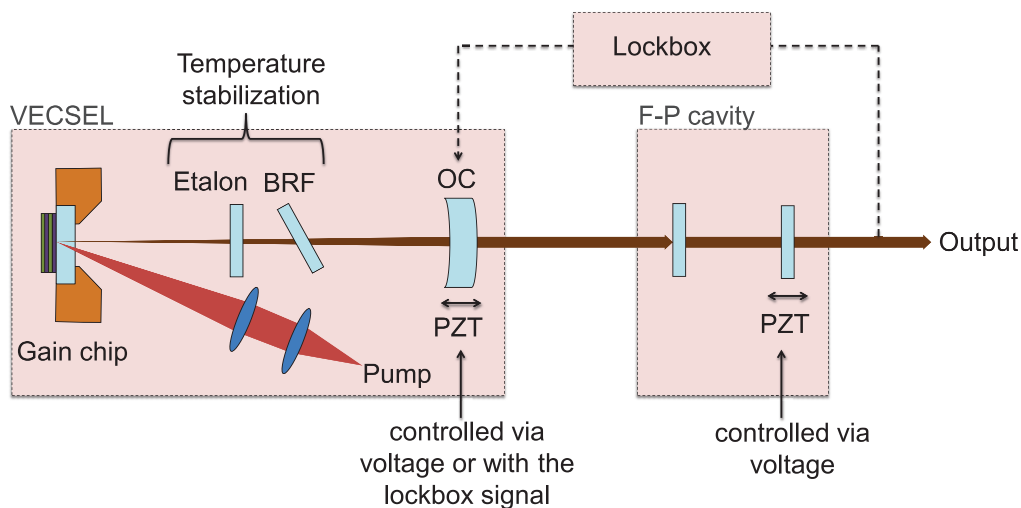

Figure 5.2: *Simplified setup used in examining the laser (i) linewidth and (ii) stability. Single longitudinal mode operation was a prerequisite for both measurements, and was verified by scanning over the FSR of the reference Fabry–Pérot cavity (PZT voltage varied) while the VECSEL cavity length was fixed to a constant PZT voltage. In (i), the VECSEL was actively stabilized, i.e. the signal arriving from the lockbox controlled the position of one of the VECSEL cavity mirror via PZT; the reference Fabry–Pérot cavity was locked to a constant PZT voltage. In (ii), only passive stabilization was used (both PZT locked to a constant voltage). Short-term laser stability was examined by measuring the amplitude fluctuation experienced by the laser system output with a power meter; long-term stability was examined with a wavemeter attached to the laser output (Fabry–Pérot cavity removed from the system). PZT stands for piezo-electric transducer, F-P for Fabry–Pérot, and FSR for free spectral range.*

The GaInAs/GaAs VECSELs showed single longitudinal mode operation at 1119 nm and 1178 nm as verified by a scanning Fabry–Pérot etalon. The output of the 1119 nm VECSEL remained fixed for several minutes as examined with a wavemeter using only passive cavity length stabilization. The frequency drift of the 1178 nm VECSEL output was estimated to be in the order of 10 MHz and 220 MHz during a measurement period of few seconds and few hours, respectively. Details from the measurements setup can be found in **Figure 5.2**. The linewidth measurement was performed only for the 2-mirror VECSEL that emitted at 1119 nm. Two different methods were utilized: In the first method, the linewidth was deduced from a beat note which was obtained by combining the VECSEL signal with a commercial fiber laser output (only passive stabilization). The second method deduced the linewidth from an error signal received from the lockbox in an actively stabilized laser system (see **Figure 5.2**). The narrowest measured linewidth was less than 300 kHz (measurement period of 4.4 ms) with the beat measurement, and less than 1 MHz (measurement period of 200 ms) with the error signal method.

To conclude, the GaInAs/GaAs VECSELs could be made to operate essentially at a single frequency, and the laser wavelength/frequency remained stable for several minutes with only passive frequency stabilization. Detailed experimental results have been reported in [P2], [P3].

5.1.2 Wavelength tuning

The wavelength of a laser can be tuned in several ways; typical methods include (i) shifting the spectral gain profile by influencing the gain medium, (ii) seeding the laser externally, (iii) introducing wavelength selective filters inside the laser cavity whose transmission peak can be spectrally adjusted, or (iv) changing the effective cavity length of a single-frequency laser. In this research, the two latter tuning techniques were used to adjust the lasing wavelength: rough wavelength tuning was performed only via spectral filtering, whereas continuous fine-tuning required both spectral filtering as well as adjustments in the effective cavity length. A BRF made of quartz was utilized as the wavelength tunable filter, whereas the effective cavity length was adjusted by changing the placement of a piezo-actuated cavity mirror. The BRF exploits birefringent properties of quartz to induce wavelength-dependent transmission losses; the operation wavelength of the laser could simply be tuned by rotating the filter plate.

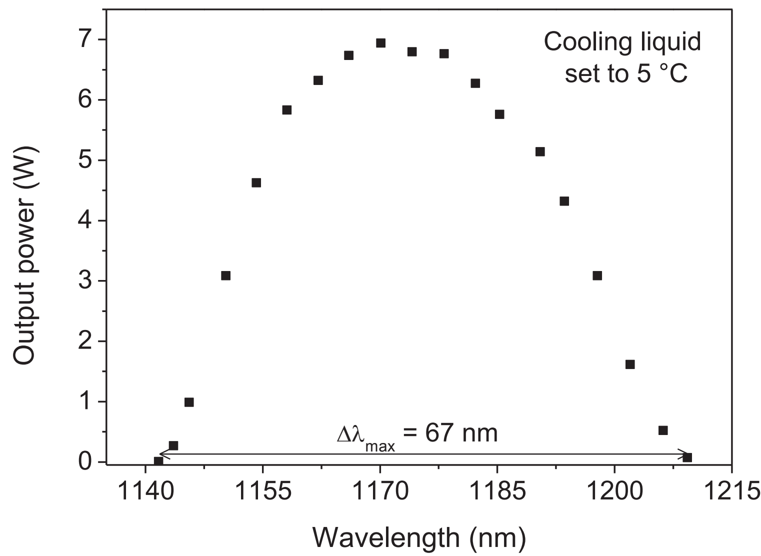

Figure 5.3: *Wavelength tuning behavior of the GaInAs/GaAs VECSELs near the center linewidth of 1178 nm achieved by rotating the BRF. The incident pump power was around 44 W.*

With only a single BRF inside a 2-mirror cavity, wavelength tuning ranges of 30–67 nm were observed with the GaInAs/GaAs VECSELs. The measured tuning ranges varied depending on the cooling capacity of the heat sink, used measurement conditions (temperature of the gain chip and coolant, and pump power level) as well as the gain mirror itself. The widest tuning range was achieved for a VECSEL designed for operation near 1178 nm; the VECSEL utilized a linear 2-mirror cavity and a 1.5 mm thick intra-cavity BRF (FSR around 1 nm). The wavelength tuning behavior of the laser can be seen in **Figure 5.3**. The laser was capable of high-power operation with a spectral width less than 1 nm FWHM (measured with 0.02 nm resolution). The measured tuning range is remarkably wide if compared to tuning ranges reported previously for GaInAs/GaAs VECSELs by other groups [47], [139], [140].

Continuous tuning near the desired operation wavelength was achieved by forcing the VECSEL to operate at a single frequency with intra-cavity filters, and by adjusting both the effective cavity length via the PZT and the filters' spectral transmission via temperature. Continuous tuning ranges on the order of a few GHz were achieved near 1120 nm and near the second harmonic wavelength of 589 nm without mode-hopping. These tuning ranges should be sufficient for the precision spectroscopic applications exploiting sodium (Na) I and magnesium (Mg) II resonances, which are the main applications for the developed lasers. The requirements

set by these applications are discribed in [P3], and a more detailed description about the output characteristics can be found in [P2]–[P4].

5.1.3 High power operation

The performance of a VECSEL gain chip is typically limited either by overheating or amplified spontaneous emission (ASE)[141]. Heat decreases the effective gain of the laser and may lead to thermal roll-over and eventually to shut down of the laser. ASE on the other hand depletes the gain from the lasing mode/modes and may even induce lateral lasing. ASE becomes increasingly significant as the pump spot and intensity is increased.

In this research, high-power operation has been enabled by several factors. First of all, the problem of overheating has been addressed by enhancing the cooling capacity of the mount, by utilizing a low operation temperature, and by using a large pump spot area (350–540 um diameter). The mount shown in **Figure 4.11 (b)** had wider cross-sections and longer length of the cooling channels than the mount shown in **Figure 4.11 (a)** in order to handle high heat loads. Coolant temperatures as low as -10 °C were utilized in order to efficiently dissipate the heat. We also used a large pump spot to distribute the heat over a larger area. On the other hand, the probability of depleting gain via ASE was also increased along with the wider pump spot. The significance of ASE as a limiting factor for the VECSEL performance was not assessed. Moreover, the mount design prevented for observing lateral lasing since the vertical edges of the chip could not be seen.

High-power operation has been realized in multimode (both transverse and longitudinal) and single-mode (both transverse and longitudinal) condition from single GaInAs/GaAsP/GaAs gain chips and reported in [P2], [P3], [P4]. The highest output powers measured were over 10 W in the single mode and over 20 W in the multimode operation regime.

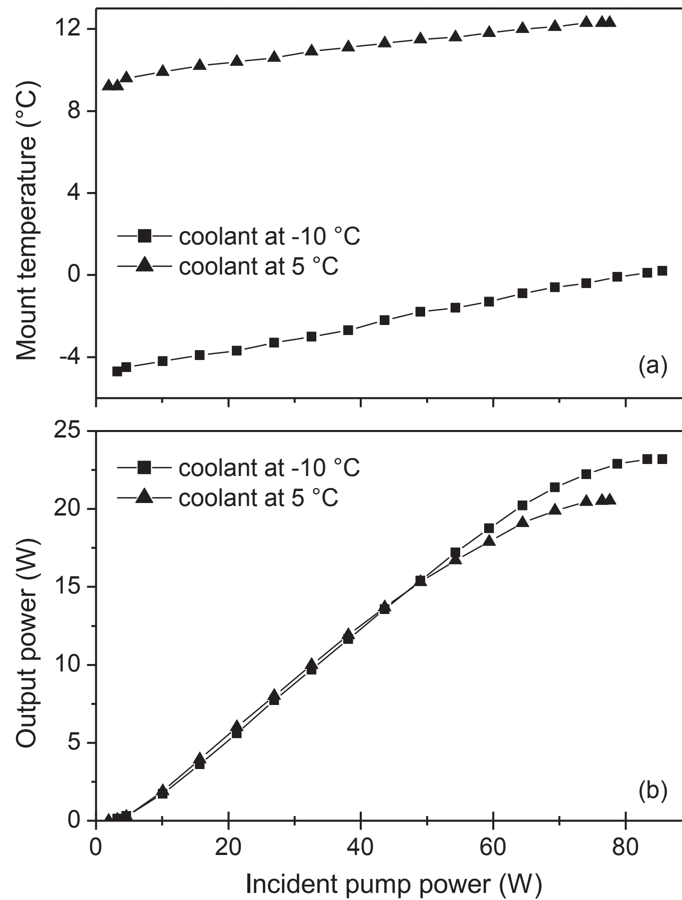

Figure 5.4: *Mount temperatures and power characteristics measured from the GaInAs/GaAs VECSEL emitting near 1178 nm at 5 °C and -10 °C coolant temperatures with 3% transmissive output coupling mirror*.

Figure 5.4 presents the power transfer curves as well as measured mount temperatures of the VECSEL emitting near 1178 nm at multiple transversal and longitudinal modes. Note that the temperatures and output powers are reported as a function of incident pump power; it was estimated that as high as 20% of the incident pump power was reflected from the uncoated air/heat spreader interface. We utilized a simple 2-mirror cavity in order to minimize additional cavity losses and a pump spot diameter of 540 µm. A wider pump spot of 715 µm was also tested, but it did not provide higher output powers than the 540 µm sized spot. As shown in **Figure 5.4 (a)**, the cooling capacity of the redesigned mount was still limited resulting in warming of the mount along with the incident pump power.

In conclusions, the developed GaInAs/GaAs gain chips proved to be capable of emitting high output powers both at single and multiple transverse as well as longitudinal modes. Overheating

was probably the main limitation for the lasing performance of the chips reported in this thesis. Namely, in later studies (yet unpublished), output powers of around 40 W (multimode) were obtained from the same gain material when cooling of the chips was enhanced and the gain chips were pumped from a larger area. Cooling was enhanced by increasing the cooling power and by utilizing a 2 mm thick diamond heat spreader.

5.2 Red mode-locked operation

The second part of the doctoral research focused on demonstrating passive mode locking of a VECSEL in the red spectral region of the electromagnetic spectrum. The mode-locked results are presented in more detail in [P5]. The gain mirror used in this study was cooled with the intra-cavity heat spreader approach.

Figure 5.5 presents the cavity configuration utilized for obtaining passive mode-locked operation with the GaInP/AlGaInP/GaAs VECSEL. The Z-shaped (4-mirror) cavity provided even more flexibility in manipulating the laser mode size on the SESAM and on the gain chip than the V-shaped (3-mirror) cavity. Adjustments of the laser mode size on the SESAM is particularly important for achieving stable mode locking [68]. The VECSEL was optically pumped with a diode-pumped solid-state laser emitting radiation at 532 nm in continuous wave mode. The pump spot had a diameter of around 115 µm on the gain chip, and the mode size on the SESAM was simulated to be around 20 µm. The gain chip was cooled with water down to 10 °C during operation, whereas the SESAM was operated at room temperature.

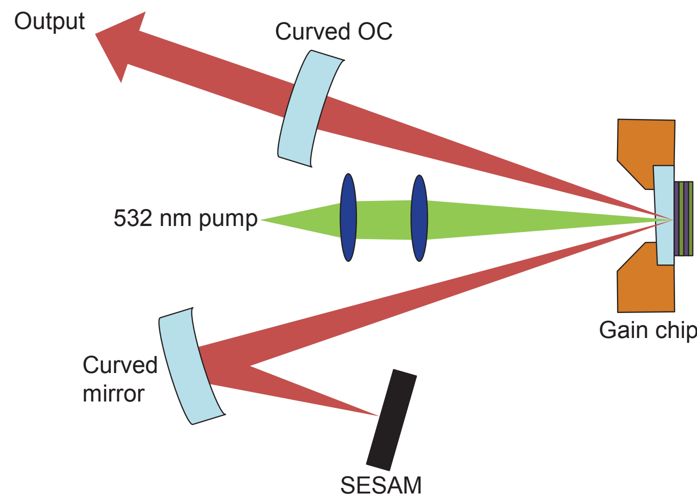

Figure 5.5: *A 4-mirror cavity utilized for achieving mode-locked operation at red wavelength*.

Before performing mode locking, the continuous-wave performance of the VECSEL was tested with the cavity shown in **Figure 5.5**, but with the exception that the SESAM was replaced with a highly reflective mirror. The VECSEL was able to emit a maximum of 143 mW at 5.5 W pump power and 10 °C cooling water temperature. With a lower cooling temperature of 5 °C, the output increased to 186 mW at 5.9 W pumping. The output power characteristic of the VECSEL measured with a cooling water temperature of 10 °C is shown in **Figure 5.6**.

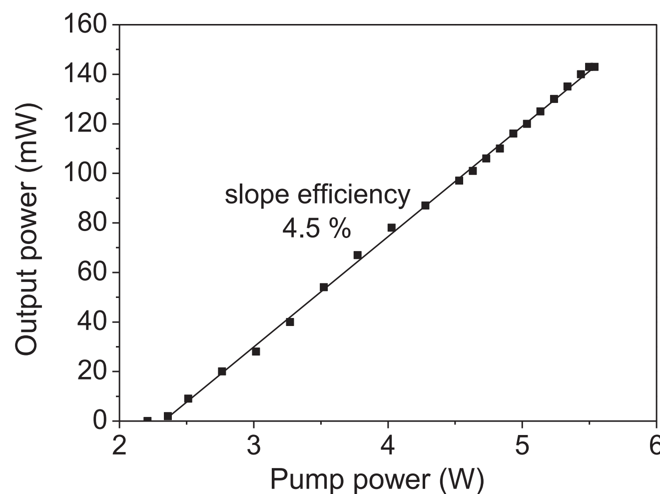

Figure 5.6: *Continuous-wave power characteristics of the 675 nm laser at cooling water temperature of 10 °C*.

Figure 5.7 presents the oscilloscope trace and the radio-frequency (RF) spectra measured from the mode-locked VECSEL. The VECSEL is clearly generating single mode-locked pulses at the fundamental frequency of 972.7 MHz with a side mode suppression ratio over 60 dB. The maximum average output power was 45 mW in the pulsed mode. The optical spectrum was centered at around 676 nm as seen in **Figure 5.8**.

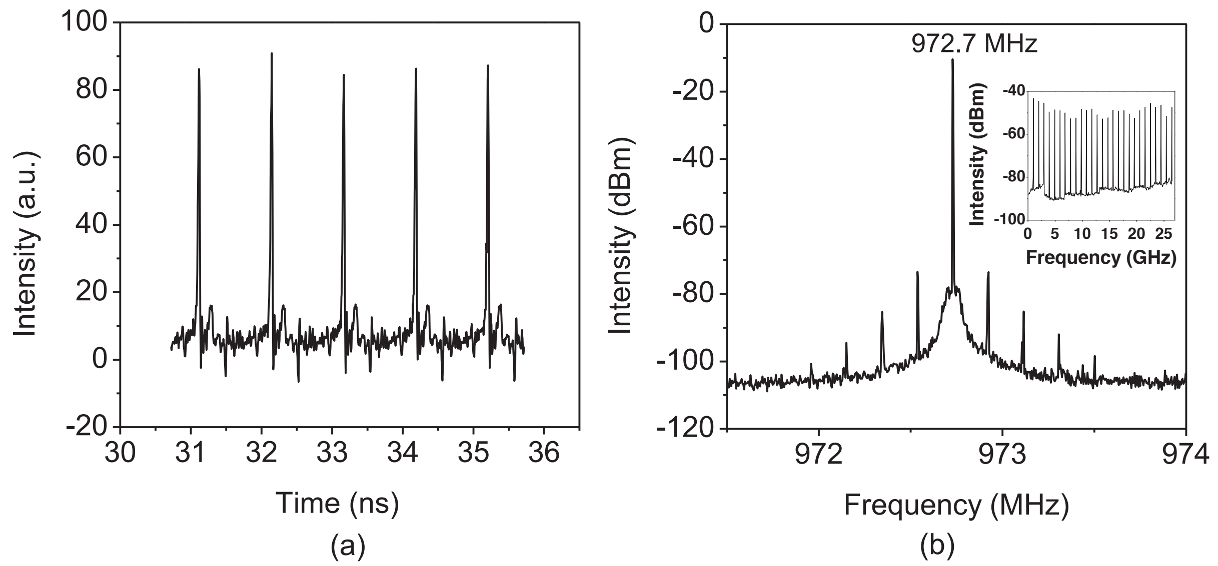

Figure 5.7: *(a) Pulse train and (b) RF spectra. The side peaks seen in the RF spectrum are 200 kHz noise caused by the pump laser drive circuitry.*

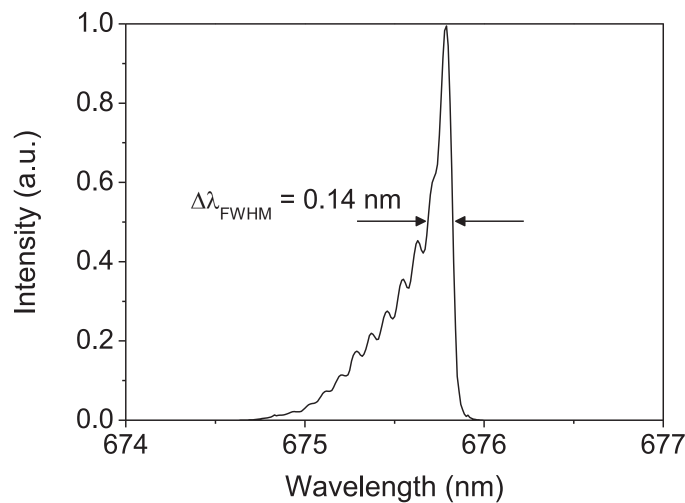

Figure 5.8: *Optical spectrum of the mode-locked 675 nm laser.*

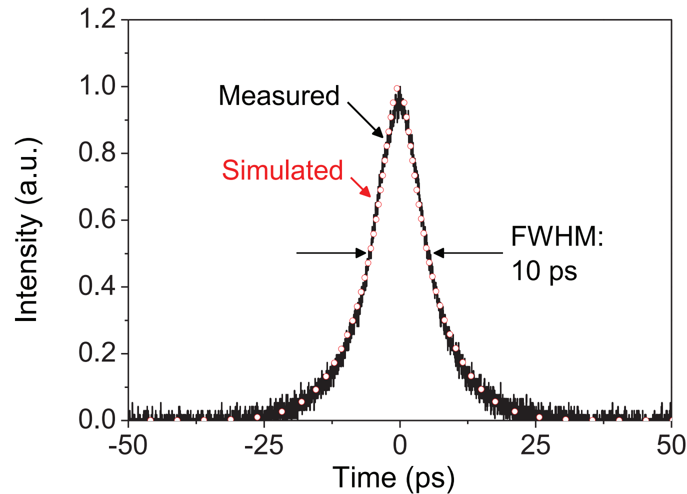

Figure 5.9: *Measured intensity autocorrelation trace (black line) and simulated autocorrelation (red circles).*

The duration of the pulses was measured with a second harmonic intensity autocorrelator. Based on this autocorrelation an estimation of the pulse structure could be reconstructed with the PICASO method [142] yielding a pulse width of 5.1 ps (FWHM). The autocorrelation simulated from these reconstructed pulses along with the measured autocorrelation trace are shown in **Figure 5.9**. The simulated autocorrelation can be seen to fit well to the measured trace. It is noteworthy, that Gaussian or hyperbolic secant functions, which are typically used to describe the laser pulse shape, could not provide an autocorrelation that would be compatible with the recorded trace, especially concerning the wings. Therefore, the laser pulse shape was retrieved with the PICASO method. The peak power of the pulses was estimated to be 15 W.

As a conclusion, passive mode locking was demonstrated for the first time (to our knowledge) with the GaInP/AlGaInP/GaAs VECSEL in the red part of the spectrum. After this report, red mode-locked operation was obtained by another group [63] as well. Their VECSEL emitted < 250 fs pulses with an average output power < 1 mW; this power is much less than obtained with the mode-locked VECSEL presented within this doctoral thesis. The repetition rate was near the same (836 MHz). These two reports show that there seems to be a growing interest for developing ultra-short pulse sources for the red spectral range.

Chapter 6

Conclusions

The main target of the doctoral work was to develop efficient VECSELs with emission at fundamental wavelengths in the range of 1.1–1.2 µm. These VECSELs are beneficial in accessing the yellow-orange wavelength range of the electromagnetic spectrum via frequency doubling. The frequency doubling experiment was left as a subject for subsequent studies, since the development of the VECSELs emitting fundamentally at near-IR [P1]–[P4] was considered by itself as a state-of-the-art achievement. The dissertation concentrated particularly on finding optimal designs as well as suitable growth parameters for realizing high-quality GaInAs/GaAsP/GaAs gain mirrors. The crystalline quality and the effect of strain compensation were assessed with photoluminescence and x-ray-diffraction based methods [P1], [P2]. As a result, partially strain-compensated (net strain from -0.03% to -0.07%; calculated with the thickness weighted method [73]), gain mirrors with high crystalline quality could be realized at the emission wavelength range of 1115–1190 nm with up to 10 QWs. Strain compensation as well as the use of reduced QW growth temperature were the two main factors enabling the high quality: strain compensation alleviated the net compressive strain induced by the QWs, whereas the low growth temperature prevented nucleation and formation of misfit dislocations in single QWs. Furthermore, PL-based dark defect imaging was found to be the most suitable method, among the ones tested in the research, for detecting relaxation-induced misfit dislocations from the gain mirrors.

Laser cavities specifically designed for high power as well as narrow-linewidth operation were constructed. Consequently, the gain mirrors demonstrated high power operation in single-frequency transverse and longitudinal [P2], [P3] as well as multimode transverse and longitudinal conditions [P4]. The emission wavelength could be tuned coarsely over a 30–67

nm span and continuously in the range of gigahertz around the central emission wavelength. Furthermore, the single-frequency lasers were able to emit stable emission for several minutes by using only passive frequency stabilization techniques. It is worth mentioning, that a record-high output power of 23 W, and a record-wide wavelength tuning range of 67 nm were reported from the gain mirror emitting near 1178 nm [P4].

In the frequency-doubled regime, the gain mirrors have demonstrated, in preliminary tests, to be capable of generating watt-level emission at 560 and 589 nm. These remarkable results demonstrate that the gain mirrors developed within this research are capable of high laser performance, and that they have potential to become efficient high-power laser sources at the yellow-orange. Moreover, the frequency-doubled output centered at 589 nm has been successfully used to detect and scan the sodium D2 resonance (reported in [P3]), which means that the gain mirror is useful for laser guide star applications. It has also been shown in [P2], and [P3] that the frequency doubled 560 nm output could, in principle, be used for a similar experiment to detect the D2 resonance line of the Mg^+ ions, which lies near 280 nm, if the output would be further frequency-doubled to the fourth harmonic of the fundamental wavelength.

In a separate project developed in parallel at ORC, the GaInAs/GaAsP/GaAs VECSELs were used to demonstrate high-power frequency doubled emission. Consequently, 20 W of output power has been reached near 588 nm with the gain mirrors developed within this dissertation work [48]. This VECSEL could be an attractive light source for guide star application if its cavity is modified further so that single longitudinal mode operation could be reached near the sodium D2 transition line. Another branch of study has focused on developing GaInAs/GaAsP/GaAs gain mirrors for the thin disk geometry (substrate removal process) utilizing the gain mirror structures developed in this thesis as the basis. So far, a maximum of 15 W of output power has been reached near 1180 nm with the thin disk approach and more is to be expected as the process is optimized further. Future development work includes increasing the output powers of the GaInAs/GaAsP/GaAs VECSELs and enhancing thermal management of the gain chips.

The second part of the dissertation concerned on the first demonstration of a passively mode-locked VECSEL emitting fundamentally at red wavelengths [P5]. The VECSEL was mode-locked with a SESAM and was capable of generating 5.1 ps pulses at the wavelength of 675 nm

with an average power of 45 mW and repetition rate of 973 MHz. The gain as well as semiconductor absorber structures are based on GaInP/AlGaInP/GaAs material system. The VECSEL has potential to be developed into a compact picosecond laser source for the red part of the spectrum. There are, however, a few issues that need to be addressed before reaching this goal. Namely, in order to reach a compact device, the bulky 532 nm solid-state laser, used in this dissertation, should be replaced by a compact diode laser source. This may not be an easy task, since currently the only suitable and commercially available pump sources are blue-emitting GaN, low power green (515 nm) and red-emitting AlGaInP laser diodes. Blue radiation is highly absorbed in the GaInP/AlGaInP/GaAs material [4], [28], whereas the red emission requires the use of more complicated in-well pumping. However, an even bigger concern is the reliability of the VECSEL; the laser performance was noticed to decrease along time in the reported red mode-locked VECSEL papers [P5], [63]. Thus, to become a practical light source, the red mode-locked VECSEL needs to be further developed, and the development work should focus especially on enhancing the material quality of the device so that sufficient reliability could be achieved.

Bibliography

[1] A. C. Tropper and S. Hoogland, 'Extended cavity surface-emitting semiconductor lasers', *Progress in Quantum Electronics*, vol. 30, no. 1, pp. 1–43, 2006.

[2] A. C. Tropper, H. D. Foreman, A. Garnache, K. G. Wilcox, and S. H. Hoogland, 'Vertical-external-cavity semiconductor lasers', *Journal of Physics D: Applied Physics*, vol. 37, no. 9, pp. R75–R85, 2004.

[3] M. Kuznetsov, 'VECSEL Semiconductor Lasers: A Path to High-Power, Quality Beam and UV to IR Wavelength by Design', in *Semiconductor Disk Lasers*, O. G. Okhotnikov, Ed. Wiley-VCH Verlag GmbH & Co. KGaA, 2010, pp. 1–71.

[4] S. Calvez, J. E. Hastie, M. Guina, O. G. Okhotnikov, and M. D. Dawson, 'Semiconductor disk lasers for the generation of visible and ultraviolet radiation', *Laser & Photonics Reviews*, vol. 3, no. 5, pp. 407–434, 2009.

[5] N. G. Basov, 'Semiconductor Lasers', in *Nobel Lectures in Physics 1963–1970*, Elsevier, Amsterdam, 1972, pp. 89–105.

[6] M. Kuznetsov, F. Hakimi, R. Sprague, and A. Mooradian, 'High-power (>0.5-W CW) diode-pumped vertical-external-cavity surface-emitting semiconductor lasers with circular TEM_{00} beams', *IEEE Photonics Technology Letters*, vol. 9, no. 8, pp. 1063–1065, 1997.

[7] M. Kuznetsov, F. Hakimi, R. Sprague, and A. Mooradian, 'Design and characteristics of high-power (>0.5-W CW) diode-pumped vertical-external-cavity surface-emitting semiconductor lasers with circular TEM_{00} beams', *IEEE Journal of Selected Topics in Quantum Electronics*, vol. 5, no. 3, pp. 561–573, 1999.

[8] Y. Kaneda, J. M. Yarborough, L. Li, N. Peyghambarian, L. Fan, C. Hessenius, M. Fallahi, J. Hader, J. V. Moloney, Y. Honda, M. Nishioka, Y. Shimizu, K. Miyazono, H. Shimatani, M. Yoshimura, Y. Mori, Y. Kitaoka, and T. Sasaki, 'Continuous-wave all-solid-state 244 nm deep-ultraviolet laser source by fourth-harmonic generation of an optically pumped semiconductor laser using $CsLiB_6O_{10}$ in an external resonator', *Optics Letters*, vol. 33, no. 15, pp. 1705–1707, 2008.

[9] M. Rahim, F. Felder, M. Fill, and H. Zogg, 'Optically pumped 5 µm IV-VI VECSEL with Al-heat spreader', *Optics Letters*, vol. 33, no. 24, pp. 3010–3012, 2008.

[10] B. Heinen, T.-L. Wang, M. Sparenberg, A. Weber, B. Kunert, J. Hader, S. W. Koch, J. V. Moloney, M. Koch, and W. Stolz, ‘106 W continuous-wave output power from vertical-external-cavity surface-emitting laser’, *Electronics Letters*, vol. 48, no. 9, pp. 516–517, 2012.

[11] P. Klopp, U. Griebner, M. Zorn, and M. Weyers, ‘Pulse repetition rate up to 92 GHz or pulse duration shorter than 110 fs from a mode-locked semiconductor disk laser’, *Applied Physics Letters*, vol. 98, no. 7, p. 071103, 2011.

[12] P. Klopp, U. Griebner, M. Zorn, A. Klehr, A. Liero, M. Weyers, and G. Erbert, ‘Mode-locked InGaAs-AlGaAs disk laser generating sub-200-fs pulses, pulse picking and amplification by a tapered diode amplifier’, *Optics Express*, vol. 17, no. 13, pp. 10820–10834, 2009.

[13] B. Rudin, V. J. Wittwer, D. J. H. C. Maas, M. Hoffmann, O. D. Sieber, Y. Barbarin, M. Golling, T. Südmeyer, and U. Keller, ‘High-power MIXSEL: an integrated ultrafast semiconductor laser with 6.4 W average power’, *Optics Express*, vol. 18, no. 26, pp. 27582–27588, 2010.

[14] K. G. Wilcox, A. C. Tropper, H. E. Beere, D. A. Ritchie, B. Kunert, B. Heinen, and W. Stolz, ‘4.35 kW peak power femtosecond pulse mode-locked VECSEL for supercontinuum generation’, *Optics Express*, vol. 21, no. 2, pp. 1599–1605, 2013.

[15] M. Scheller, T.-L. Wang, B. Kunert, W. Stolz, S. W. Koch, and J. V. Moloney, ‘Passively modelocked VECSEL emitting 682 fs pulses with 5.1W of average output power’, *Electronics Letters*, vol. 48, no. 10, pp. 588 –589, 2012.

[16] M. Butkus, E. A. Viktorov, T. Erneux, C. J. Hamilton, G. Maker, G. P. A. Malcolm, and E. U. Rafailov, ‘85.7 MHz repetition rate mode-locked semiconductor disk laser: fundamental and soliton bound states’, *Optics Express*, vol. 21, no. 21, pp. 25526–25531, 2013.

[17] E. J. Saarinen, A. Rantamäki, A. Chamorovskiy, and O. G. Okhotnikov, ‘200 GHz 1 W semiconductor disc laser emitting 800 fs pulses’, *Electronics Letters*, vol. 48, no. 21, pp. 1355–1357, 2012.

[18] J. R. Orchard, D. T. D. Childs, L. C. Lin, B. J. Stevens, D. M. Williams, and R. A. Hogg, ‘Design Rules and Characterisation of Electrically Pumped Vertical External Cavity Surface Emitting Lasers’, *Japanese Journal of Applied Physics*, vol. 50, no. 4S, p. 04DG05, 2011.

[19] A. Mooradian, A. Shchegrov, A. Tandon, and G. Yoffe, ‘External-Cavity Surface-Emitting Diode Lasers’, in *Semiconductor Disk Lasers*, O. G. Okhotnikov, Ed. Wiley-VCH Verlag GmbH & Co. KGaA, 2010, pp. 263–304.

[20] Y. Barbarin, M. Hoffmann, W. P. Pallmann, I. Dahhan, P. Kreuter, M. Miller, J. Baier, H. Moench, M. Golling, T. Südmeyer, B. Witzigmann, and U. Keller, ‘Electrically Pumped Vertical External Cavity Surface Emitting Lasers Suitable for Passive Modelocking’, *IEEE Journal of Selected Topics in Quantum Electronics*, vol. 17, no. 6, pp. 1779–1786, 2011.

[21] B. Sumpf, K.-H. Hasler, P. Adamiec, F. Bugge, F. Dittmar, J. Fricke, H. Wenzel, M. Zorn, G. Erbert, and G. Tränkle, ‘High-Brightness Quantum Well Tapered Lasers’, *IEEE Journal of Selected Topics in Quantum Electronics*, vol. 15, no. 3, pp. 1009–1020, 2009.

[22] M. Mikulla, ‘Tapered High-Power, High-Brightness Diode Lasers: Design and Performance’, in *High-Power Diode Lasers*, R. Diehl, Ed. Springer Berlin Heidelberg, 2000, pp. 265–288.

[23] C. Fiebig, G. Blume, C. Kaspari, D. Feise, J. Fricke, M. Matalla, W. John, H. Wenzel, K. Paschke, and G. Erbert, ‘12W high-brightness single-frequency DBR tapered diode laser’, *Electronics Letters*, vol. 44, no. 21, pp. 1253–1255, 2008.

[24] S. R. Bowman, ‘High-power diode-pumped solid-state lasers’, *Optical Engineering*, vol. 52, no. 2, p. 021012, 2013.

[25] T. Schwarzbäck, R. Bek, F. Hargart, C. A. Kessler, H. Kahle, E. Koroknay, M. Jetter, and P. Michler, ‘High-power InP quantum dot based semiconductor disk laser exceeding 1.3 W’, *Applied Physics Letters*, vol. 102, no. 9, p. 092101, 2013.

[26] T. Schwarzbäck, H. Kahle, M. Eichfelder, W.-M. Schulz, R. Roßbach, M. Jetter, and P. Michler, ‘Wavelength tunable red AlGaInP-VECSEL emitting at around 660 nm’, *Proceedings of SPIE*, vol. 7919, p. 79190B, 2011.

[27] T. Schwarzbäck, M. Eichfelder, W.-M. Schulz, R. Roßbach, M. Jetter, and P. Michler, ‘Short wavelength red-emitting AlGaInP-VECSEL exceeds 1.2 W continuous-wave output power’, *Applied Physics B*, vol. 102, no. 4, pp. 789–794, 2010.

[28] A. Smith, J. E. Hastie, H. D. Foreman, T. Leinonen, M. Guina, and M. D. Dawson, ‘GaN diode-pumping of red semiconductor disk laser’, *Electronics Letters*, vol. 44, no. 20, pp. 1195–1196, 2008.

[29] J. Hastie, S. Calvez, M. Dawson, T. Leinonen, A. Laakso, J. Lyytikäinen, and M. Pessa, ‘High power CW red VECSEL with linearly polarized TEM00 output beam’, *Optics Express*, vol. 13, no. 1, pp. 77–81, 2005.

[30] J. E. Hastie, S. Calvez, M. D. Dawson, T. Leinonen, and M. Pessa, ‘0.3 W cw red microchip VECSEL’, in *Conference on Lasers and Electro-Optics (CLEO)*, 2005, vol. 2, pp. 1390 – 1392.

[31] J. E. Hastie, L. G. Morton, A. J. Kemp, M. D. Dawson, A. B. Krysa, and J. S. Roberts, ‘Tunable ultraviolet output from an intracavity frequency-doubled red vertical-external-cavity surface-emitting laser’, *Applied Physics Letters*, vol. 89, no. 6, p. 061114, 2006.

[32] P. J. Schlosser, J. E. Hastie, S. Calvez, A. B. Krysa, and M. D. Dawson, ‘InP/AlGaInP quantum dot semiconductor disk lasers for CW TEM_{00} emission at 716–755 nm’, *Optics Express*, vol. 17, no. 24, pp. 21782–21787, 2009.

[33] T. Wunderer, J. E. Northrup, Z. Yang, M. Teepe, A. Strittmatter, N. M. Johnson, P. Rotella, and M. Wraback, ‘In-well pumping of InGaN/GaN vertical-external-cavity surface-emitting lasers’, *Applied Physics Letters*, vol. 99, no. 20, p. 201109, 2011.

[34] T. Wunderer, J. E. Northrup, Z. Yang, M. Teepe, N. M. Johnson, P. Rotella, and M. Wraback, ‘In-Well Pumped Blue GaN-Based Vertical-External-Cavity Surface-Emitting Lasers’, *Japanese Journal of Applied Physics*, vol. 52, no. 8S, p. 08JG11, 2013.

[35] G. B. Kim, J.-Y. Kim, J. Lee, J. Yoo, K.-S. Kim, S.-M. Lee, S. Cho, S.-J. Lim, T. Kim, and Y. Park, 'End-pumped green and blue vertical external cavity surface emitting laser devices', *Applied Physics Letters*, vol. 89, no. 18, p. 181106, 2006.

[36] J.-Y. Kim, S. Cho, S.-J. Lim, J. Yoo, G. B. Kim, K.-S. Kim, J. Lee, S.-M. Lee, T. Kim, and Y. Park, 'Efficient blue lasers based on gain structure optimizing of vertical-external-cavity surface-emitting laser with second harmonic generation', *Journal of Applied Physics*, vol. 101, no. 3, p. 033103, 2007.

[37] A. Hein, F. Demaria, A. Kern, S. Menzel, F. Rinaldi, R. Rösch, and P. Unger, 'Efficient 460-nm Second-Harmonic Generation With Optically Pumped Semiconductor Disk Lasers', *IEEE Photonics Technology Letters*, vol. 23, no. 3, pp. 179–181, 2011.

[38] J. Chilla, Q.-Z. Shu, H. Zhou, E. Weiss, M. Reed, and L. Spinelli, 'Recent advances in optically pumped semiconductor lasers', *Proceedings of SPIE*, vol. 6451, p. 645109, 2007.

[39] L. E. Hunziker, C. Ihli, and D. S. Steingrube, 'Miniaturization and Power Scaling of Fundamental Mode Optically Pumped Semiconductor Lasers', *IEEE Journal of Selected Topics in Quantum Electronics*, vol. 13, no. 3, pp. 610–618, 2007.

[40] L. Fan, T.-C. Hsu, M. Fallahi, J. T. Murray, R. Bedford, Y. Kaneda, J. Hader, A. R. Zakharian, J. V. Moloney, S. W. Koch, and W. Stolz, 'Tunable watt-level blue-green vertical-external-cavity surface-emitting lasers by intracavity frequency doubling', *Applied Physics Letters*, vol. 88, no. 25, p. 251117, 2006.

[41] J. L. A. Chilla, S. D. Butterworth, A. Zeitschel, J. P. Charles, A. L. Caprara, M. K. Reed, and L. Spinelli, 'High-power optically pumped semiconductor lasers', *Proceedings of SPIE*, vol. 5332, pp. 143–150, 2004.

[42] M. Jacquemet, M. Domenech, G. Lucas-Leclin, P. Georges, J. Dion, M. Strassner, I. Sagnes, and A. Garnache, 'Single-frequency cw vertical external cavity surface emitting semiconductor laser at 1003 nm and 501 nm by intracavity frequency doubling', *Applied Physics B*, vol. 86, no. 3, pp. 503–510, 2007.

[43] A. Hein, S. Menzel, and P. Unger, 'High-power high-efficiency optically pumped semiconductor disk lasers in the green spectral region with a broad tuning range', *Applied Physics Letters*, vol. 101, no. 11, p. 111109, 2012.

[44] A. J. Maclean, A. J. Kemp, S. Calvez, J.-Y. Kim, T. Kim, M. D. Dawson, and D. Burns, 'Continuous Tuning and Efficient Intracavity Second-Harmonic Generation in a Semiconductor Disk Laser With an Intracavity Diamond Heatspreader', *IEEE Journal of Quantum Electronics*, vol. 44, no. 3, pp. 216–225, 2008.

[45] J. Lee, S. Lee, T. Kim, and Y. Park, '7W high-efficiency continuous-wave green light generation by intracavity frequency doubling of an end-pumped vertical external-cavity surface emitting semiconductor laser', *Applied Physics Letters*, vol. 89, no. 24, p. 241107, 2006.

[46] S. Hilbich, W. Seelert, V. Ostroumov, C. Kannengiesser, R. v. Elm, J. Mueller, E. Weiss, H. Zhou, and J. Chilla, 'New wavelengths in the yellow-orange range between 545 nm and 580 nm generated by an intracavity frequency-doubled optically pumped semiconductor laser', *Proceedings of SPIE*, vol. 6451, p. 64510C, 2007.

[47] M. Fallahi, L. Fan, Y. Kaneda, C. Hessenius, J. Hader, H. Li, J. V. Moloney, B. Kunert, W. Stolz, S. W. Koch, J. Murray, and R. Bedford, '5-W Yellow Laser by Intracavity Frequency Doubling of High-Power Vertical-External-Cavity Surface-Emitting Laser', *IEEE Photonics Technology Letters*, vol. 20, no. 20, pp. 1700 –1702, 2008.

[48] E. Kantola, T. Leinonen, S. Ranta, M. Tavast, and M. Guina, 'High-efficiency 20 W yellow VECSEL', *Optics Express*, vol. 22, no. 6, pp. 6372–6380, 2014.

[49] Y. Kaneda, M. Fallahi, J. Hader, J. V. Moloney, S. W. Koch, B. Kunert, and W. Stoltz, 'Continuous-wave single-frequency 295 nm laser source by a frequency-quadrupled optically pumped semiconductor laser', *Optics Letters*, vol. 34, no. 22, pp. 3511–3513, 2009.

[50] C. Hessenius, P. Y. Guinet, M. Lukowski, J. Moloney, and M. Fallahi, '589nm single-frequency VECSEL for sodium guidestar applications', *Proceedings of SPIE*, vol. 8242, p. 82420E, 2012.

[51] T. Leinonen, V.-M. Korpijärvi, A. Härkönen, and M. Guina, '7.4W yellow GaInNAs-based semiconductor disk laser', *Electronics Letters*, vol. 47, no. 20, pp. 1139 –1440, 2011.

[52] E. Gerster, I. Ecker, S. Lorch, C. Hahn, S. Menzel, and P. Unger, 'Orange-emitting frequency-doubled GaAsSb/GaAs semiconductor disk laser', *Journal of Applied Physics*, vol. 94, no. 12, pp. 7397–7401, 2003.

[53] J. Rautiainen, O. G. Okhotnikov, D. Eger, S. A. Zolotovskaya, K. A. Fedorova, and E. U. Rafailov, 'Intracavity generation of 610 nm light by periodically poled near-stoichiometric lithium tantalate', *Electronics Letters*, vol. 45, no. 3, pp. 177–179, 2009.

[54] J. Rautiainen, A. Härkönen, V.-M. Korpijärvi, P. Tuomisto, M. Guina, and O. G. Okhotnikov, '2.7 W tunable orange-red GaInNAs semiconductor disk laser', *Optics Express*, vol. 15, no. 26, pp. 18345–18350, 2007.

[55] A. Härkönen, J. Rautiainen, M. Guina, J. Konttinen, P. Tuomisto, L. Orsila, M. Pessa, and O. G. Okhotnikov, 'High power frequency doubled GaInNAs semiconductor disk laser emitting at 615 nm', *Optics Express*, vol. 15, no. 6, pp. 3224–3229, 2007.

[56] J. Rautiainen, A. Härkönen, P. Tuomisto, J. Konttinen, L. Orsila, M. Guina, and O. G. Okhotnikov, '1W at 617 nm generation by intracavity frequency conversion in semiconductor disk laser', *Electronics Letters*, vol. 43, no. 18, pp. 980–981, 2007.

[57] M. Butkus, J. Rautiainen, O. G. Okhotnikov, C. J. Hamilton, G. P. A. Malcolm, S. S. Mikhrin, I. L. Krestnikov, D. A. Livshits, and E. U. Rafailov, 'Quantum Dot Based Semiconductor Disk Lasers for 1–1.3µm', *IEEE Journal of Selected Topics in Quantum Electronics*, vol. 17, no. 6, pp. 1763–1771, 2011.

[58] A. Rantamäki, A. Sirbu, A. Mereuta, E. Kapon, and O. G. Okhotnikov, '3 W of 650 nm red emission by frequency doubling of wafer-fused semiconductor disk laser', *Optics Express*, vol. 18, no. 21, pp. 21645–21650, 2010.

[59] Coherent Inc., 'Optically pumped semiconductor lasers: power, precision, performance - based on semiconductor lasers'. Coherent Inc., Brochure, 2010.

[60] N. S. Sadick and R. Weiss, ‘The Utilization of a New Yellow Light Laser (578 nm) for the Treatment of Class I Red Telangiectasia of the Lower Extremities’, *Dermatologic Surgery*, vol. 28, no. 1, pp. 21–25, 2002.

[61] W. G. Telford, ‘Chapter 15 - Lasers in Flow Cytometry’, in *Methods in Cell Biology*, vol. 102, E. H. Zbigniew Darzynkiewicz, Ed. Academic Press, 2011, pp. 373–409.

[62] O. Casel, D. Woll, M. A. Tremont, H. Fuchs, R. Wallenstein, E. Gerster, P. Unger, M. Zorn, and M. Weyers, ‘Blue 489-nm picosecond pulses generated by intracavity frequency doubling in a passively mode-locked optically pumped semiconductor disk laser’, *Applied Physics B*, vol. 81, no. 4, pp. 443–446, 2005.

[63] R. Bek, H. Kahle, T. Schwarzbäck, M. Jetter, and P. Michler, ‘Mode-locked red-emitting semiconductor disk laser with sub-250 fs pulses’, *Applied Physics Letters*, vol. 103, no. 24, p. 242101, 2013.

[64] M. Herrera, D. González, R. García, M. Hopkinson, P. Navaretti, M. Gutiérrez, and H. Y. Liu, ‘Structural and optical properties of high In and N content GaInNAs quantum wells’, *Thin Solid Films*, vol. 483, no. 1–2, pp. 185–190, 2005.

[65] D. C. Houghton, M. Davies, and M. Dion, ‘Design criteria for structurally stable, highly strained multiple quantum well devices’, *Applied Physics Letters*, vol. 64, no. 4, pp. 505–507, 1994.

[66] A. Periasamy, P. Wodnicki, X. F. Wang, S. Kwon, G. W. Gordon, and B. Herman, ‘Time-resolved fluorescence lifetime imaging microscopy using a picosecond pulsed tunable dye laser system’, *Review of Scientific Instruments*, vol. 67, no. 10, pp. 3722–3731, 1996.

[67] T. Liu, J. Wang, G. I. Petrov, V. V. Yakovlev, and H. F. Zhang, ‘Photoacoustic generation by multiple picosecond pulse excitation’, *Medical Physics*, vol. 37, no. 4, pp. 1518–1521, 2010.

[68] T. Südmeyer, D. J. H. C. Maas, and U. Keller, ‘Mode-Locked Semiconductor Disk Lasers’, in *Semiconductor Disk Lasers*, O. G. Okhotnikov, Ed. Wiley-VCH Verlag GmbH & Co. KGaA, 2010, pp. 213–261.

[69] H. A. Macleod, *Thin-Film Optical Filters, Fourth Edition*. CRC Press, 2010.

[70] J. J. Coleman, ‘Strained layer quantum well heterostructure lasers’, in *Quantum Well Lasers*, P. S. Zory, Ed. San Diego: Academic Press, 1993, pp. 367–413.

[71] J. J. Coleman, ‘Strained-layer InGaAs quantum-well heterostructure lasers’, *IEEE Journal of Selected Topics in Quantum Electronics*, vol. 6, no. 6, pp. 1008–1013, 2000.

[72] D. J. Dunstan, ‘Strain and strain relaxation in semiconductors’, *Journal of Materials Science: Materials in Electronics*, vol. 8, no. 6, pp. 337–375, 1997.

[73] N. J. Ekins-Daukes, K. Kawaguchi, and J. Zhang, ‘Strain-Balanced Criteria for Multiple Quantum Well Structures and Its Signature in X-ray Rocking Curves’, *Crystal Growth & Design*, vol. 2, no. 4, pp. 287–292, 2002.

[74] S. W. Corzine, R. S. Geels, J. W. Scott, R.-H. Yan, and L. A. Coldren, ‘Design of Fabry-Perot surface-emitting lasers with a periodic gain structure’, *IEEE Journal of Quantum Electronics*, vol. 25, no. 6, pp. 1513–1524, 1989.

[75] Y. Morozov, T. Leinonen, M. Morozov, S. Ranta, M. Saarinen, V. Popov, and M. Pessa, ‘Effect of pump reflections in vertical external cavity surface-emitting lasers’, *New Journal of Physics*, vol. 10, no. 6, p. 063028, 2008.

[76] ‘The Essential Macleod (Version 8.13.97(ie))’. Thin Film Center Inc, 1995-2006.

[77] M. Henini, *Molecular Beam Epitaxy: From Research to Mass Production*, 1st ed. Elsevier Science and Technology, 2012.

[78] W. J. Alford, T. D. Raymond, and A. A. Allerman, ‘High power and good beam quality at 980 nm from a vertical external-cavity surface-emitting laser’, *Journal of the Optical Society of America B*, vol. 19, no. 4, pp. 663–666, 2002.

[79] M. Guina, A. Härkönen, V.-M. Korpijärvi, T. Leinonen, and S. Suomalainen, ‘Semiconductor Disk Lasers: Recent Advances in Generation of Yellow-Orange and Mid-IR Radiation’, *Advances in Optical Technologies*, vol. 2012, pp. 1–19, 2012.

[80] A. J. Maclean, R. B. Birch, P. W. Roth, A. J. Kemp, and D. Burns, ‘Limits on efficiency and power scaling in semiconductor disk lasers with diamond heatspreaders’, *Journal of the Optical Society of America B*, vol. 26, no. 12, pp. 2228–2236, 2009.

[81] A. Chernikov, J. Herrmann, M. Koch, B. Kunert, W. Stolz, S. Chatterjee, S. W. Koch, T.-L. Wang, Y. Kaneda, J. M. Yarborough, J. Hader, and J. V. Moloney, ‘Heat Management in High-Power Vertical-External-Cavity Surface-Emitting Lasers’, *IEEE Journal of Selected Topics in Quantum Electronics*, vol. 17, no. 6, pp. 1772–1778, 2011.

[82] T.-L. Wang, Y. Kaneda, J. M. Yarborough, J. Hader, J. V. Moloney, A. Chernikov, S. Chatterjee, S. W. Koch, B. Kunert, and W. Stolz, ‘High-Power Optically Pumped Semiconductor Laser at 1040 nm’, *IEEE Photonics Technology Letters*, vol. 22, no. 9, pp. 661–663, 2010.

[83] S. Lutgen, T. Albrecht, P. Brick, W. Reill, J. Luft, and W. Späth, ‘8-W high-efficiency continuous-wave semiconductor disk laser at 1000 nm’, *Applied Physics Letters*, vol. 82, no. 21, pp. 3620–3622, 2003.

[84] B. Rudin, A. Rutz, M. Hoffmann, D. J. H. C. Maas, A.-R. Bellancourt, E. Gini, T. Südmeyer, and U. Keller, ‘Highly efficient optically pumped vertical-emitting semiconductor laser with more than 20 W average output power in a fundamental transverse mode’, *Optics Letters*, vol. 33, no. 22, pp. 2719–2721, 2008.

[85] ‘WinLase (Version 2.1. Professional)’. Dr. C. Horvath & Dr. F. Loesel, 1995-2004.

[86] M. Schmid, S. Benchabane, F. Torabi-Goudarzi, R. Abram, A. I. Ferguson, and E. Riis, ‘Optical in-well pumping of a vertical-external-cavity surface-emitting laser’, *Applied Physics Letters*, vol. 84, no. 24, pp. 4860–4862, 2004.

[87] S.-S. Beyertt, M. Zorn, T. Kübler, H. Wenzel, M. Weyers, A. Giesen, G. Tränkle, and U. Brauch, ‘Optical in-well pumping of a semiconductor disk laser with high optical efficiency’, *IEEE Journal of Quantum Electronics*, vol. 41, no. 12, pp. 1439–1449, 2005.

[88] W. Zhang, T. Ackemann, S. McGinily, M. Schmid, E. Riis, and A. I. Ferguson, ‘Operation of an optical in-well-pumped vertical-external-cavity surface-emitting laser’, *Applied Optics*, vol. 45, no. 29, pp. 7729–7735, 2006.

[89] H. A. Haus, 'Mode-locking of lasers', *IEEE Journal of Selected Topics in Quantum Electronics*, vol. 6, no. 6, pp. 1173–1185, 2000.

[90] O. Svelto, *Principles of Lasers*, 4th ed. Springer Science & Business Media, 1998.

[91] U. Keller and A. C. Tropper, 'Passively modelocked surface-emitting semiconductor lasers', *Physics Reports*, vol. 429, no. 2, pp. 67–120, 2006.

[92] M. J. Lederer, V. Kolev, B. Luther-Davies, H. H. Tan, and C. Jagadish, 'Ion-implanted InGaAs single quantum well semiconductor saturable absorber mirrors for passive mode-locking', *Journal of Physics D: Applied Physics*, vol. 34, no. 16, pp. 2455–2464, 2001.

[93] N. G. Anderson, W. D. Laidig, R. M. Kolbas, and Y. C. Lo, 'Optical characterization of pseudomorphic $In_xGa_{1-x}As$–GaAs single-quantum-well heterostructures', *Journal of Applied Physics*, vol. 60, no. 7, pp. 2361–2367, 1986.

[94] Y. Q. Wei, S. M. Wang, X. D. Wang, Q. X. Zhao, M. Sadeghi, I. Tångring, and A. Larsson, 'Long-wavelength InGaAs/GaAs quantum-well lasers grown by molecular beam epitaxy', *Journal of Crystal Growth*, vol. 278, no. 1–4, pp. 747–750, 2005.

[95] D. Schlenker, T. Miyamoto, Z. Chen, F. Koyama, and K. Iga, 'Growth of highly strained GaInAs/GaAs quantum wells for 1.2 μm wavelength lasers', *Journal of Crystal Growth*, vol. 209, no. 1, pp. 27–36, 2000.

[96] P. W. Hutchinson and P. S. Dobson, 'Defect structure of degraded GaAlAs-GaAs double heterojunction lasers', *Philosophical Magazine*, vol. 32, no. 4, pp. 745–754, 1975.

[97] J. E. Ayers, *Heteroepitaxy of Semiconductors: Theory, Growth, and Characterization*, EBook. CRC Press, 2007.

[98] M. Grundmann, J. Christen, D. Bimberg, A. Fischer-Colbrie, and R. Hull, 'Misfit dislocations in pseudomorphic $In_{0.23}Ga_{0.77}As$/GaAs quantum wells: Influence on lifetime and diffusion of excess excitons', *Journal of Applied Physics*, vol. 66, no. 5, pp. 2214–2216, 1989.

[99] J. Jiménez, 'Laser diode reliability: crystal defects and degradation modes', *Comptes Rendus Physique*, vol. 4, no. 6, pp. 663–673, 2003.

[100] J. W. Matthews and A. E. Blakeslee, 'Defects in epitaxial multilayers: I. Misfit dislocations', *Journal of Crystal Growth*, vol. 27, pp. 118–125, 1974.

[101] B. Elman, E. S. Koteles, P. Melman, K. Ostreicher, and C. Sung, 'Low substrate temperature molecular beam epitaxial growth and the critical layer thickness of InGaAs grown on GaAs', *Journal of Applied Physics*, vol. 70, no. 5, pp. 2634–2640, 1991.

[102] S. M. Wang, T. G. Andersson, and M. J. Ekenstedt, 'Temperature-dependent transition from two-dimensional to three-dimensional growth in highly strained $In_xGa_{1-x}As$/GaAs ($0.36 \leq x \leq 1$) single quantum wells', *Applied Physics Letters*, vol. 61, no. 26, pp. 3139–3141, 1992.

[103] S. Guha, A. Madhukar, and K. C. Rajkumar, 'Onset of incoherency and defect introduction in the initial stages of molecular beam epitaxical growth of highly strained $In_xGa_{1-x}As$ on GaAs(100)', *Applied Physics Letters*, vol. 57, no. 20, pp. 2110–2112, 1990.

[104] A. G. Cullis, D. J. Norris, T. Walther, M. A. Migliorato, and M. Hopkinson, 'Stranski-Krastanow transition and epitaxial island growth', *Physical Review B*, vol. 66, no. 8, p. 081305, 2002.

[105] C. Heyn, 'Critical coverage for strain-induced formation of InAs quantum dots', *Physical Review B*, vol. 64, no. 16, p. 165306, 2001.

[106] M. J. Ekenstedt, S. M. Wang, and T. G. Andersson, 'Temperature-dependent critical layer thickness for $In_{0.36}Ga_{0.64}As$/GaAs single quantum wells', *Applied Physics Letters*, vol. 58, no. 8, pp. 854–855, 1991.

[107] C. W. Snyder, B. G. Orr, D. Kessler, and L. M. Sander, 'Effect of strain on surface morphology in highly strained InGaAs films', *Physical Review Letters*, vol. 66, no. 23, pp. 3032–3035, 1991.

[108] M. J. Ekenstedt, T. G. Andersson, and S. M. Wang, 'Temperature-dependent relaxation and growth phenomena in strained In(x)Ga(1-x)As layers grown on GaAs', *Physical Review B*, vol. 48, no. 8, pp. 5289–5299, 1993.

[109] A. Riposan, J. Mirecki Millunchick, and C. Pearson, 'Critical film thickness dependence on As flux in In0.27Ga0.73As/GaAs(001) films', *Applied Physics Letters*, vol. 90, no. 9, p. 091902, 2007.

[110] A. Ohtake and M. Ozeki, 'Growth mode of In(x)Ga(1-x)As (0<~x<~0.5) on GaAs(001) under As-deficient conditions', *Physical Review B*, vol. 65, no. 15, p. 155318, 2002.

[111] N. Grandjean, J. Massies, M. Leroux, J. Leymarie, A. Vasson, and A. M. Vasson, 'Improved GaInAs/GaAs heterostructures by high growth rate molecular beam epitaxy', *Applied Physics Letters*, vol. 64, no. 20, pp. 2664–2666, 1994.

[112] J. Massies, N. Grandjean, and V. H. Etgens, 'Surfactant mediated epitaxial growth of $In_xGa_{1-x}As$ on GaAs (001)', *Applied Physics Letters*, vol. 61, no. 1, pp. 99–101, 1992.

[113] M. R. Pillai, S.-S. Kim, S. T. Ho, and S. A. Barnett, 'Growth of $In_xGa_{1-x}As$/GaAs heterostructures using Bi as a surfactant', *Journal of Vacuum Science & Technology B*, vol. 18, no. 3, pp. 1232–1236, 2000.

[114] J. C. Harmand, L. H. Li, G. Patriarche, and L. Travers, 'GaInAs/GaAs quantum-well growth assisted by Sb surfactant: Toward 1.3 μm emission', *Applied Physics Letters*, vol. 84, no. 20, pp. 3981–3983, 2004.

[115] T. J. Gosling, R. Bullough, S. C. Jain, and J. R. Willis, 'Misfit dislocation distributions in capped (buried) strained semiconductor layers', *Journal of Applied Physics*, vol. 73, no. 12, pp. 8267–8278, 1993.

[116] M. E. Twigg, 'Line tension of extended double kinks in thin films', *Journal of Applied Physics*, vol. 68, no. 10, pp. 5109–5114, 1990.

[117] X. Liu, A. Prasad, J. Nishio, E. R. Weber, Z. Liliental-Weber, and W. Walukiewicz, 'Native point defects in low-temperature-grown GaAs', *Applied Physics Letters*, vol. 67, no. 2, pp. 279–281, 1995.

[118] K. S. Kim, J. R. Yoo, S. M. Lee, S. J. Lim, J. Y. Kim, J. H. Lee, S. H. Cho, T. Kim, and Y. J. Park, 'Highly efficient InGaAs QW vertical external cavity surface emitting lasers emitting at 1060 nm', *Journal of Crystal Growth*, vol. 287, no. 2, pp. 629–632, 2006.

[119] W. E. Hoke, P. J. Lemonias, and A. Torabi, 'Reduction of oxygen contamination in InGaP and AlGaInP films grown by solid source molecular beam epitaxy', *Journal of Vacuum Science & Technology B*, vol. 16, no. 6, pp. 3041–3047, 1998.

[120] W. E. Hoke and P. J. Lemonias, 'Practical aspects of solid source molecular beam epitaxial growth of phosphorus-containing films', *Journal of Vacuum Science & Technology B*, vol. 17, no. 5, pp. 2009–2014, 1999.

[121] N. Xiang, A. Tukiainen, J. Dekker, J. Likonen, and M. Pessa, 'Oxygen-related deep level defects in solid-source MBE grown GaInP', *Journal of Crystal Growth*, vol. 227–228, pp. 244–248, 2001.

[122] T. Leinonen, 'The design and fabrication of lasing semiconductor nanostructures employing vertical-cavity geometry', Doctoral dissertation, Tampere University of Technology, Tampere, Finland, 2007.

[123] U. Pietsch, V. Holy, and T. Baumbach, *High-Resolution X-Ray Scattering: From Thin Films to Lateral Nanostructures*. Springer Science & Business Media, 2004.

[124] T. Dieing and B. F. Usher, 'Wafer curvature in molecular beam epitaxy grown heterostructures', *Physical Review B*, vol. 67, no. 5, p. 054108, 2003.

[125] P. L. Gourley, R. M. Biefeld, and L. R. Dawson, 'Elimination of dark line defects in lattice-mismatched epilayers through use of strained-layer superlattices', *Applied Physics Letters*, vol. 47, no. 5, pp. 482–484, 1985.

[126] Y. Ohizumi, T. Tsuruoka, and S. Ushioda, 'Formation of misfit dislocations in GaAs/InGaAs multiquantum wells observed by photoluminescence microscopy', *Journal of Applied Physics*, vol. 92, no. 5, pp. 2385–2390, 2002.

[127] P. L. Gourley, I. J. Fritz, and L. R. Dawson, 'Controversy of critical layer thickness for InGaAs/GaAs strained-layer epitaxy', *Applied Physics Letters*, vol. 52, no. 5, pp. 377–379, 1988.

[128] D. H. Rich, T. George, W. T. Pike, J. Maserjian, F. J. Grunthaner, and A. Larsson, 'Cathodoluminescence and transmission electron microscopy study of dark line defects in thick $In_{0.2}Ga_{0.8}As$/GaAs multiple quantum wells', *Journal of Applied Physics*, vol. 72, no. 12, pp. 5834–5839, 1992.

[129] S. Ranta, T. Leinonen, M. Tavast, T. V. Hakkarainen, I. Suominen, and M. Guina, 'Strain compensation of InGaAs/GaAs SDL gain mirrors grown by molecular beam epitaxy', *Proceedings of SPIE*, vol. 8242, p. 824211, 2012.

[130] J. Zou, D. J. H. Cockayne, and B. F. Usher, 'Temperature-dependent generation of misfit dislocations in $In_{0.2}Ga_{0.8}As$/GaAs single heterostructures', *Applied Physics Letters*, vol. 68, no. 5, pp. 673–674, 1996.

[131] X. W. Liu, A. A. Hopgood, B. F. Usher, H. Wang, and N. S. J. Braithwaite, 'Formation of misfit dislocations in strained-layer $GaAs/In_xGa_{1-x}As/GaAs$ heterostructures during postfabrication thermal processing', *Journal of Applied Physics*, vol. 94, no. 12, pp. 7496–7501, 2003.

[132] L. Toikkanen, A. Tukiainen, M. Dumitrescu, S. Viitala, V. Rimpiläinen, I. Hirvonen, and M. Pessa, 'Phosphide based Molecular Beam Epitaxy for High Power Short-Wavelength Diode Lasers', *Physica Scripta*, vol. 2004, no. T114, pp. 161–163, 2004.

[133] D. Vignaud and F. Mollot, 'Conduction band offset in the $Al(x)Ga(y)In(1-x-y)P/Ga_{0.52}In_{0.48}P$ system as studied by luminescence spectroscopy', *Journal of Applied Physics*, vol. 93, no. 1, pp. 384–389, 2003.

[134] I. Vurgaftman, J. R. Meyer, and L. R. Ram-Mohan, 'Band parameters for III–V compound semiconductors and their alloys', *Journal of Applied Physics*, vol. 89, no. 11, pp. 5815–5875, 2001.

[135] M. A. Afromowitz, 'Refractive index of $Ga_{1-x}Al_xAs$', *Solid State Communications*, vol. 15, no. 1, pp. 59–63, 1974.

[136] M. A. Afromowitz, 'Thermal conductivity of $Ga_{1-x}Al_xAs$ alloys', *Journal of Applied Physics*, vol. 44, no. 3, pp. 1292–1294, 1973.

[137] A. J. Kemp, G. J. Valentine, J.-M. Hopkins, J. E. Hastie, S. A. Smith, S. Calvez, M. D. Dawson, and D. Burns, 'Thermal management in vertical-external-cavity surface-emitting lasers: finite-element analysis of a heatspreader approach', *IEEE Journal of Quantum Electronics*, vol. 41, no. 2, pp. 148–155, 2005.

[138] Z. L. Liau, 'Semiconductor wafer bonding via liquid capillarity', *Applied Physics Letters*, vol. 77, no. 5, pp. 651–653, 2000.

[139] L. Fan, C. Hessenius, M. Fallahi, J. Hader, H. Li, J. V. Moloney, W. Stolz, S. W. Koch, J. T. Murray, and R. Bedford, 'Highly strained InGaAs/GaAs multiwatt vertical-external-cavity surface-emitting laser emitting around 1170 nm', *Applied Physics Letters*, vol. 91, no. 13, p. 131114, 2007.

[140] C. Borgentun, C. Hessenius, J. Bengtsson, M. Fallahi, and A. Larsson, 'Widely Tunable High-Power Semiconductor Disk Laser With Nonresonant AR-Assisted Gain Element on Diamond Heat Spreader', *IEEE Photonics Journal*, vol. 3, no. 5, pp. 946–953, 2011.

[141] R. G. Bedford, M. Kolesik, J. L. A. Chilla, M. K. Reed, T. R. Nelson, and J. V. Moloney, 'Power-limiting mechanisms in VECSELs', *Proceedings of SPIE*, vol. 5814, pp. 199–208, 2005.

[142] J. W. Nicholson and W. Rudolph, 'Noise sensitivity and accuracy of femtosecond pulse retrieval by phase and intensity from correlation and spectrum only (PICASO)', *Journal of the Optical Society of America B*, vol. 19, no. 2, pp. 330–339, 2002.

P1

Publication 1

S. Ranta, T. Hakkarainen, M. Tavast, J. Lindfors, T. Leinonen, and M. Guina, "Strain compensated 1120 nm GaInAs/GaAs vertical external-cavity surface-emitting laser grown by molecular beam epitaxy," *Journal of Crystal Growth*, vol. 335, no. 1, pp. 4–9, 2011.
http://www.sciencedirect.com/science/article/pii/S002202481100738X

© 2011 Elsevier Limited. Reproduced with permission.

Strain compensated 1120 nm GaInAs/GaAs vertical external-cavity surface-emitting laser grown by molecular beam epitaxy

Sanna Ranta[a], Teemu Hakkarainen[a], Miki Tavast[a], Jukka Lindfors[a], Tomi Leinonen[a], and Mircea Guina[a]

[a]Optoelectronics Research Centre, Tampere University of Technology,

P.O. Box 692, FIN-33101 Tampere, Finland,

sanna.ranta@tut.fi, teemu.hakkarainen@tut.fi, miki.tavast@tut.fi, jukka.lindfors@tut.fi, tomi.leinonen@tut.fi, mircea.guina@tut.fi

Corresponding author: Sanna Ranta, sanna.ranta@tut.fi, TEL +358 40 198 1070

FAX +358 3 3115 3400

Abstract

We report on the development of high quality, strain compensated gain mirror for 1120 nm vertical external-cavity surface-emitting lasers (VECSELs). The gain mirror was grown by molecular beam epitaxy and comprised a total of six $Ga_{0.69}In_{0.31}As$ quantum wells. The effect of the strain compensation has been assessed by measuring the curvature of the wafer and by mapping the photoluminescence to identify the non-emissive dark areas. We demonstrate that ~91 % strain compensation with $GaAs_{0.85}P_{0.15}$ is sufficient to remove the dark lines corresponding to areas with structural defects in the gain mirror structure. Rapid thermal annealing studies revealed that the strain compensation is efficient in preventing the appearance of dark lines even for samples that were annealed at temperatures as high as 700 °C for a considerable time. The strain compensated gain mirror was used to demonstrate a VECSEL emitting at 1120 nm.

Keywords

A3. Molecular beam epitaxy, B2. Semiconducting III-V materials, B3. Vertical external cavity surface emitting lasers, B3. Semiconductor disk lasers, B3. Strain compensation

Main text:

1. Introduction

Optically-pumped vertical external-cavity surface-emitting lasers (OP-VECSELs) have shown outstanding lasing characteristics for a broad wavelength range, extending from UV to mid-IR [1, 2]. The VECSEL technology enables high brightness levels unattainable by using other semiconductor lasers. At the same time, the VECSEL concept takes full benefit of the wavelength versatility provided by semiconductor gain media. Furthermore, the external cavity enables manipulation of spectral and temporal laser characteristics, such as frequency conversion [3], wavelength tuning [4], linewidth narrowing [5], and ultrashort pulse generation via mode locking [6].

The most mature VECSEL technology is based on GaAs/AlGaAs distributed Bragg reflectors (DBR) and GaInAs quantum wells (QWs) covering a spectral range around 1040–1060 nm. At wavelengths shorter than 960 nm the GaInAs QWs start to suffer from poor carrier confinement and above 1100 nm, the QWs become too highly strained [7]. There is indeed a strong interest to expand the wavelength range covered by GaAs-based VECSELs towards longer wavelengths. In particular, VECSELs emitting within 1120–1200 nm are very attractive for generating frequency-doubled yellow-orange radiation required for optical clocks and other high impact applications in medicine, high-precision spectroscopy, and astronomy. Emission within this wavelength range can be achieved by using dilute nitride (GaInNAs/GaAs) QWs [8] or InAs/GaAs quantum dots (QDs) [9]. Although these material systems can alleviate the strain limitation associated with GaInAs/GaAs QWs, they also have certain pitfalls. In particular, reducing the amount of N-related defects in dilute-nitrides requires extensive optimization of the growth, while the QD gain structures exhibit lower modal gain than QW structures and offer less flexibility in designing the gain region; as a consequence the output powers available from QD VECSELs is significantly lower than the levels provided by QW-based VECSELs. Alternatively, the emission wavelengths of GaInAs QWs can be extended above the 1100 nm by careful optimization of the growth conditions to avoid formation of structural defects and/or transition to 3D growth mode. By lowering the temperature during the growth of GaInAs/GaAs QWs and by using a high V/III ratio

several groups have demonstrated high quality laser diodes with emission around 1.2 µm, using both MOVPE [10, 11] and MBE [12]. Compared to laser diodes, VECSELs have much thicker active regions and operate with higher intracavity power densities and under more severe thermal load. Therefore, the exploitation of highly strained GaInAs/GaAs QWs for achieving efficient emission from VECSELs is more difficult and requires the deployment of strain compensation [13]. Strain compensated GaInAs/GaAs QWs have enabled VECSELs operation at wavelengths up to 1197 nm [14]. Nevertheless the previous reports have mainly focused on device operation rather than providing fabrication details concerning the strain compensation and its impact on reducing the structural defects linked to device lifetime.

In this paper we report on the development of strain compensated GaInAs/GaAs VECSEL gain mirror for operation at 1120 nm. In particular, we take a first step towards studying the link between strain compensation and formation of structural defects. The effectiveness of the strain compensation is quantitatively assessed by measuring the wafer curvature and by mapping the photoluminescence over the wafer to identify the non-emissive areas, in this case dark lines. We also compare the evolution of the dark lines after rapid thermal annealing of strain compensated and uncompensated structures. The presence of dark lines results in reduced efficiency and ultimately reduced device life-time. In terms of applications, the development of 1120 nm VECSELs is motivated by the need for frequency-stable high power lasers emitting at around 560 nm which are required in high precision optical clocks; this wavelength range can be reached via intracavity conversion of 1120 nm VECSELs.

2. Description of the structures studied

The 1120 nm VECSEL gain mirror was developed in three phases. First, the growth temperature of the GaInAs QWs was optimized by investigating photoluminescence measured from a set of *single-QW calibration samples*. These samples comprised one QW embedded within GaAs barriers that were surrounded by carrier-confining AlAs layers. Second, the material quality of active region was examined with x-ray diffraction methods. For this study we used *active region samples* that contained only semiconductor layers forming the active region, i.e. a VECSEL gain mirror without the DBR. The purpose of this phase was to optimize the active

region growth parameters prior to full gain mirror structure growth, and to analyze how the compressive strain introduced by the multiple QWs affects the crystal quality of the active region and whether strain compensation is able to improve its quality. Third, for a more thorough study of the strain effects and for demonstrating VECSEL operation, complete semiconductor structures, also called *gain mirrors*, for an 1120 nm VECSEL were fabricated and characterized. The gain mirrors were grown in flip-chip arrangement [15, 16], i.e. the DBR was grown on top of the gain region and the structure was mounted top-side down after which the substrate was removed to leave the active region facing the cavity side of the laser. This design is preferred for volume manufacturing of VECSEL gain mirrors and for alleviating the etalon effect associated with the intra-cavity heat spreader approach [17, 18]. Photoluminescence mapping was used to reveal the crystal quality of the gain mirrors.

The gain mirror design is shown in detail in Fig. 1(a). The DBR consisted of 23 pairs of AlAs/GaAs layers pairs that lead to a simulated reflectance of 99.89 % at the central wavelength of 1115 nm, as shown in Fig. 1(b). The number of DBR layer pairs was chosen as a compromise to minimize the compressive strain, and thermal impedance associated with the mirror, while still maintaining a high reflectance. The total thickness of the DBR was 4.1 μm.

The active region comprised a total of six 7-nm thick $Ga_{0.69}$ $In_{0.31}As$ QWs embedded within pump-absorbing GaAs barriers. The QWs were designed to exhibit a room temperature peak gain/photoluminescence at ~1105 nm and thus to take into account the red shift during optical pumping. The amount of indium needed to reach the desired QW emission wavelength was first approximated with the 8-band *k.p*-model and then experimentally fine-tuned using photoluminescence calibration samples. To achieve emission at 1120 nm, while preserving a good optical quality of the semiconductor crystal, we used GaAsP strain compensation layers between the QWs; the location of the strain compensation layers is shown in Fig. 1(a). The QWs were evenly placed within the active region and were separated by an optical distance of half-wavelength. The air-semiconductor interface was located at an optical distance of one wavelength apart from the topmost QW (see Fig. 1(a)). Here the optical distances are defined for a wavelength of 1115 nm. We also grew samples with two

closely spaced QWs; each QW-pair located at an optical distance of half-wavelength apart from each other. These QW-samples, however, exhibited poor crystalline quality (possibly due to relaxation of the thick strain compensation layers that had to be utilized to maintain the net strain near zero). The gain mirror employed an antiresonant design in order to eliminate the strong cavity enhancement associated with a cavity resonance that limits the wavelength tuning. A 50-nm thick $Ga_{0.51}In_{0.49}P$ layer was used as a window layer; it also served as an etch stop layer for the substrate removal process.

For the strain compensation, the *strain-thickness* product of a QW was balanced with the opposite sign *strain-thickness* product of a GaAsP layer. The amount of compensation as well as the composition and thickness of the GaAsP layers were chosen such that the tensile strain of individual GaAsP layers would be below the relaxation limit and the net strain of the structure would be near zero. Fig. 2 shows an estimation of the critical layer thickness for GaAsP as a function of P composition using Matthews and Blakeslee approximation [7]. The GaAsP layer thickness required to fully compensate one 7 nm $Ga_{0.69}In_{0.31}As$ QW is indicated with a dotted line in Fig. 2. One can observe that the required GaAsP layer thickness to achieve full compensation for a reasonable P composition is larger than the relaxation limit of the GaAsP layer. In order to preserve high crystalline quality, the net strain of the gain region was left slightly compressive. We chose to use a 27-nm thick $GaAs_{0.85}P_{0.15}$ layer, exhibiting ~0.54 % misfit tensile strain, for compensating ~91% of the compressive strain associated with a single 7-nm thick $Ga_{0.69}In_{0.31}As$ QW. Although the critical thickness of $GaAs_{0.85}P_{0.15}$ is according to Matthews and Blakeslee around 21 nm, we succeeded to grow photoluminescence calibration samples containing two QWs and two 27 nm thick $GaAs_{0.85}P_{0.15}$ layers without any dark line defects. Increasing the P content of the 27-nm thick GaAsP layers by 1 % (to 16 %) resulted in the occurrence of few small dark lines. Based on these observations we can infer that the 27-nm thick $GaAs_{0.85}P_{0.15}$ layers are grown near their stability limit above which it is energetically favourable for the layer to partially relax. Simulations revealed that an active region structure comprising six 27-nm thick $GaAs_{0.85}P_{0.15}$ and six 7-nm thick $Ga_{0.69}In_{0.31}As$ layers is able to absorb ~58 % of an incident 808 nm pump light (the wavelength used to pump the gain mirror for VECSEL operation).

The semiconductor structures were grown by solid-source molecular beam epitaxy (MBE) on GaAs (100) substrates. The MBE-reactor was equipped with valved As and P cracker cells. The group III fluxes were controlled by mechanical shutters; group V fluxes only by the cracker's needle valve. A 30-second-long growth interruption was utilized to adjust the As and P fluxes before and after the growth of $GaAs_{0.85}P_{0.15}$ strain compensation and $Ga_{0.51}In_{0.49}P$ window layers. The As and P fluxes necessary to produce $GaAs_{0.85}P_{0.15}$ were calibrated with 2-period $GaAs_xP_{1-x}$ /GaAs superlattice samples prior to the active region and gain mirror sample growths. An x-ray diffraction scan was performed for the superlattice samples from which the incorporation of P could be estimated by fitting a simulation model to the x-ray diffraction data. The GaAs barriers and $GaAs_{0.85}P_{0.15}$ strain compensation layers were grown at 580–590 °C; the temperature was measured with an Ircon Modline infrared thermometer. The optimal QW growth temperature is about 500 °C, according to the single-QW photoluminescence study (presented in section 3). The $Ga_{0.51}In_{0.49}P$ window layer was grown in typical growth conditions: at 500 °C and in phosphorus overpressure. In order to change the sample temperature, we used a growth interruption step of 7 min on both sides of each QW. A 4-minute-long interruption was applied before and after the growth of the $Ga_{0.51}In_{0.49}P$ window layer. A thin low-temperature-grown GaAs layer was used to protect the QW interfaces and $Ga_{0.51}In_{0.49}P$ window layer surface against the interruptions. The V/III beam equivalent pressure (BEP) ratio was 25 for the $Ga_{0.69}In_{0.31}As$ QWs, 27 for $GaAs_{0.85}P_{0.15}$ strain compensation layers and 30 for the GaAs barriers. The DBR was grown with a BEP ratio of 50 for AlAs and 30 for GaAs. The growth rate for the QW, GaAs barriers and $GaAs_{0.85}P_{0.15}$ strain compensation layers was around 1 μm/h, while the AlAs and $Ga_{0.51}In_{0.49}P$ window layers were grown at 0.83 μm/h and 1.25 μm/h rates, respectively.

3. Results and discussions

In the first part of the study we optimized the growth temperature of a single GaInAs QW. The photoluminescence intensity of the single-QW calibration samples for different growth temperatures is shown in Fig. 3. The growth temperatures were measured with a thermocouple and whenever possible with a pyrometer; we should point out here that the pyrometer could not measure reliably temperatures below 500 °C.

The highest photoluminescence intensity was obtained for a growth temperature of 500 °C, which corresponds to a 545 °C thermocouple reading. From QWs grown at 565 °C as well as 370 °C (thermocouple readings) we could not observe any photoluminescence and therefore the curves corresponding to these growth temperatures are not included in Fig. 3. At 565 °C the growth mode of the highly strained GaInAs layers most probably evolved from 2D growth to island-like 3D growth. On the other hand, the low growth temperature of 370 °C likely caused a high amount of nonradiative centres within the structure. Both the 3D growth mode and the formation of nonradiative centres deteriorate the material quality of the QWs. The optimal growth temperature of GaInAs is therefore a trade-off: the growth temperature should be as high as possible to prevent the occurrence of nonradiative centres but still low enough to obtain 2D growth.

As shown in Fig. 3, the photoluminescence wavelength in this study was 20–25 nm longer than the target wavelength for the QW peak gain. The wavelength was adjusted to 1105 nm for the active region and gain mirror samples by introducing slightly less indium in the QWs. It was assumed that the QWs with lower In content would exhibit the same growth temperature behaviour as the QWs used in the growth temperature optimization study. Consequently, the GaInAs QWs of the active region and gain mirror samples were grown at 545 °C.

In the second part of the study, we analyzed the effect of strain compensation on the crystal quality of the active region by comparing two active region samples, one with and one without GaAsP strain compensation layers. The structural quality of these samples was analyzed around the (004) and (113) reciprocal space points for both [011] and [01-1] directions with an x-ray diffractometer using Cu k-alpha radiation. The (113) reciprocal space mapping was performed in grazing exit configuration. Fig. 4 reveals the diffracted intensity distribution of the active region samples around (113) point of the reciprocal space for the [01-1] direction. The narrow peaks and Pendellösung features shown in Fig. 4 indicate good crystalline quality. Furthermore, a relaxation analysis based on the (113) reciprocal space maps indicated 0 ± 0.5 % relaxation for the QWs and GaAsP strain compensation layers in both of the samples. We would like to point out, however, that even a 0.5 % strain relaxation would result in multiple dislocations over the area of a 100-μm-diameter

pump spot. Therefore we needed to examine the possible existence of strain related defects by other means. This defect study was performed for the active region as well as gain mirror samples as described later on in the paper. Since the (113) maps revealed that the GaAsP layers exhibit zero strain relaxation within the accuracy of the reciprocal space measurement, we could determine the actual P content of the GaAsP layers from the (004) ω-2θ diffraction patterns measured for both the strain compensated active region and gain mirror samples. By simulating the measured diffraction patterns we estimated that the phosphorus percentage within the GaAsP strain compensation layers was ~11 % for the active region and ~15 % for the gain mirror, whereas the P composition target was 15 % for both of the samples. The presence of two group V materials, As and P, complicated the growth of GaAsP since they are both supplied in excess to the growth chamber. The difficulty in maintaining a stabile As/P ratio over different growth runs explains the difference in the P content of GaAsP layers used for the structures studied. The $GaAs_{0.89}P_{0.11}$ layers resulted in a net strain compensation of about 68 %.

To estimate the residual strain remaining after the epitaxial growth, we measured the strain induced bending of the wafers and fit the measurements with a theoretical model employed by Dieing and Usher [19].The measurements were done with 2 mm steps over a range of 32 mm in both [011] and [01-1] directions. A GaAs (100) substrate was used as a reference. The measurements for the wafer curvatures are presented in Table 1. These results show that the strain compensated active region is slightly compressively strained as was targeted. Additionally the uncompensated active region has half the radius of curvature of the strain compensated active region. The measurements are in fairly good agreement with the calculations. The bending of the substrate, which was not included in the calculations, could explain the deviation observed between the values for the experimental and theoretical curvature.

In the third and final part of our study we examined the lateral crystal quality of the gain mirror by photoluminescence mapping to reveal irregularities in the luminescence intensity. The photoluminescence map was measured by illuminating a 1.2×0.9 mm^2 area of the wafer at a time with 808 nm radiation. The output from this area was imaged with a CCD camera having an 850 nm long-wave pass filter in front. Fig. 5 shows

typical photoluminescence maps recorded from an uncompensated and a ~91 % strain compensated gain mirror structures. The strain compensated gain mirror has a very low density of any irregularities in comparison to the uncompensated gain mirror that contains clearly visible dark lines. We also performed photoluminescence mapping for the 68 % strain compensated and uncompensated active region samples. We didn't, however, observe any differences between the maps; both of the samples had a high crystalline quality. We believe that the cumulative strain arising from the mismatch between the AlAs and GaAs layers forming the DBR together with the strain added by an active region induces the dark line defects in the gain mirror structure that is not strain compensated.

The evolution of the dark lines under thermal stress was examined by performing a rapid thermal annealing (RTA) of the reference and the strain compensated gain mirrors. For this study the gain mirrors were cut into 3 × 3 mm^2 samples and were capped with 5 × 5 mm^2 pieces of GaAs to prevent arsenic outdiffusion and to ensure that the surface of the samples stays as intact as possible. The samples were annealed for 1 min, 2 min, 4 min and 8 min at 700 °C, 750 °C and 800 °C in a RTA station. Every sample was photoluminescence mapped before and after the RTA. Apparently, the ~91 % strain compensated gain mirror was more resistant to the heat stress than the uncompensated gain mirror. A sufficiently high and long RTA treatment caused, however, dark line defects to appear in the ~91 % strain compensated gain material as well. The 700 °C RTA treatment did not affect the strain compensated structures even after 8 min annealing. Our observations regarding RTA are in good agreement with previous reports revealing that post-growth thermal processing leads to appearance of dark lines in GaAs/GaInAs/GaAs structures annealed for 10 min at 770 °C [20]. It has also been shown that the dark line defects that appear during growth cannot be eliminated by post-growth thermal processing [21] and hence the presence of dark lines is a major concern regarding the device lifetime.

The performance of the strain compensated gain mirror was tested in a V-shaped VECSEL cavity, schematically presented in Fig. 6. The wafer was cut into 1.5 × 1.5 mm^2 chips. Then the chips were top-side down attached to a silicon-diamond composite heat spreader and the substrate was removed by wet etching with NH_4OH–H_2O solution. An antireflection coating was applied on top of the surface exposed after substrate

removal, i.e. the $Ga_{0.51}In_{0.49}P$ window layer. Finally the composite diamond was attached to a copper mount that was cooled by water during the laser measurement; the water temperature was 16 °C.

The laser mode size on the gain mirror was simulated to be 100 µm in diameter. The pump light was focused to a 128 µm diameter spot on the gain mirror. The VECSEL emitted a power of 525 mW when pumped with 4 W of 808 nm radiation. The emission spectrum was quite broad and centred at 1120 nm. The output beam had a symmetric Gaussian profile for the entire pump power range used in the experiment. We did not observe any sign of degradation of the output characteristics during prolonged laboratory operation. The relatively low value of the differential slope, of about 22 %, is most likely caused by incomplete absorption of the pump power by the GaAs barrier layers. In addition, the low thermal conductivity of the silicon-diamond composite heat spreader ($4.9\ W \cdot cm^{-1} \cdot K^{-1}$ [22]) most probably limited the output power of the laser. More recent experiments indicate improved laser operation with a 10 QW 1120 nm GaInAs/GaAs gain mirror bonded to a chemical vapour deposited (CVD) diamond heat spreader (thermal conductivity $20\ W \cdot cm^{-1} \cdot K^{-1}$ [23]); a total of 3 W has been obtained with a 350 µm pump spot diameter. We believe that the laser performance can be further improved by optimizing the laser cavity and the fabrication process. A more comprehensive study of the CVD diamond heat spreader VECSEL and its characteristics will be reported elsewhere.

4. Conclusions

A high quality GaInAs VECSEL gain mirror was grown and characterized. The strain arising from $Ga_{0.69}In_{0.31}As$ QWs was ~91 % compensated with $GaAs_{0.85}P_{0.15}$ layers. The effect of the strain compensation has been assessed by measuring the curvature of the wafers and by mapping the photoluminescence to identify the non-emissive dark areas. We demonstrated that ~91 % strain compensation was sufficient to remove the dark lines corresponding to areas with structural defects and prevented appearance of dark line even for gain mirrors that had been annealed at temperatures as high as 700 °C. It was shown that only ~68 % compensation was needed to grow a high quality active region. However, for a full gain mirror the compensation might not be enough due to the compressive strain added by the DBR. A VECSEL with a gain mirror comprising 6 QWs produced a total of 525 mW at 1120 nm for 4 W of pump power. The output power of the device can be further

increased by adding more QWs in the active region to enhance the material gain. Furthermore, diamond could be used as a heat spreader since it has higher thermal conductivity than the composite diamond used in the reported experiments. Further work will focus on power scaling, intra-cavity frequency conversion to generate high-brightness 560 nm radiation, and wavelength extension of the strain compensated gain mirrors towards 1200 nm.

Acknowledgements

This study was financially supported by Areté Associates and the Academy of Finland (within project #128364). The main author would like to acknowledge the graduate school of the Tampere University of Technology, Emil Aaltonen Foundation, and Jenny and Antti Wihuri Foundation for financial support. The authors would like to acknowledge Dr. Antti Laakso for the GaInAs QW energy band calculations, Dr. Antti Härkönen for assisting in the photoluminescence mapping studies and for many useful discussions, Mr. Ilpo Suominen for helping with the VECSEL gain mirror processing, and Mr. Jari Nikkinen for evaporating the antireflection coatings for the gain mirror.

References

[1] S. Calvez, J.E. Hastie, M. Guina, O.G. Okhotnikov, M. D. Dawson, Semiconductor disk lasers for the generation of visible and ultraviolet radiation, Laser & Photon. Rev. 3 (2009) 407–434

[2] N. Schulz, J.-M. Hopkins, M. Rattunde, D. Burns, J. Wagner, High-brightness long-wavelength semiconductor disk lasers, Laser & Photon. Rev. 2 (2008) 160–181

[3] J. Chilla, S. Butterworth, A. Zeitschel, J. Charles, A Caprara, M. Reed, L. Spineli, High-power optically pumped semiconductor lasers, Proc. SPIE 5332 (2004) 143–150

[4] J. Paajaste, S. Suomalainen, R. Koskinen, A. Härkönen, M. Guina, M. Pessa, High-power and broadly tunable GaSb-based optically pumped VECSELs emitting near 2 µm, J. of Cryst. Growth 311 (2009) 1917–1919

[5] A. Laurain, M. Myara, G. Beaudoin, I. Sagnes, A. Garnache, Multiwatt-power highly-coherent compact single-frequency tunable Vertical-External-Cavity-Surface-Emitting–Semiconductor-Laser, Opt. Express 18 (2010) 14627–14636

[6] S. Hoogland, S. Dhanjal, A.C. Tropper, J.S. Roberts, R. Haring, R. Paschotta, F. Morier-Genoud, U. Keller, Passively mode-locked diode-pumped surface-emitting semiconductor laser, IEEE Photon. Technol. Lett. 12 (2000) 1135–1137

[7] J.W. Matthews, A.E. Blakeslee, Defects in epitaxial multilayers: I. Misfit dislocations, J. Cryst. Growth 27 (1974) 118–125

[8] M. Guina, T. Leinonen, A. Härkönen, M. Pessa, High-power disk lasers based on dilute nitride heterostructures, New J. Phys. 11 (2009) 125019

[9] A. Strittmatter, T.D. Germann, J. Pohl, U.W. Pohl, D. Bimberg, J. Rautiainen, M. Guina, O.G. Okhotnikov, 1040 nm vertical external cavity surface emitting laser based on InGaAs quantum dots grown in the Stranski-Krastanow regime, Electron. Lett. 44 (2008) 290–291

[10] D. Schlenker, T. Miyamoto, Z. Chen, F. Koyama, K. Iga, Growth of highly strained GaInAs/GaAs quantum wells for 1.2 µm wavelength lasers, J. Cryst. Growth 209 (2000) 27–36

[11] Y.K. Su, W.C. Chen, C.T. Wan, H.C. Yu, R.W. Chuang, M.C. Tsai, K.Y. Cheng, C. Hu, Seth Tsau, Optimization of the highly strained InGaAs/GaAs quantum well lasers grown by MOVPE, J. Cryst. Growth 310 (2008) 3615–3620

[12] G. Adolfsson, S.M. Wang, M. Sadeghi, A. Larsson, High-performance long-wavelength InGaAs/GaAs multiple quantum-well lasers grown by molecular beam epitaxy, Electron. Lett. 43 (2007) 454–456

[13] K.S. Kim, J.R. Yoo, S.M. Lee, S.J. Lim, J.Y. Kim, J.H. Lee, S.H. Cho, T. Kim, Y.J. Park, Highly efficient InGaAs QW vertical external cavity surface emitting lasers emitting at 1060 nm, J. Cryst. Growth 287 (2006) 629–632

[14] L. Fan, C. Hessenius, M. Fallahi, J. Hader, H. Li, J.V. Moloney, W. Stolz, S.W. Koch, J.T. Murray, R. Bedford, Highly strained InGaAs/GaAs multiwatt vertical-external-cavity surface-emitting laser emitting around 1170 nm, Appl. Phys. Lett. 91 (2007) 131114

[15] M. Kuznetsov, F. Hakimi, R. Sprague, A. Mooradian, High-power (>0.5-W CW) diode-pumped vertical-external-cavity surface-emitting semiconductor lasers with circular TEM_{00} beams, IEEE Photon. Technol. Lett. 9 (1997) 1063–1065

[16] S. Lutgen, T. Albrecht, P. Brick, W. Reill, J. Luft, W. Späth, 8-W high-efficiency continuous-wave semiconductor disk laser at 1000 nm, Appl. Phys. Lett. 82 (2003) 3620–3622

[17] W.J. Alford, T.D. Raymond, A.A. Allerman, High power and good beam quality at 980 nm from a vertical external-cavity surface-emitting laser, J. Opt. Soc. Am. B 19 (2002) 663–666

[18] J.-M. Hopkins, S. A. Smith, C. W. Jeon, H.D. Sun, D. Burns, S. Calvez, M. D. Dawson, T. Jouhti, M. Pessa, 0.6 W CW GaInNAs vertical external-cavity surface emitting laser operating at 1.32 μm, Electron. Lett. 40 (2004) 30–31

[19] T. Dieing, B. F. Usher, Wafer curvature in molecular beam epitaxy grown heterostructures, Phys. Rev. B 67 (2003) 054108

[20] F. Bugge, U. Zeimer, H. Wenzel, G. Erbert, M. Weyers, Interdiffusion in highly strained InGaAs-QWs for high power laser diode applications, J. Cryst. Growth 272 (2004) 531–537

[21] S.M. Wang, I. Tangring, Q.F. Gu, M. Sadeghi, A. Larsson, X.D. Wang, C.H. Ma, I.A. Buyanova, W.M. Chen, Metamorphic InGaAs quantum wells for light emission at 1.3-1.6 μm, Thin Solid Films 515 (2007) 4348–4351

[22] J.E. Hastie, J.-M. Hopkins, S. Calvez, Chan Wook Jeon, D. Burns, R. Abram, E. Riis, A.I. Ferguson, M.D. Dawson, 0.5-W single transverse-mode operation of an 850-nm diode-pumped surface-emitting semiconductor laser, IEEE Photon. Technol. Lett. 15 (2003) 894–896

[23] P. Millar, R.B. Birch, A.J. Kemp, D. Burns, Synthetic diamond for intracavity thermal management in compact solid-state lasers," IEEE J. Quantum Electron. 44(2008) 709–717

Figure captions

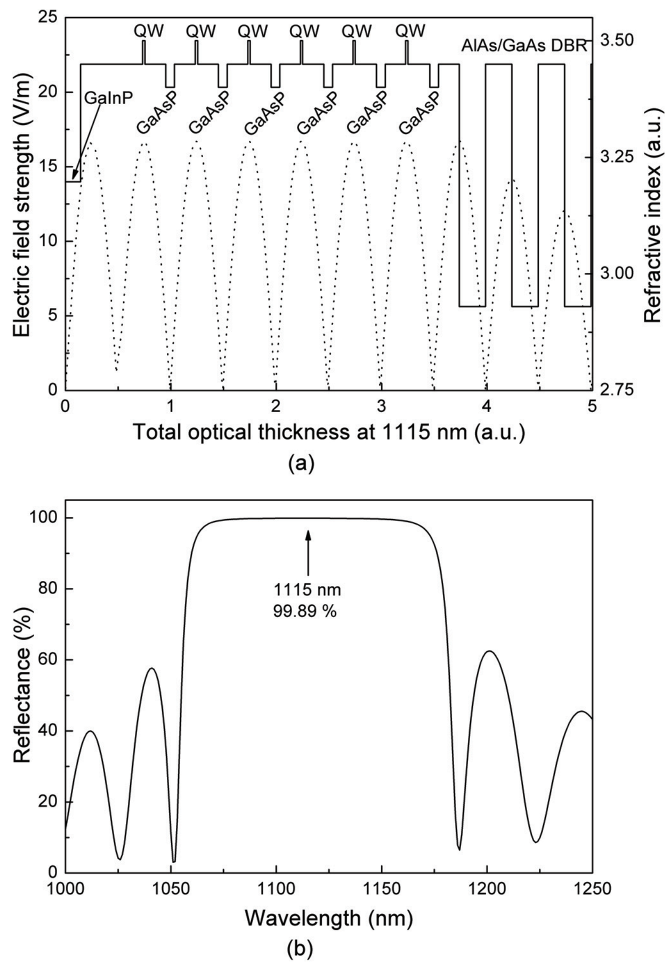

Fig. 1. (a) Electric field distribution (dotted line) and refractive index profile (solid line) of the VECSEL gain mirror structure. A section of the DBR is shown on the right side of the picture. The air-semiconductor interface is located at “zero” point on the optical thickness axis (the structure corresponds to final device for which the substrate has been removed leaving exposed the GaInP etch-stop/window layer). (b) Simulated DBR reflectivity.

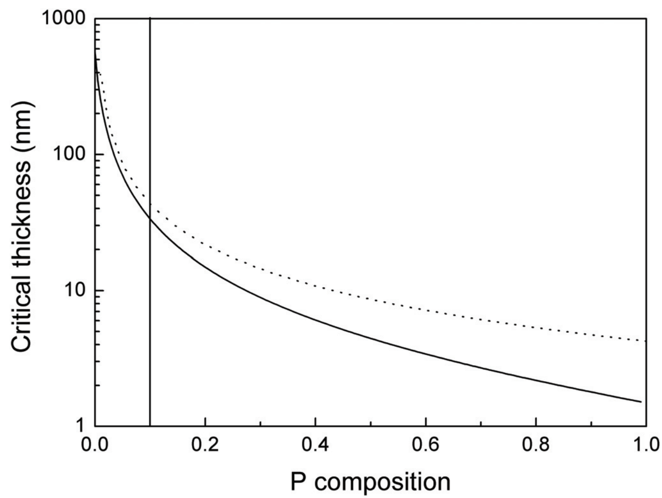

Fig. 2. Critical thickness of GaAsP as a function of P composition calculated with the model of Matthews and Blakeslee. The dotted line represents the thickness of a single GaAsP layer required to fully compensate the compressive strain of a single 7-nm thick $Ga_{0.69}In_{0.31}As$ QW. The vertical line indicates the critical thicknesses for $GaAs_{0.85}P_{0.15}$.

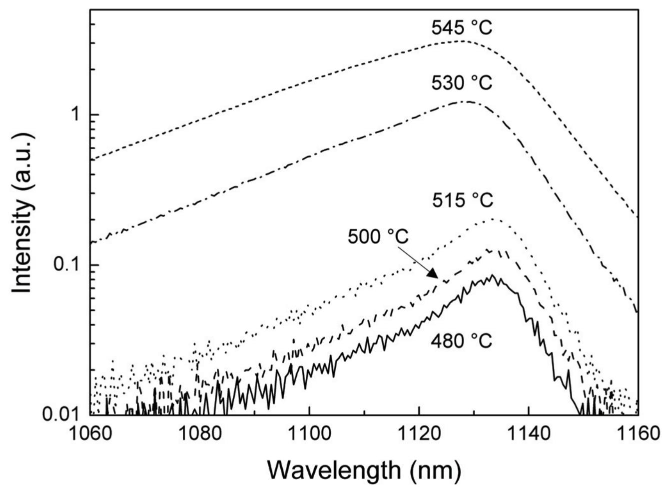

Fig. 3. Photoluminescence from GaInAs single-QW calibration samples grown at different growth temperatures. The reported temperatures have been measured with a thermocouple.

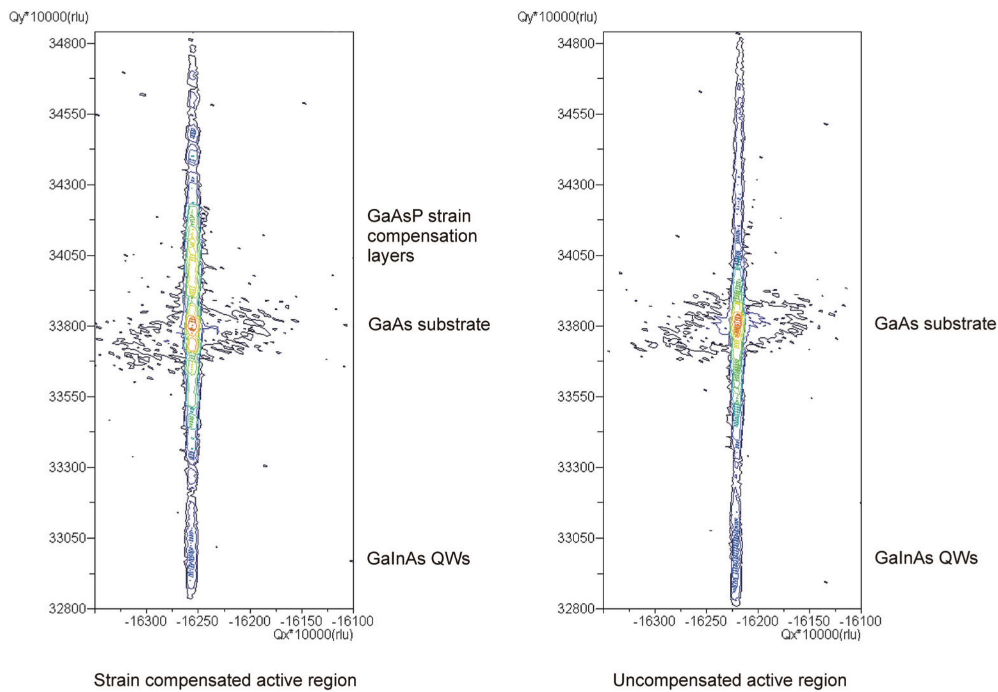

Fig. 4. (113) reciprocal space maps taken in direction [01-1] for the strain compensated and uncompensated active region samples. The diffraction peaks related to the strain compensation layers, substrate and QWs are indicated on the right side of each graph.

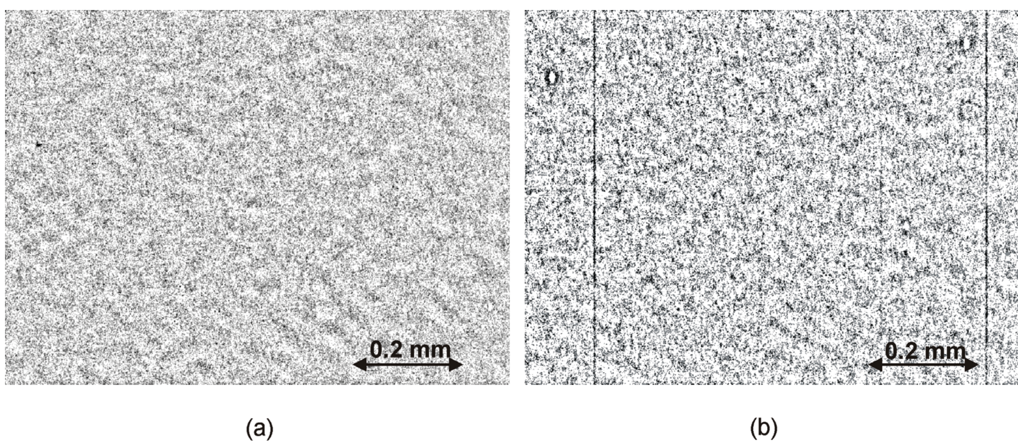

Fig. 5. A typical photoluminescence map from (a) ~91% compensated and (b) uncompensated 6 QW VECSEL gain mirrors. The original pictures were altered by ImageJ-software to highlight the PL peculiarities. The wavy pattern is caused by speckle.

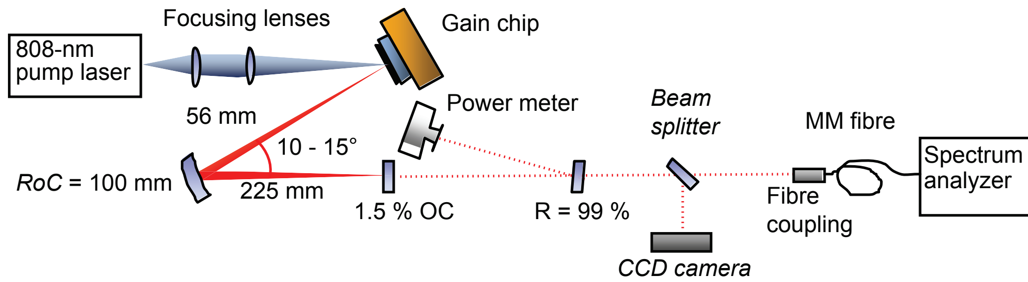

Fig. 6. VECSEL measurement setup. The laser cavity is formed between the gain mirror and the plane output coupler that has a transmission of 1.5 % at 1120 nm. The folding mirror has a 100 mm radius of curvature (RoC).

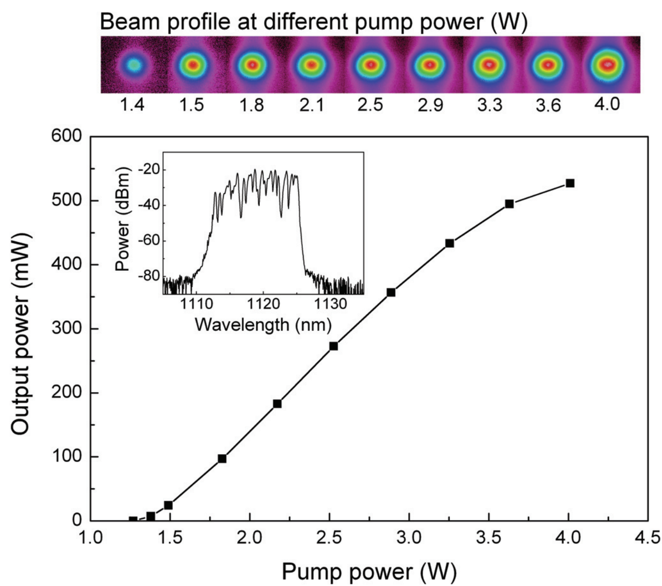

Fig. 7. Output power characteristics and beam profile measured at various pump powers. The emission spectrum (inset graph) corresponds to an output power of 527 mW.

Tables

Table 1. Experimental and theoretical wafer curvatures for 68 % compensated active region sample, uncompensated active region sample and GaAs (100) substrate. The curvatures are reported in $\times 10^{-2}$ (m^{-1}) units.

Sample	Curvature [011]	Curvature [01-1]	Theoretical mean curvature
68 % compensated active region	2.0 ± 0.013	1.5 ± 0.012	1.4
Uncompensated active region	4.5 ± 0.027	3.5 ± 0.018	3.9
GaAs(100) substrate	0.25 ± 0.011	0.78 ± 0.041	-

Publication 2

P2

S. Ranta, M. Tavast, T. Leinonen, R. Epstein, and M. Guina, ”Narrow linewidth 1118/559 nm VECSEL based on strain compensated GaInAs/GaAs quantum-wells for laser cooling Mg-ions,” *Optical Materials Express*, vol. 2, no. 8, pp. 1011–1019, 2012.

© 2012 Optical Society of America. Reproduced with permission.

This paper was published in Optical Materials Express and is made available as an electronic reprint with the permission of OSA. The paper can be found at the following URL on the OSA website: http://www.opticsinfobase.org/ome/abstract.cfm?uri=ome-2-8-1011. Systematic or multiple reproduction or distribution to multiple locations via electronic or other means is prohibited and is subject to penalties under law.

Narrow linewidth 1118/559 nm VECSEL based on strain compensated GaInAs/GaAs quantum-wells for laser cooling of Mg-ions

Sanna Ranta,[1,*] Miki Tavast,[1] Tomi Leinonen,[1] Ryan Epstein,[2] and Mircea Guina[1]

[1]Optoelectronics Research Centre, Tampere University of Technology, P.O. Box 692, FIN-33101 Tampere, Finland
[2]Areté Associates, 1225 Ken Pratt Boulevard, Suite 206, Longmont, CO 80501, USA
**Sanna.Ranta@tut.fi*

Abstract: We report on the development of an optically-pumped vertical external-cavity surface-emitting laser emitting near 1120 nm using strain compensated quantum wells. The development is motivated by the need to achieve narrow linewidth emission at ~280 nm via fourth harmonic generation, which is required to cool Mg^+ ions. The gain mirror had a top-emitting geometry, was grown by molecular beam epitaxy and comprised GaInAs/GaAs quantum wells strain compensated by GaAsP layers; the strain compensation was instrumental for achieving a dislocation free epitaxial structure without dark lines. We demonstrate VECSEL operation at a fundamental wavelength close to 1118 nm with a linewidth of less than 300 kHz. Using a lithium triborate crystal we achieved frequency doubling to ~559 nm with an output power of 1.1W.

©2012 Optical Society of America

OCIS codes: (140.3460) Lasers; (140.3480) Lasers, diode-pumped; (140.3515) Lasers, frequency doubled; (140.3600) Lasers, tunable; (140.5960) Semiconductor lasers; (140.7260) Vertical cavity surface emitting lasers; (140.7270) Vertical emitting lasers.

References and links

1. T. W. Hänsch and A. L. Schawlow, "Cooling of gases by laser radiation," Opt. Commun. **13**(1), 68–69 (1975).
2. M. Kuznetsov, F. Hakimi, R. Sprague, and A. Mooradian, "High-power (>0.5-W CW) diode-pumped vertical-external-cavity surface-emitting semiconductor lasers with circular TEM_{00} beams," IEEE Photon. Technol. Lett. **9**(8), 1063–1065 (1997).
3. M. Rahim, F. Felder, M. Fill, and H. Zogg, "Optically pumped 5 µm IV-VI VECSEL with Al-heat spreader," Opt. Lett. **33**(24), 3010–3012 (2008).
4. A. Härkönen, M. Guina, O. Okhotnikov, K. Rößner, M. Hümmer, T. Lehnhardt, M. Müller, A. Forchel, and M. Fischer, "1-W antimonide-based vertical external cavity surface emitting laser operating at 2-µm," Opt. Express **14**(14), 6479–6484 (2006).
5. T. L. Wang, Y. Kaneda, J. M. Yarborough, J. Hader, J. V. Moloney, A. Chernikov, S. Chatterjee, S. W. Koch, B. Kunert, and W. Stolz, "High-power optically pumped semiconductor laser at 1040 nm," IEEE Photon. Technol. Lett. **22**(9), 661–663 (2010).
6. J. E. Hastie, L. G. Morton, A. J. Kemp, M. D. Dawson, A. B. Krysa, and J. S. Roberts, "Tunable ultraviolet output from an intracavity frequency-doubled red vertical-external-cavity surface-emitting laser," Appl. Phys. Lett. **89**(6), 061114 (2006).
7. T. Leinonen, S. Ranta, M. Tavast, M. Guina, and R. J. Epstein, "Narrow Linewidth 1120 nm Semiconductor Disk Laser Based on strain compensated GaInAs quantum wells," in Lasers, Sources, and Related Photonic Devices, OSA Technical Digest (CD) (Optical Society of America, 2012), paper AW4A.18.
8. Y. Kaneda, J. M. Yarborough, L. Li, N. Peyghambarian, L. Fan, C. Hessenius, M. Fallahi, J. Hader, J. V. Moloney, Y. Honda, M. Nishioka, Y. Shimizu, K. Miyazono, H. Shimatani, M. Yoshimura, Y. Mori, Y. Kitaoka, and T. Sasaki, "Continuous-wave all-solid-state 244 nm deep-ultraviolet laser source by fourth-harmonic generation of an optically pumped semiconductor laser using $CsLiB_6O_{10}$ in an external resonator," Opt. Lett. **33**(15), 1705–1707 (2008).
9. J. Paul, Y. Kaneda, T. Wang, C. Lytle, J. Moloney, and J. Jones, "Precision Spectroscopy of Atomic Mercury in the Deep Ultraviolet Based on Fourth-Harmonic Generation from an Optically Pumped External-Cavity Semiconductor Laser," in Conference on Lasers and Electro-Optics, OSA Technical Digest (CD) (Optical Society of America, 2010), paper CTuS6.
10. Y. Kaneda, M. Fallahi, J. Hader, J. V. Moloney, S. W. Koch, B. Kunert, and W. Stoltz, "Continuous-wave single-frequency 295 nm laser source by a frequency-quadrupled optically pumped semiconductor laser," Opt. Lett. **34**(22), 3511–3513 (2009).

11. S. Ranta, T. Hakkarainen, M. Tavast, J. Lindfors, T. Leinonen, and M. Guina, "Strain compensated 1120 nm GaInAs/GaAs vertical external-cavity surface-emitting laser grown by molecular beam epitaxy," J. Cryst. Growth **335**(1), 4–9 (2011).
12. W. Alford, T. Raymond, and A. Allerman, "High power and good beam quality at 980 nm from a vertical external-cavity surface-emitting laser," J. Opt. Soc. Am. B **19**(4), 663–666 (2002).
13. M. Kuznetsov, F. Hakimi, R. Sprague, and A. Mooradian, "Design and characteristics of high-power (>0.5-W CW) diode-pumped vertical-external-cavity surface-emitting semiconductor lasers with circular TEM_{00} beams," IEEE J. Sel. Top. Quantum Electron. **5**(3), 561–573 (1999).
14. J. Jiménez, "Laser diode reliability: crystal defects and degradation modes," C. R. Phys. **4**(6), 663–673 (2003).
15. S. M. Wang, T. G. Andersson, and M. J. Ekenstedt, "Temperature-dependent transition from two-dimensional to three-dimensional growth in highly strained $In_xGa_{1-x}As/GaAs$ ($0.36 \le x \le 1$) single quantum wells," Appl. Phys. Lett. **61**(26), 3139–3141 (1992).
16. X. Liu, A. Prasad, J. Nishio, E. R. Weber, Z. Liliental-Weber, and W. Walukiewicz, "Native point defects in low-temperature-grown GaAs," Appl. Phys. Lett. **67**(2), 279–281 (1995).
17. Z. L. Liau, "Semiconductor wafer bonding via liquid capillarity," Appl. Phys. Lett. **77**(5), 651–653 (2000).
18. M. Herrmann, V. Batteiger, S. Knünz, G. Saathoff, Th. Udem, and T. W. Hänsch, "Frequency metrology on single trapped ions in the weak binding limit: the 3s(1/2)-3p(3/2) transition in 24Mg+," Phys. Rev. Lett. **102**(1), 013006 (2009).
19. M. A. Holm, D. Burns, A. I. Ferguson, and M. D. Dawson, "Actively stabilized single-frequency vertical-external-cavity AlGaAs laser," IEEE Photon. Technol. Lett. **11**(12), 1551–1553 (1999).

1. Introduction

Laser cooling [1] and trapping of atoms or ions require narrow linewidth (< 1 MHz), frequency-stable light sources that operate in resonance with specific atomic transitions. Laser cooling is commonly performed using either dye or fiber lasers. Dye lasers offer a wide range of wavelengths from the visible to near infrared but the high cost of pump lasers, the size, and the need of constant dye solution maintenance are a drawback. Fiber lasers are capable of generating high output power with excellent beam quality but only at the distinct energy bands determined by the pump-laser-active ions. This wavelength limitation can be overcome by placing the fiber laser as part of an optical parametric oscillator (OPO). The complexity of such OPOs, however, increases their manufacturing costs impeding their implementation to various applications. The drawbacks associated with the current laser solutions used in atom cooling could be alleviated by using a relatively novel type of laser architecture, which is the optically-pumped vertical external-cavity surface-emitting laser (VECSEL), also referred to as semiconductor disk laser (SDL) [2]. The VECSELs make use of semiconductor gain media and resemble many of the design features characterising the solid state disk lasers.

By combining the power scaling capability of disk laser concepts with the gain provided by semiconductor structures, VECSELs are capable of generating high lateral mode quality beams with high output powers over a range of emission wavelengths spanning from ultraviolet to mid-infrared [3–6]. These properties, together with the ability to tailor the emission of the semiconductor gain medium, are unique advantages of this laser platform. In addition, optical elements, such as birefringent filters and etalons, can be added to the cavity to filter out any unwanted cavity modes and to allow tuning of the wavelength and narrow bandwidth operation [7].

This report is focused on leveraging the advantages offered by VECSEL concepts to a wavelength range that would enable obtaining 280 nm radiation required for cooling of Mg^+ ions. Fourth harmonic generation to deep ultraviolet has been already demonstrated using VECSELs but at wavelengths that are not suitable for cooling of Mg^+ ions [8–10]. In particular we describe the design and fabrication of the strain compensated gain mirrors required for achieving narrow linewidth emission in VECSEL with fundamental wavelength at ~1118 nm.

2. Design and fabrication

The structure of the gain mirror is presented in Fig. 1. It consists of a 25.5-pair AlAs/GaAs DBR and a GaInAs/GaAs/GaAsP gain section. The indium molar fraction of the quantum wells (QWs) was ~31% as estimated by measuring ω-2θ x-ray diffraction (XRD) patterns. The XRD measurements used for estimating the In composition are shown in Fig. 2, and are also proof of a high structural quality of the gain mirror. The compressive strain associated

with each of the 7 nm thick QWs was compensated by a tensile-strained 30-nm-thick GaAsP layer with an estimated phosphorous molar fraction of 13%. The thickness of each tensile GaAsP layer is in fact compensating about 90% of the compressive strain-thickness product of each QW. According to our studies, without strain compensation, the structure would exhibit relaxation of the QWs and consequently have a high density of dark line defects [11]. Compared to the structure we reported in [11], the amount of QWs was increased from 6 to 10, and the gain mirror processing was substantially simplified by switching from flip-chip architecture [2] to top-emitting, i.e. intracavity heat-spreader, approach [12]. Both changes should result in improved capabilities for high power operation. In particular, for the type of output coupling we have used in our experiments, a gain mirror comprising 10 QWs appears to be optimal for high power operation [13].

Besides reducing the efficiency via non-radiative recombination and increased heating, the presence of dislocations is detrimental to laser life time [14] and therefore the strain compensation is mandatory for gain mirrors incorporating a relatively high amount of In. GaAsP strain compensation has been previously utilized in MOVPE grown GaInAs/GaAs gain mirror [10]. However, our strain compensation strategy differs in terms of GaAsP composition and thickness from the one described in [10], where only slightly strained $GaAs_{0.97}P_{0.03}$ layers have been utilized. Moreover, the precise thicknesses of the $GaAs_{0.97}P_{0.03}$ layers are not revealed in [10] but the small amount of phosphorus implies much larger thickness (about a factor of 4), if similar level of strain compensation is targeted. Most likely, significant amount of pump light is absorbed in such thick strain compensation layers with low P content, whereas in our case, the pump light is absorbed mainly in the GaAs barrier layers.

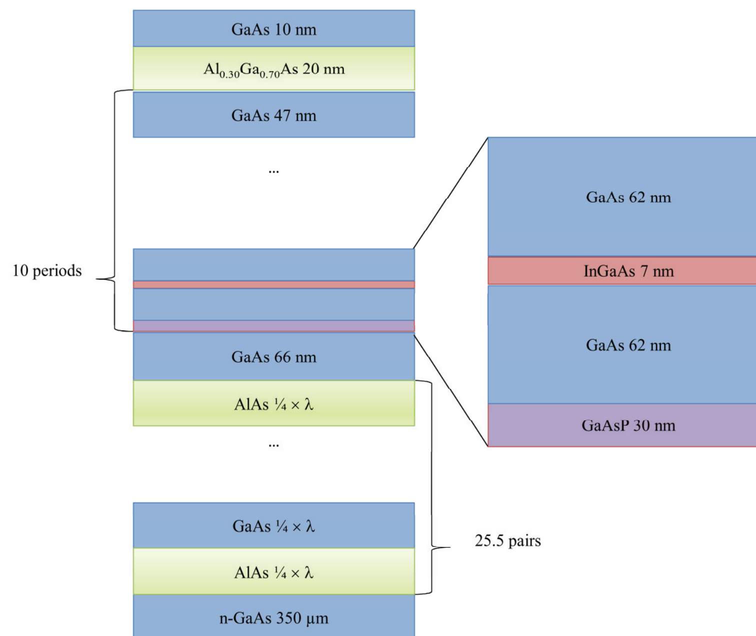

Fig. 1. The structure of the gain mirror.

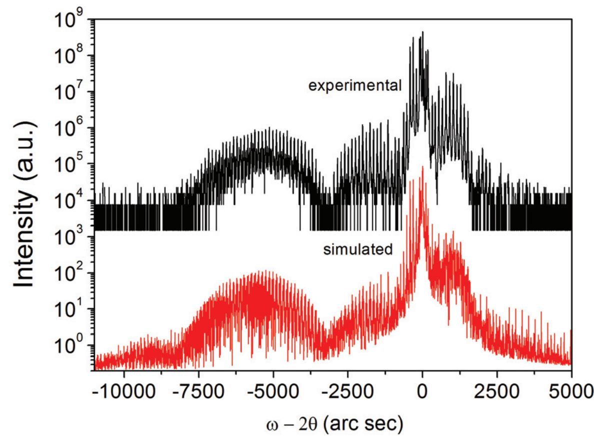

Fig. 2. Experimental and simulated (004) ω-2θ x-ray diffraction patterns. The fine structure pattern and the narrow diffraction peaks indicate a high crystalline quality.

The optical thickness of the gain region was chosen such that the etalon formed between the DBR and the gain mirror surface would be anti-resonant with the laser operation wavelength. This configuration provides a wide gain bandwidth and a wider wavelength tuning range. The structure was grown by solid-source molecular beam epitaxy (SSMBE) on a (001) n-GaAs substrate. To reach high luminescence efficiency, the QW growth temperature was optimized by fabricating several samples containing one QW. The quality assessment was performed by comparing the intensities of their photoluminescence (PL) signals. The optimization yielded a growth temperature of 545 °C, measured by the thermocouple mounted on the substrate holder. This corresponds to a pyrometer reading of about 500 °C. The PL peak intensity *versus* thermocouple reading is presented in Fig. 3. Using the room temperature PL setup available, we could not detect any PL signal for the extreme growth temperatures of T = 370 °C and 565 °C (thermocouple reading). A possible explanation for the poor PL signal at the high temperature is the relaxation of the GaInAs layer leading to growth mode transition from 2D to 3D and subsequent generation of misfit dislocations in the crystal [15]. We believe that the poor PL signal at the low growth temperatures is caused by structural defects such as arsenic antisites and gallium vacancies [16].

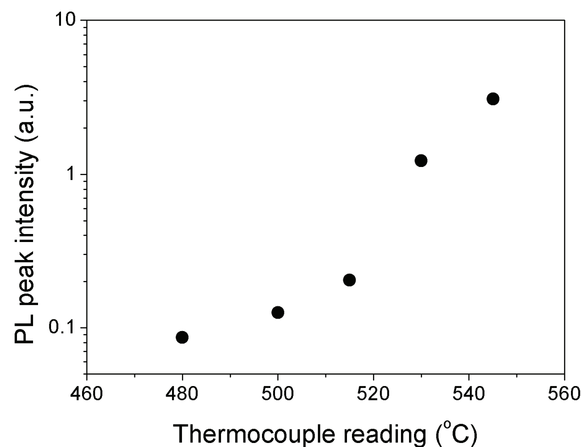

Fig. 3. Photoluminescence peak intensity from single-QW samples grown at different temperatures. The 370 °C and 565 °C data point were excluded from the figure since no emission was obtained at these temperatures using the available room temperature PL system.

The strain compensation and GaAs barrier layers were grown at a typical growth temperature of 580–590 °C (pyrometer measurements). The growth was stopped between these layers and the QWs in order to ramp the temperature to adequate levels ensuring high quality growth. The stop band of the DBR and the surface PL peak are centered at 1123 nm and 1121 nm, respectively, as shown in Fig. 4. The success of the strain compensation was investigated by measuring a PL map of the gain mirror that would point out any dark line or dark spot defects. The measurement revealed a very low dark spot density and absence of dark lines. Most likely, these dark spot defects originated from the substrates. The ω-2θ x-ray diffraction spectra, shown in Fig. 2, did not reveal any signs of strain relaxation or diffusion scattering from crystal defects.

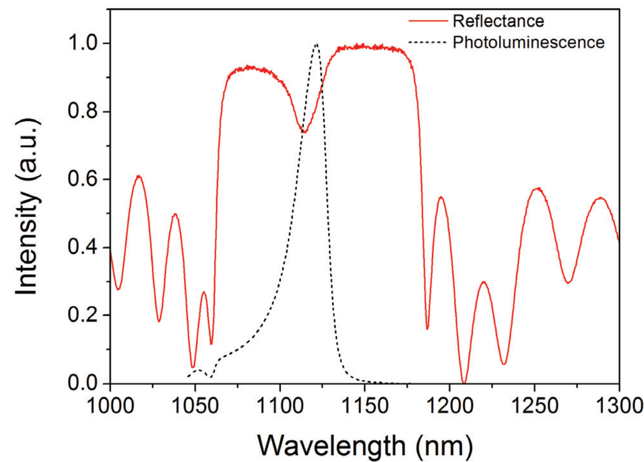

Fig. 4. Normalized surface photoluminescence (PL) and reflectance curves recorded from the gain mirror after growth. The dip in the reflectivity characteristic is caused by QW absorption.

After the epitaxial growth and material characterizations, a 2.5 mm × 2.5 mm chip was cleaved from the wafer and capillary bonded [17] on the epi-side to a 3 mm × 3 mm diamond heat spreader that has a 2° wedge. Water was used to pull the two surfaces into contact and eventually to bond them together by intermolecular surface forces. A slight pressure was applied to the chip-diamond interface during and after bonding to ensure firm contact. The single-crystal synthetic diamond had a surface roughness (R_a) below 5 nm and a surface flatness of <5 interference fringes in reflection at 632.8 nm. The surface roughness of the semiconductor chip was determined by using an atomic force microscope from a 3 µm × 3 µm sized scan area. The measurement was performed at two different locations on the gain chip, yielding a roughness of ~0.17 nm (R_a-value). The wedged geometry of the diamond heat spreader alleviates the etalon effects that would otherwise perturb the laser spectrum. The heat spreader was clamped with an intervening indium foil to a cooled copper sample holder (Fig. 5). An antireflective coating was deposited on the air-diamond interface in order to reduce the intracavity reflection at the lasing wavelength and further weaken the subcavity etalon effect. The antireflective coating comprised altogether two layers, a TiO_2 layer and a SiO_2 layer. The reflectance minimum was targeted at the 1120 nm laser wavelength but the coating provided also significantly reduced reflectivity (R<12%) at the pump emission wavelength of 808 nm for an 8° incidence angle.

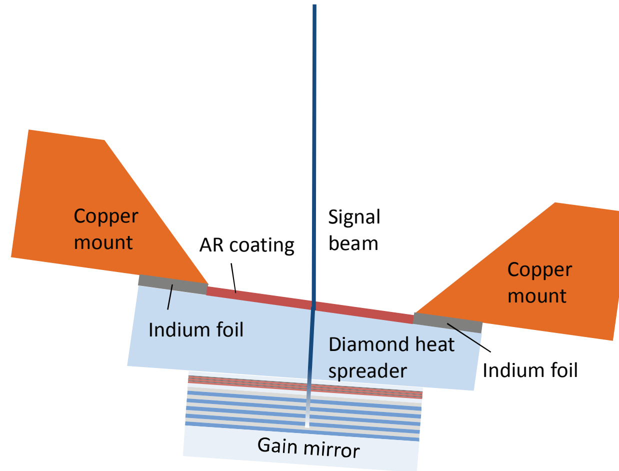

Fig. 5. Schematic showing the gain mirror attachment to the wedged diamond heat spreader and the diamond attachment to the copper mount with indium.

3. Laser setups and characterization

The gain mirror was first used for generating narrow linewidth light close to 559.271 nm via second harmonic generation (SHG), which can be further frequency doubled to reach the $^{24}Mg^{+}$ D2 transition wavelength of 279.635 nm [18]. For this purpose, we assembled a cavity as depicted in Fig. 6. The cavity comprised a 3 mm thick birefringent (BRF) filter and a 1 mm thick uncoated yttrium aluminum garnet (YAG) etalon for wavelength tuning and linewidth narrowing. A 15 mm long rectangular lithium triborate crystal (LBO) crystal was used for SHG. The LBO crystal was antireflective coated for 1120 nm and 560 nm wavelengths, and was placed about 5 mm away from the 4 mm thick fused silica cavity end mirror. To achieve efficient nonlinear conversion the LBO crystal was heated at about 88 °C. The distance from the gain mirror to the folding mirror was 263 mm while the distance from the folding mirror to the flat end mirror was 108 mm. The mode size ($1/e^2$ diameter) on the semiconductor chip was estimated to be 273 µm in horizontal direction and 308 µm in vertical direction. The angle of the folding mirror was ~11°. The coating of the cavity mirrors were chosen such that the light beam at the fundamental frequency could not escape the cavity while the frequency doubled light could exit the cavity only through the cavity folding mirror. The end mirror coating was also designed to minimize the phase shift between the fundamental and second harmonic frequency light. The laser was pumped with an 808 nm pump laser that was fiber coupled to a 200 µm core fiber and focused to a spot diameter ($1/e^2$ diameter) of ~390 µm.

Up to 1.1 W was achieved at 560 nm with an incident pump power of 30 W, which should enable achieving 100–200 mW at 280 nm [10], high enough for the ion-cooling experiments. The wavelength of the laser was determined by comparing the number of interference oscillations with those of a HeNe laser in a home-built Michelson interferometer. The output wavelength of the laser was adjusted by rotating the BRF. While it was possible to get within ~50 pm of the desired wavelength of 559.271 nm, it was found that the laser wavelength jumped by ~170 pm when tuning the BRF. We suspect the jumps to be associated with etalons formed by the optical elements of the cavity. Because of this wavelength jump we were not able to perform accurate linewidth measurement; the wavelength could not be tuned close enough to emission of a reference laser to observe the beat signal.

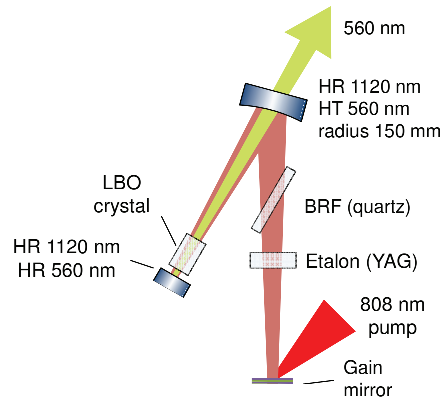

Fig. 6. Cavity configuration for the narrow linewidth SHG experiment.

In order to eliminate the wavelength discriminating behavior and to measure the laser linewidth, a straight cavity without the LBO crystal was constructed (see Fig. 7). Also the etalon was omitted because it was not needed for achieving single frequency operation. In this configuration, the laser would operate in a single-frequency mode depending on the BRF angle and the pump power. The laser still exhibited wavelength jumps on the scanning Fabry-Perot etalon when the cavity length was varied or the BRF angles were adjusted. However, the step was measured to be as small as 7.6 pm, which was the same as the wavelength step size of the wavemeter we used for measuring the emission wavelength. At 1118.5 nm, 7.6 pm corresponds to 1.8 GHz, whereas the cavity free spectral range was 0.82 GHz, which is below the resolution of the wavemeter. Therefore, we could not verify whether the jumps observed by the scanning Fabry-Perot etalon were longitudinal modes of the cavity. By simplifying the cavity, we were able to significantly improve the tuning of the laser by reducing the magnitude of the wavelength jumps.

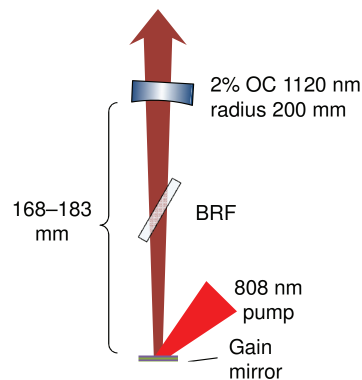

Fig. 7. The cavity used for the narrow linewidth fundamental wavelength emission experiment.

Figure 8(a) shows the power conversion graph of the laser corresponding to a temperature of the cooling water set to 15 °C. The kinks in the graph are most likely due to sudden changes to higher transversal mode operation or a sudden wavelength jump. The maximum output power was limited by the available pump power. The maximum optical conversion efficiency was about 25%. Figure 8(b) shows the output power *versus* emission wavelength when the wavelength was tuned by rotating the BRF and the pump power was kept constant at 30 W. The total tuning range reached was 31 nm. During the tuning experiment, the laser

operated mostly in a single frequency mode, i.e., it would occasionally emit multiple frequencies as observed with the scanning Fabry-Perot etalon. To measure the emission linewidth, the laser was tuned close to the desired wavelength and pumped with 9 W to reach about 0.8 W of output power and a beat measurement between the laser and a commercial fiber laser (Menlo Systems) was performed. The assessment of linewidth at higher output power was not possible because the chiller used for cooling the gain mirror did not have adequate capacity to keep the temperature constant for the period required to carry out the measurement. The beams from both lasers were directed via a single mode fiber to a single high-bandwidth photodetector and the beat signal was recorded using a spectrum analyzer (Agilent). The measured beat signal is shown in Fig. 9. The beat width was below the 300 kHz resolution bandwidth of the spectrum analyzer. The use of narrower measurement bandwidth was not possible because it would require a longer sweep time during which the wavelength of the laser drifted outside the measurement window. The wavelength drift could have been eliminated or reduced significantly by introducing active wavelength stabilization to the cavity [19]. This, however, could not be implemented to the cavity in this experiment but will be implemented in the future design of the laser cavity.

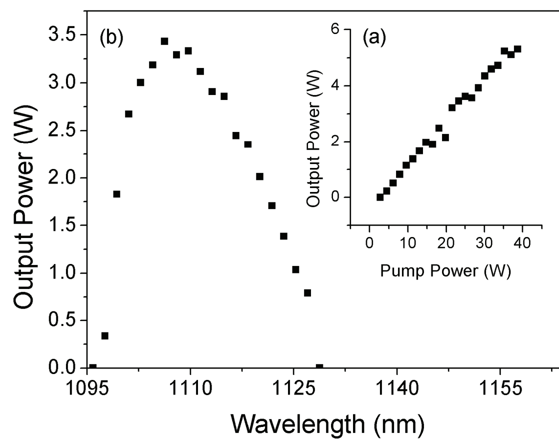

Fig. 8. Graphs recorded during the power conversion (a) and corresponding wavelength tuning (b).

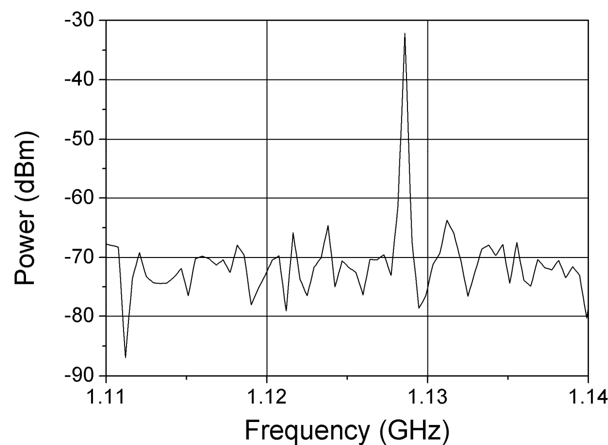

Fig. 9. Beat signal measured at 4.4 ms sweep time of the spectrum analyzer.

4. Conclusion

We have shown that GaInAs/GaAs-based VECSELs are a promising technology to cool Mg^+ ions. According to our experiments, strain compensation and a fairly low growth temperature were necessary to reach high crystalline quality for a gain mirror comprising 10 GaInAs QWs. In particular, we have identified an optimal growth temperature of 500 °C (pyrometer reading) for the QWs. The strain compensation was achieved by using 30-nm-thick GaAsP layers with a P concentration of 13%. We were able to reach ~5.5 W at 1118 nm with 30 W of pump power. A linewidth of less than 300 kHz could be measured for an output power of 0.8 W at the fundamental wavelength of 1118 nm with 9 W of pump power. Linewidth measurements at higher pump power were not possible due to the technical limitations of the cooling system available. Furthermore, we were able to demonstrate 1.1 W output power at 559 nm with 30 W of pump power by second harmonic intracavity conversion. Our results prove that it would be possible to generate continuous tuning at the half-frequency of Mg^+ ion photoionization wavelength using VECSEL technology.

Acknowledgments

This work was supported by the US National Institute of Standards and Technology, the Academy of Finland (grant 128364) and the graduate school of the Tampere University of Technology. The authors are grateful to Dr. Härkönen for evaporating the antireflective coating on the diamond heat spreader for the VECSEL and Dr. Sandalphon for technical assistance with the laser system.

Publication 3

P3

W.J. Alford, G.J. Fetzer, R.J. Epstein, Sandalphon, N. Van Lieu, S. Ranta, M. Tavast, T. Leinonen, and M. Guina, "Optically pumped semiconductor lasers for precision spectroscopic applications," *IEEE Journal of Quantum Electronics*, vol. 49, no. 8, pp. 719–727, 2013.

© 2013 Institute of Electrical and Electronics Engineers. Reprinted with permission.

In reference to IEEE copyrighted material which is used with permission in this thesis, the IEEE does not endorse any of Tampere University of Technology's products or services. Internal or personal use of this material is permitted. If interested in reprinting/republishing IEEE copyrighted material for advertising or promotional purposes or for creating new collective works for resale or redistribution, please go to
http://www.ieee.org/publications_standards/publications/rights/rights_link.html
to learn how to obtain a License from RightsLink.

This is the author's version of an article that has been published in this journal. Changes were made to this version by the publisher prior to publication.
The final version of record is available at http://dx.doi.org/10.1109/JQE.2013.2270912

Optically Pumped Semiconductor Lasers for Precision Spectroscopic Applications

William J. Alford, Gregory J. Fetzer, Ryan J. Epstein, Sandalphon, Neil Van Lieu, Sanna Ranta, Miki Tavast, Tomi Leinonen, and Mircea Guina

***Abstract*—Optically pumped semiconductor lasers in conjunction with intra-cavity frequency conversion and tuning elements offer high continuous-wave power, narrow linewidth, and broad tunability. As a result they are well suited to precision spectroscopic applications. We describe the development and testing of optically pumped semiconductor lasers operating at fundamental wavelengths of 1119 and 1178 nm. The fourth and second harmonic wavelengths are resonant with transitions in Mg II and Na I, respectively. We demonstrate continuously tunable, single-frequency lasers with watt-level average power at 1119 nm, 1178 nm, and 589 nm.**

***Index Terms*—Lasers, semiconductor lasers, quantum well laser, surface emitting lasers, and optical harmonic generation**

I. Introduction

A number of applications based on precision spectroscopy of atoms have moved out of the lab and still more are poised to do so in the near future. Sodium laser guide stars [1] used by the astronomical community are an example of an established application. The rapidly progressing field of quantum optics is opening doors to high performance computing, sensitive and high precision measurements of physical parameters, and fundamental research. It is likely that developments in this field will soon move out of the lab and enable high bandwidth information transfer, ultrafast computing, and other applications requiring precise knowledge of time, frequency, or other physical variables. This could result in practical quantum optical sensors such as atomic magnetometers [2,3], atom interferometer gyroscopes [4], and atomic clocks [5]. The use of trapped ions as quantum bits represents one of the promising avenues for scalable quantum information processing [6-8]. Laser cooling of atoms and ions is critical for quantum information processing and many other quantum optical applications. These exciting fields of study rely on narrow-linewidth, resonantly tuned lasers to interrogate or change the state of atoms, ions, and molecules.

Dye lasers have been used for many years for spectroscopic research and applications. Their advantages are broad spectral coverage, high gain from the active media, and maturity of the technology. However, the inconvenience of using dye and the requirement for a bright pump illumination source render this a poor candidate for many applications.

Fiber lasers or fiber amplifiers coupled to diode laser seeds can provide narrow linewidths, reasonable powers, and excellent beam quality in compact packages. Coupled with nonlinear frequency conversion methods, such lasers meet with acceptance in specific wavelength regions; however, broad spectral coverage is not currently available, limiting their applicability.

Semiconductor diode laser technology is appropriate for some applications and often provides a robust solution. Electrically pumped semiconductor laser technology has benefited from large investments by the telecom industry to produce single-frequency, low-noise devices with excellent side mode suppression. Unfortunately, these lasers are not available in a wide variety of wavelengths and costs for custom wavelengths are substantial. VCSEL (vertical cavity surface emitting laser) and DFB (distributed feedback) lasers provide modest powers (1-100 mW) at narrow linewidths of approximately 10 MHz. Narrower linewidth operation is possible by incorporating external cavities and some very capable systems exist at a few relevant wavelengths. External cavity diode lasers are generally limited to modest power (tens of milliwatts). Applications requiring higher laser power therefore require an amplifier, which often results in output of poor beam quality.

OPSLs (optically pumped semiconductor lasers), also known as VECSELs (vertical external-cavity surface emitting lasers), are 'vertically' emitting lasers similar to VCSELs but with superior power scaling potential and transverse mode control. They have inherent advantages as laser sources for precision spectroscopic applications [9]. Foundry costs to reach new wavelengths are relatively low because OPSLs, grown with MBE (molecular beam epitaxy) or MOCVD (metal-organic chemical vapor deposition), require little post-growth processing. OPSLs require no lateral confinement regions, electrical contacts, or other features across the wafer requiring

Manuscript received February X, 2013. This work was supported in part by the U.S. Department of Commerce under SB134109CN0070 and National Science Foundation SBIR Grant IIP-0956879.
W. J. Alford is a consultant based out of Lafayette CO, USA.
G. J. Fetzer, R. J. Epstein, and N. Van Lieu are with Areté Associates, 2500 Trade Center Ave., Longmont CO 80501 USA. R. J. Epstein is currently with Lockheed Martin Space Systems Company, Littleton CO, USA. (email: gfetzer@arete.com)
Sandalphon is with Cinnabar Optics, Erie CO USA.
S. Ranta, M. Tavast, T. Leinonen, and M. Guina are with the Optoelectronics Research Center, Tampere University of Technology, Korkeakoulunkatu 3, 33720 Tampere Finland.
Digital Object Identifier xxxxxx.

Copyright (c) 2013 IEEE. Personal use is permitted. For any other purposes, permission must be obtained from the IEEE by emailing pubs-permissions@ieee.org.

This is the author's version of an article that has been published in this journal. Changes were made to this version by the publisher prior to publication.
The final version of record is available at http://dx.doi.org/10.1109/JQE.2013.2270912

masks for post-growth processing. Band-gap engineering of the lasing material allows for broad coverage of wavelengths, which can in turn provide wavelengths ranging from the infrared to the UV through nonlinear frequency conversion [9]. The excellent beam quality and multi-watt powers at fundamental wavelengths provided by OPSLs, make single-step or sequential frequency conversion processes practical. Single spatial and longitudinal mode operation can be achieved with modest optical arrangements [10-12] and frequency stabilization is achieved using standard techniques [13,14].

OPSLs have been designed and used for quantum optical applications, for example for cooling of Cs atoms related to atomic clock applications [15, 16]. Paul et al [17] recently reported the development of an OPSL with sequential frequency doubling to reach well into the ultraviolet for cooling of Hg atoms. Laser cooling of solids has been demonstrated by Albrecht et al [18] using a 1020 nm OPSL to achieve a 20 K temperature drop of Yb:YLF within the OPSL cavity.

Several applications are of interest for the 589 nm sodium wavelength. In addition to atomic state manipulation and cooling, a particularly interesting application is the use of lasers to create laser guide stars in the upper atmosphere to allow correction of atmospheric distortion using adaptive optics. Astronomical laser guide star systems typically require 10-50 W of 589 nm output, though often, sodium fluorescence returns resulting from as little as 4 W on the sky are sufficient to “close the loop” on the adaptive optics.

This paper discusses development and testing of OPSLs targeted for precision spectroscopic applications. We demonstrate simultaneous multi-watt output power and continuous single-frequency tuning at the precise wavelengths required for Na and Mg applications. Specifically, gain materials and laser designs were produced to exploit resonances in Mg II (280 nm) and Na I (589 nm). To this end gain materials were produced to operate at the fundamental wavelengths of 1119 nm and 1178 nm. The semiconductor materials were assembled to form ‘gain chips’ incorporating a high reflector and gain medium in one monolithic semiconductor component. The gain chips were integrated into laser cavities designed for single-frequency, continuously tunable operation at the fundamental wavelengths. Previously we have reported 5.5 W at 1118 nm [11] and 14.2 W at 1178 nm [19] with OPSLs capable of single frequency operation at select wavelengths but lacking continuous tuning. Continuous single-frequency tuning is critical for precision spectroscopic applications typically requiring wavelengths tuned-to and tunable-about fixed atomic resonances. The requirements [20-24] and achievements of the 1119 nm and 1178 nm efforts are summarized in Table 1. The requirements are typical of a variety of precision spectroscopic applications.

Section II discusses the gain material design, growth and characterization of the semiconductor gain region. Section III discusses laser design and implementation. OPSL characterization results are discussed in Section IV. A brief summary of results is provided in Section V.

Table 1 Laser performance objectives and achievements.

Parameter	Requirement	Achievement
Wavelength	**1119 nm**	**1119 nm**
Power	> 1 W	4 W
Tuning	1.0 GHz	2.0 GHz
Linewidth	< 1 MHz	0.9 MHz
Beam Quality	TEM_{00}	TEM_{00}
Wavelength	**1178/ 589 nm**	**1178/589 nm**
Power	15 /6 W	11 /3 W
Tuning	± 5 GHz (589 nm)	± 5 GHz
Linewidth	<50 MHz	<50 MHz
Beam Quality	TEM_{00}	TEM_{00}

II. DESIGN, GROWTH, AND CHARACTERIZATION

A schematic of the semiconductor gain structure (gain chip or gain mirror) is shown in Fig. 1. A very high reflectivity DBR (distributed Bragg reflector) is grown on a GaAs substrate. A quantum well (QW) gain region is grown on top of the DBR. A diamond heat spreader is bonded to the top of the structure. Pump light enters the structure through the heat spreader.

The 1119 nm and 1178 nm gain chips contained a 10-QW GaInAs/GaAs gain region and a 25.5-pair AlAs/GaAs DBR used as the laser cavity high reflector. The separation between the room-temperature QW peak photoluminescence wavelength and the target operation wavelength of the structures was designed to be about 15–20 nm. Periodically spaced, 7 nm thick QWs were sandwiched between GaAs layers that provided the bulk of the optical absorption of the pump laser. A thin $GaAs_{0.89}P_{0.11}$ layer located equidistant between adjacent QWs was used to reduce the strain resulting from the lattice mismatch between the QWs and the GaAs. The indium composition of the QWs was measured by X-ray diffraction to be 32% and 35% for the 1119 nm and 1178 nm gain chips, respectively. The strain compensation layers were 30 nm thick in the 1119 nm and 32 nm in the 1178 nm gain chip structure. A 20 nm thick $Al_{0.33}Ga_{0.67}As$ window layer prevented non-radiative surface recombination of carriers. Both structures were finalized with a 10 nm thick capping layer to passivate the surfaces of the AlGaAs window layers.

The QWs were located at the antinodes, and the GaAsP layers at the nodes, of the standing optical wave pattern formed between the DBR and the external cavity mirror of the OPSL. The 1119 nm structure was designed to be resonant, i.e. such that the capping layer and the DBR form a resonant cavity for the operational wavelength [25]. The 1178 nm structure was designed to be antiresonant, i.e. such that the capping layer and the DBR form a non-resonant cavity for the operational wavelength. Resonant structures provide higher gain at the resonant wavelength but demonstrate restricted tuning while antiresonant structures demonstrate reduced gain with increased tuning range. The reduced gain bandwidth of

Copyright (c) 2013 IEEE. Personal use is permitted. For any other purposes, permission must be obtained from the IEEE by emailing pubs-permissions@ieee.org.

This is the author's version of an article that has been published in this journal. Changes were made to this version by the publisher prior to publication.
The final version of record is available at http://dx.doi.org/10.1109/JQE.2013.2270912

resonant structures is beneficial for obtaining single-frequency operation with limited tuning [25, 26]. Resonant structures are preferred for fixed wavelength operation if the QW peak gain wavelength and the chip resonant wavelength are equal at the chip operating temperature. Uncertainties in the optimum 1178 nm structure growth motivated us to use a non-resonant structure despite the fixed wavelength for this application.

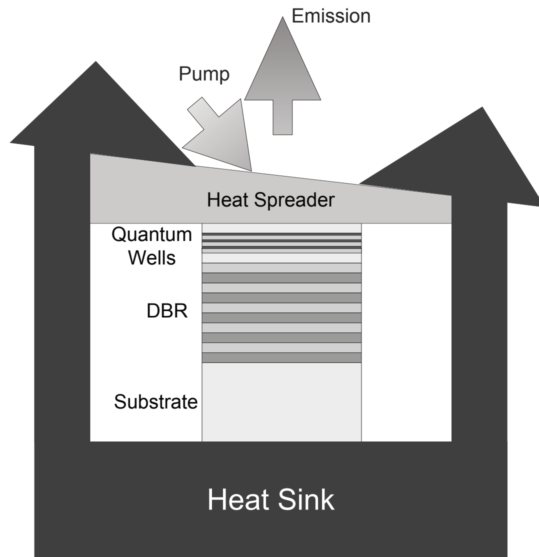

Fig. 1. Schematic of semiconductor gain structure and mounting scheme.

The gain chips were grown by solid-source MBE on a 2-inch n-GaAs substrate. The growth advanced from the DBR to the active region, window layer and finally to the cap. During the growth of the 1178-nm-emitting QWs, the sample manipulator temperature was set to 460 °C which is lower than the typical manipulator temperature of 565 °C used for the less-strained GaInAs QWs emitting near 1000 nm. The 1119-nm-emitting QWs were grown at 545 °C manipulator temperature. The lower growth temperature increased the critical thickness of the material and thus mitigated the formation of misfit dislocations. The GaAs absorption layers, $GaAs_{0.89}P_{0.11}$ strain compensation layers, DBR layers, window layers and cap layers were grown at about 670 °C (manipulator set temperature). The higher growth temperature, as compared to the growth temperature of the QWs, was necessary for achieving good crystalline quality for the $GaAs_{0.89}P_{0.11}$ layers. The growth was interrupted near every QW in order to adjust the growth temperature to the higher value. The manipulator temperature setting of 670°C corresponded to 580 °C as measured by a pyrometer that yields the growth temperature of the layer more accurately. The low temperature cut-off of the pyrometer was around 500 °C, which is above the growth temperature of the QWs. Therefore, it was not possible to measure the QW growth temperature with the pyrometer. The growth rates for all layers ranged from 0.8 to 1.1 μm/h, except for the window layer that had a growth rate of 0.5 μm/h for the 1119 nm gain chip and 0.6 μm/h for the 1178 nm gain chip.

The wafers were characterized by reflectance, photoluminescence (PL), and x-ray diffraction measurements. The measured reflectance and photoluminescence graphs are shown in Fig. 2 for both the 1119 nm and 1178 nm gain chips. The photoluminescence signal was measured from a cleaved sample edge in order to eliminate impact of the micro-cavity formed between the DBR and the sample surface. For the 1119 nm structure, the wavelength corresponding to the PL peak at low pump-powers was 1122 nm, i.e. 2 nm longer than the target wavelength. This negative detuning is most likely a result of an unexpected deviation in the reactor calibrations. The PL emission peak for the 1178 nm structure was at 1159 nm. To assess the crystalline quality of the gain chips we used photoluminescence mapping capable of revealing dark defects. These maps revealed that the gain chips contained some dark spot defects but no dark line defects.

After wafer characterization, 2.5 × 2.5 mm^2 chips were cut from the substrates and attached on the surface of synthetic 3 × 3 × 0.3 mm^3 diamonds via capillary bonding. The diamond was attached from its opposite surface to a water-cooled copper heat sink with the aid of a 50 μm thick indium foil. The copper heat sink had a clear aperture of 1.5 mm in diameter to allow optical pumping and extraction of laser light. The diamond had a 2° wedge to mitigate the etalon effect that can result from reflections at the diamond surface. Finally the chips were anti-reflective coated with one TiO_2 layer and one SiO_2 layer, deposited on the top diamond surface. The aim of the coating is to reduce reflection loss from the diamond–air interface for both the pump and OPSL wavelengths.

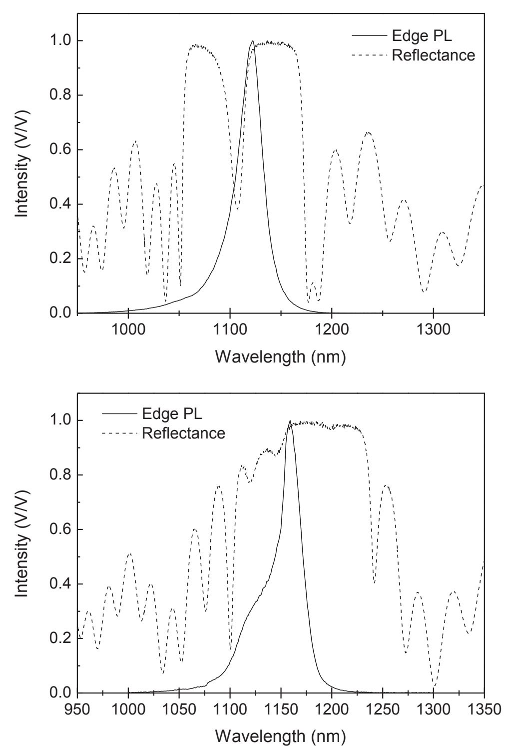

Fig. 2. Photoluminescence and reflectance of 1119 nm (top) and 1178 nm (bottom) semiconductor gain chips.

Copyright (c) 2013 IEEE. Personal use is permitted. For any other purposes, permission must be obtained from the IEEE by emailing pubs-permissions@ieee.org.

III. Laser Design and Fabrication

Two OPSL cavity configurations were used, one for producing fundamental wavelength output and the other for producing second harmonic output. Fig. 3 shows a schematic of the two-mirror cavity used to produce single-frequency output at the fundamental laser wavelength. The cavity consists of the semiconductor gain chip, a single-plate birefringent filter (BRF), an etalon, and a curved output coupler (OC). The BRF was a 3 mm thick plate of quartz inserted in the cavity at Brewster's angle. The BRF provided sufficient wavelength selectivity to tune over a few 10's of nm. The BRF alone (no etalon) typically resulted in a few longitudinal modes lasing though at times the output consisted of a single longitudinal mode. Reliable single longitudinal mode operation required the use of a 1 mm thick, uncoated YAG (yttrium aluminum garnet) etalon inserted at near-normal angle of incidence. The curvature of the output coupler and the cavity length were chosen to produce a TEM00 resonator mode size on the semiconductor gain chip less than the pump spot size. The maximum fundamental output power was obtained with an output coupler reflectivity of ~98%. The typical cavity length was 13 cm while the curvature of the output coupler was 15 cm. The output coupler was mounted to a PZT (piezoelectric transducer) to allow fine adjustments of the cavity length.

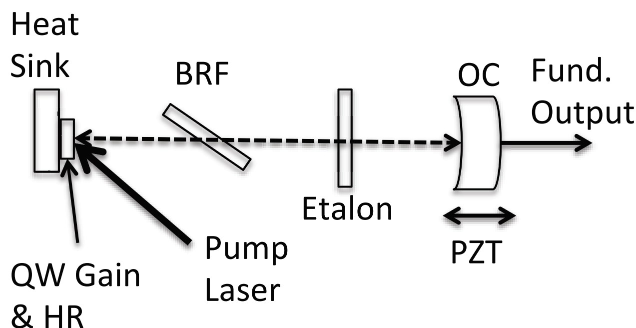

Fig. 3. Two-mirror cavity with frequency selective elements.

Fig. 4 shows the three-mirror cavity used to produce single-frequency output at the second harmonic of the fundamental laser wavelength. The cavity is similar to the two-mirror fundamental cavity with the addition of an intra-cavity turning mirror, mounted to a PZT, and a nonlinear crystal, LBO (lithium triborate), for second harmonic generation (SHG). The cavity is designed to produce a waist at the semiconductor gain chip and also in the LBO. The intra-cavity turning mirror and the output coupler are both high transmission at the SHG wavelength, thus producing SHG output in two directions. A single-beam output can be obtained from this cavity by using a high reflectivity coating for the second harmonic on the OC, resulting in a single SHG beam exiting the intra-cavity turning mirror. The 15 mm LBO crystal was cut for Type I noncritical phase matching with propagation down the x-axis of the crystal. The fundamental wavelength is P-polarized relative to the LBO Brewster surfaces and the SHG is S-polarized. To maximize the intra-cavity power at the fundamental wavelength the output coupler and intra-cavity turning mirror have high reflectivity at the fundamental wavelength.

A fiber coupled diode laser operating at 808 nm was used to pump the OPSLs. The fiber had a 400 μm diameter and could deliver over 50 W of laser power. Lenses focused the fiber output onto the semiconductor gain chip to a diameter of 350-450 μm. The gain mirror cooling water temperature was typically set in the range of 5-15 °C. Diagnostics of the OPSL output included a calibrated laser power meter, an IR wavelength meter (1 pm resolution), a scanning confocal Fabry-Perot etalon with a 1.5 GHz free spectral range, and a CMOS camera.

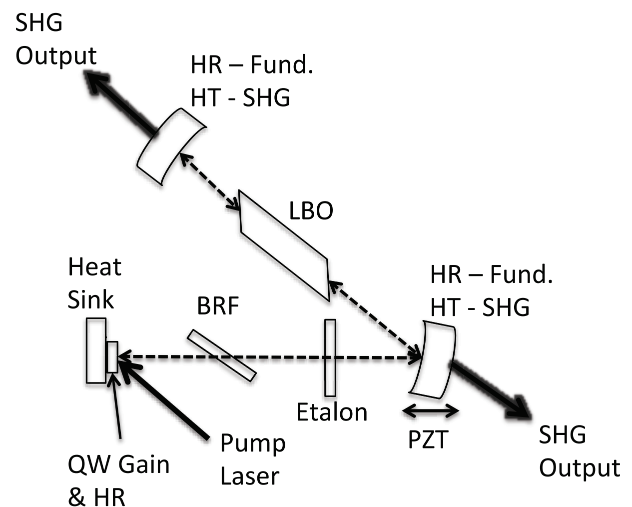

Fig. 4. Three-mirror cavity with frequency selection and SHG.

Stable single-frequency output is obtained by temperature stabilizing the intra-cavity frequency selective elements (the BRF and etalon) and by passive stabilization of the cavity length. The BRF and etalon temperatures are actively stabilized approximately 10-30 °C above ambient with commercial temperature controllers. Passive stabilization of the cavity length is achieved by mounting cavity components on a vibrationally isolated breadboard and by enclosing the breadboard to minimize air movement. Single frequency tuning of the laser is, somewhat awkwardly, achieved by manually tuning the temperature set points and the cavity length (through the PZT). Better, standard techniques for stabilization and tuning can straightforwardly be applied to the OPSLs. It is worth noting that the short, periodic gain structure in OPSLs eliminates spatial hole burning, which combined with the homogeneous broadening of the QWs means OPSLs can rather easily be made to run single frequency.

Copyright (c) 2013 IEEE. Personal use is permitted. For any other purposes, permission must be obtained from the IEEE by emailing pubs-permissions@ieee.org.

This is the author's version of an article that has been published in this journal. Changes were made to this version by the publisher prior to publication.
The final version of record is available at http://dx.doi.org/10.1109/JQE.2013.2270912

IV. Results

A. 1119 nm laser

A typical 1119 nm laser output power versus pump power is shown in Fig. 5 for a two-mirror cavity. Approximately 4 W is obtained with a maximum optical-to-optical efficiency slightly over 10%. Day to day variations in the pump focusing alignment, cavity alignment, and loss due to intra-cavity elements led to slight variations in the output power but the maximum power was always approximately 4 W. The 10% efficiency is attractive for a single frequency OPSL though higher efficiencies have been obtained with short-cavity-length OPSLs containing no intra-cavity elements [10]. Fig. 6 shows the spatial profile of the OPSL output for an output power of 4.3 W. As mentioned above, the pump spot is slightly larger than the lowest order mode of the laser cavity in order to promote efficient operation on the TEM00 mode of this low-gain laser. We did not quantitatively measure the beam quality of the output to verify TEM00 operation but the beam is seen to be single peaked with reasonable azimuthal symmetry.

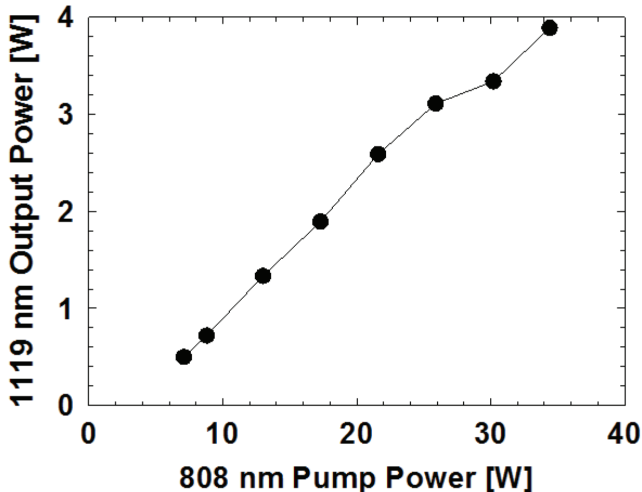

Fig. 5. Output power of a two-mirror OPSL cavity operating at ~1119 nm.

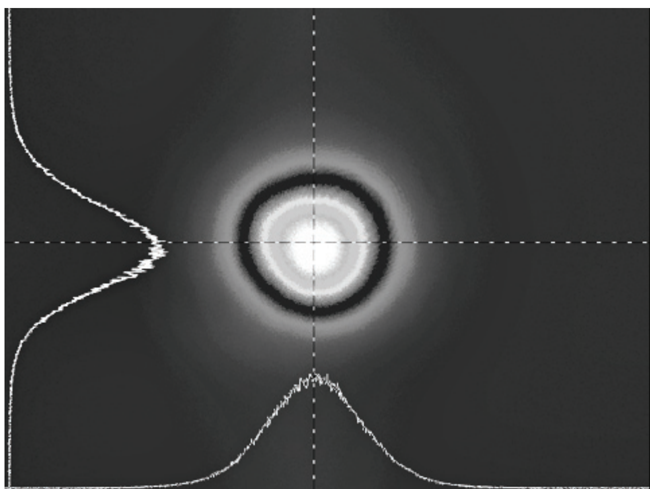

Fig. 6. Spatial profile of 1119 nm OPSL output.

Fig. 7 shows a scanning Fabry-Perot trace for the OPSL output. The output is seen to be single longitudinal mode (SLM) due to the line narrowing of the birefringent filter and the etalon. As noted above, certain wavelengths exhibited stable SLM operation with just the birefringent filter in the laser cavity but this SLM operation was not maintained as the laser wavelength was tuned and was easily interrupted by mechanical disturbance of the laser. Micro-etalon effects in the gain chip may be the reason for particular wavelengths operating SLM with just the BRF.

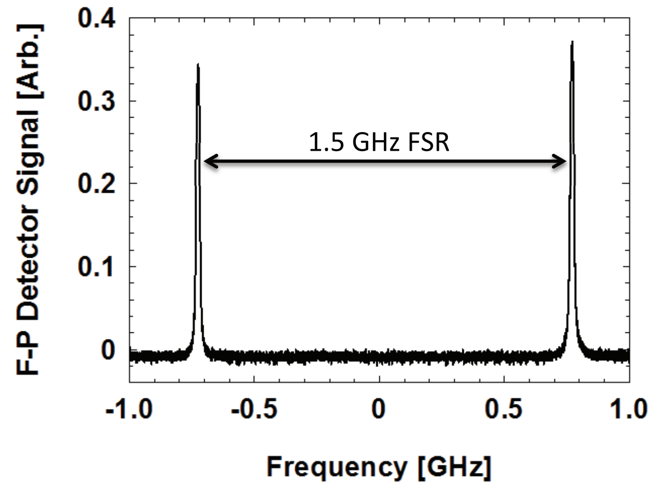

Fig. 7. Scanning Fabry-Perot (1.5 GHz Free Spectral Range) trace for the 1119 nm OPSL output.

We verified the OPSL could be tuned to the 1118.542 nm wavelength required for frequency quadrupling to obtain the 280 nm resonant wavelength of Mg II. Fixed wavelength operation with temperature stabilization resulted in SLM operation for many minutes with only passive cavity length stabilization – constant PZT voltage and a laser breadboard enclosure. The linewidth of the OPSL output was estimated by locking the laser to the side of a Fabry-Perot fringe (Fig. 7) using a commercial ‘lockbox’ with proportional and integral feedback to the cavity mirror PZT. Analysis of the error signal resulted in a 0.9 MHz root-mean-square frequency deviation over 200 ms.

B. 1178/589 nm laser

The 1178 nm OPSL was operated in two-mirror and three-mirror configurations. The 1178 nm output power of the two-mirror cavity using a cooling water temperature of 15 °C is shown in Fig. 8 for the bare cavity, cavity with birefringent filter, and cavity with birefringent filter & etalon. The maximum output power, ~12 W, was obtained for an output coupler with reflectivity of 97.5%. The maximum output power dropped by only ~10% with the additional intra-cavity elements required for reliable single-frequency operation. The additional loss of the BRF and etalon does however, lower the pump power at which thermal rollover is observed. This is not surprising given the low-gain nature of ‘vertical’ semiconductor lasers - due to the very short gain length. Subsequent work using gain chips from the same wafer and

Copyright (c) 2013 IEEE. Personal use is permitted. For any other purposes, permission must be obtained from the IEEE by emailing pubs-permissions@ieee.org.

This is the author's version of an article that has been published in this journal. Changes were made to this version by the publisher prior to publication.
The final version of record is available at http://dx.doi.org/10.1109/JQE.2013.2270912

lower operating temperatures reported up to 14.2 W of 1178 nm output power with a BRF in the cavity [19].

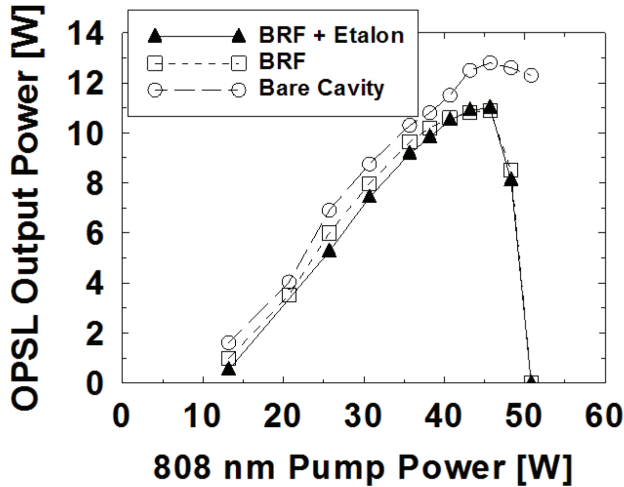

Fig. 8. Output power of the two-mirror OPSL cavity operating at ~1178 nm.

Fig. 9 shows the broad tuning obtained with the 1178 nm OPSL using a two-mirror cavity with the etalon removed and a pump power of 26 W. The OPSL tuning was obtained by angle tuning the BRF; the observed tuning range of over 30 nm is typical of OPSL technology. The peak of the tuning curve is slightly below the desired wavelength of 1178 nm at this pump power level, as expected from the photoluminescence peak wavelength being below 1178 nm. Thus the gain structure is well suited for high power 1178 nm operation. Note that the temperature of the gain region during laser operation is higher than the temperature during photoluminescence measurements (Fig. 2) resulting in a peak laser wavelength closer to the operational wavelength of 1178 nm than the peak of the luminescence.

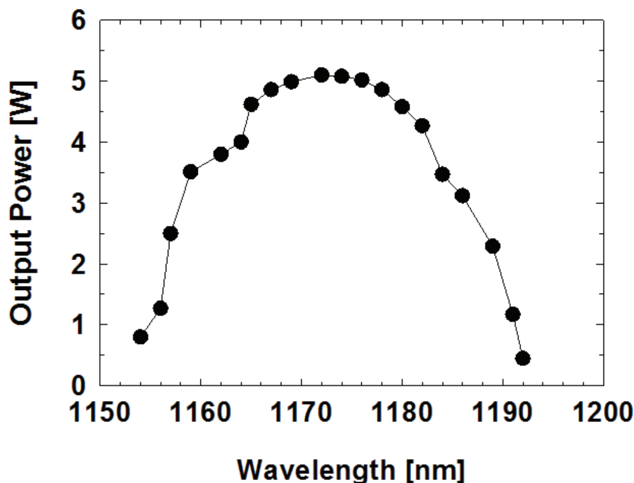

Fig. 9. Output power of the two-mirror OPSL cavity tuned in the vicinity of 1178 nm with the birefringent filter.

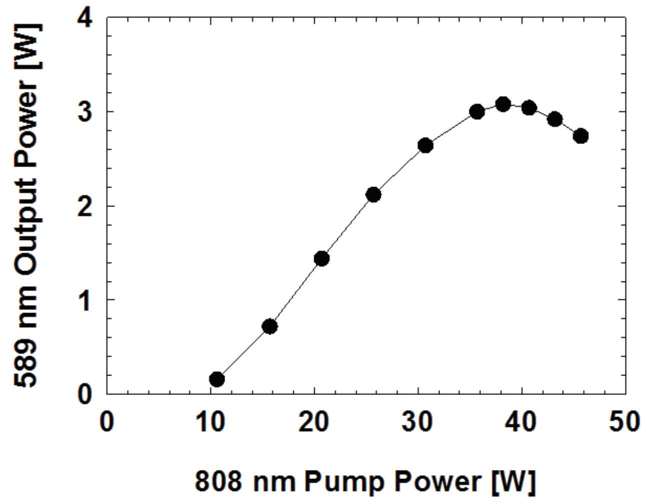

Fig. 10. Output power of the frequency-doubled, three-mirror OPSL cavity producing ~589 nm.

The frequency-doubled output power of the three-mirror OPSL is shown in Fig. 10 where the 589 nm output power is the sum of yellow emitted from the two bulk cavity mirrors (two beams). We obtain a maximum of 3.1 W at a pump power of 38 W for a pump diode-to-yellow efficiency of 8%. This efficiency is similar to results in the literature for mostly non-SLM OPSLs [27-29] but is less than the highest efficiency of ~30% obtained for non-SLM operation [30-32].

The SHG conversion efficiency has not been optimized, primarily due to limitations of optics we had available. Based on the fundamental performance shown in Fig. 8 we can estimate an intra-cavity fundamental laser power of 480 W (12W/0.025 for 2.5% output coupling) each way. Given the additional loss of the LBO crystal we might reasonably expect 300-400 W of intra-cavity power. Assuming optimum output coupling with the LBO crystal is slightly less than fundamental operation, say 2%, we can readily focus into a 15 mm LBO crystal with 300-400 W to produce the desired 2% loss of the fundamental, resulting in 6-8 W of SHG output. Thus, we expect that the optimization of the waist size in the LBO crystal would result in roughly twice as much SHG output than we observed.

Fig. 11 shows the spatial profile of the 589 nm beam for an output power of 3.1 W. As with the 1119 nm output discussed above, we did not make a quantitative measurement of the beam quality to verify TEM00 operation. Disregarding the high-frequency structure due to an experimental measurement artifact, the beam is seen to be single peaked with reasonable azimuthal symmetric.

Copyright (c) 2013 IEEE. Personal use is permitted. For any other purposes, permission must be obtained from the IEEE by emailing pubs-permissions@ieee.org.

This is the author's version of an article that has been published in this journal. Changes were made to this version by the publisher prior to publication.
The final version of record is available at http://dx.doi.org/10.1109/JQE.2013.2270912

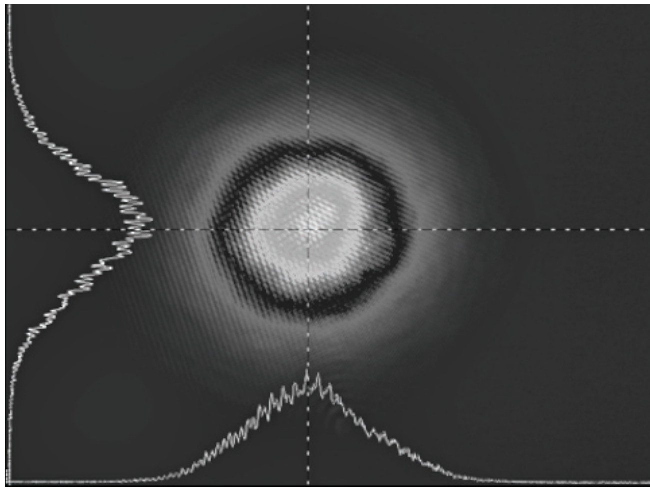

Fig. 11. Spatial profile of the 589 nm OPSL output. The high-frequency structure is an experimental artifact.

Fig. 12 shows the scanning Fabry-Perot data obtained by sending both the 1178 nm and the 589 nm light through the scanning Fabry-Perot. Both wavelengths are seen to be single frequency and the 589 nm trace shows a PZT period of half the 1178 nm trace, as expected. The short-term (seconds) frequency stability of the 1178 nm output was observed to be of order 10 MHz as determined from amplitude fluctuations observed with fixed Fabry-Perot voltage. The long-term wavelength drift over a few hours was observed to be ±1 pm (~220 MHz) as determined by the wavelength meter. Tuning of the 589 nm output is accomplished by temperature tuning the BRF and etalon along with cavity length tuning with the mirror PZT.

A scan of the 589 nm output through the sodium D2 transition is shown in Fig. 13. Many astronomical observatories use the sodium D2 transition for laser guide star work. The plotted absorption signal is obtained using a balanced detector that subtracts the detected light transmitted through the sodium cell from a portion of the beam incident on the sodium cell. The sodium cell is 7.5 cm long and heated to 77 °C. The model data shown in Fig. 13 is obtained by calculating the lineshape obtained from Doppler broadened D2a and D2b transitions separated by 1.8 GHz. Though the signal-to-noise ratio is limited, the observed absorption agrees well with the modeled absorption lineshape.

V. Summary

We demonstrated continuously tunable, high power, single-frequency output at 1119 nm, 1178 nm, and 589 nm. The 589 nm result is the first multi-watt, single-frequency OPSL reported in the literature with continuous tuning at the sodium resonance. The demonstrated OPSL output wavelengths, powers, and frequency characteristics are consistent with requirements for a number of precision spectroscopic applications and in the case of the 589 nm laser is sufficient for stimulating the formation of laser guide stars in the upper atmosphere. OPSLs are well suited to these applications because the materials can be tailored to meet the wavelengths of interest and multi-watt output power can be achieved in reasonably compact packages. Tunable single frequency operation is obtained with straightforward optical techniques. Future endeavors involve reducing the footprint of the lasers for instrumentation applications and scaling to higher power for guide star applications.

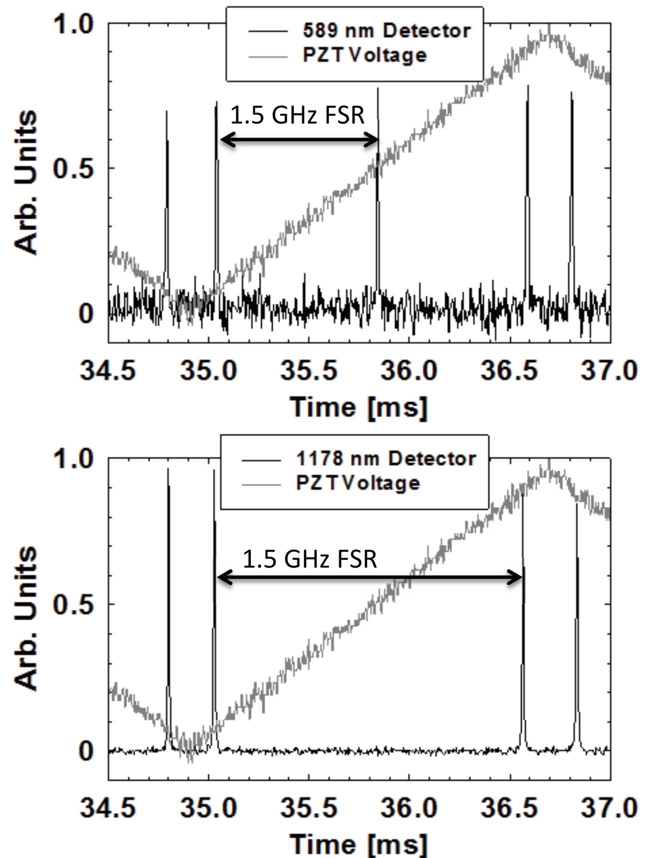

Fig. 12. Scanning Fabry-Perot (1.5 GHz FSR) traces for the three-mirror OPSL cavity operating at 1178 nm (lower trace) and intra-cavity frequency-doubled to produce 589 nm (upper trace). The gray trace shows the voltage ramp applied to the PZT on the cavity fold mirror.

Copyright (c) 2013 IEEE. Personal use is permitted. For any other purposes, permission must be obtained from the IEEE by emailing pubs-permissions@ieee.org.

This is the author's version of an article that has been published in this journal. Changes were made to this version by the publisher prior to publication.
The final version of record is available at http://dx.doi.org/10.1109/JQE.2013.2270912

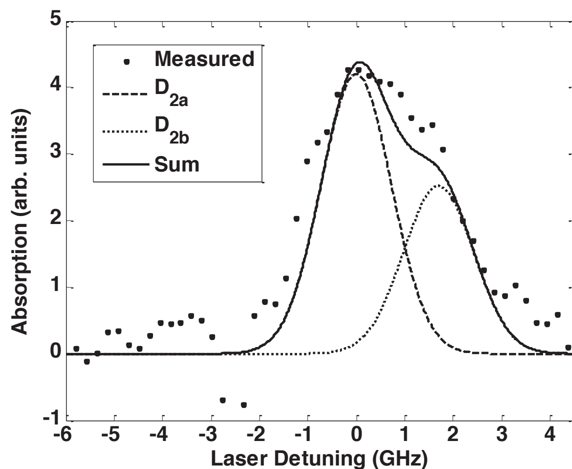

Fig. 13. Measured absorption signal (points) recorded while scanning the 1178/589 nm OPSL through the Na D2 resonance. The solid curves show the modeled absorption for the Doppler broadened Na D2a and D2b components as well as the total resulting absorption.

ACKNOWLEDGMENT

R. J. Epstein and G. J. Fetzer, acknowledge many fruitful discussions with Dr. J. T. Murray.

REFERENCES

[1] M. C. Liu, "Astronomical science with laser guide star adaptive optics: a brief review, a current snapshot, and a bright future," *Proc. SPIE*, vol. 6272, pp. 62720H-62720H-11, 2006.

[2] I. K. Kominis, T. W. Kornack, J. C. Allredm, and M. V. Romalis, "A sub femtotesla multichannel atomic magnetometer," *Nature,* vol. 422, pp. 596-599, 2003.

[3] V. Acosta, M. P. Ledbetter, S. M. Rochester, D. Budker, D. F. Jackson-Kimball, D. C. Hovde, W. Gawlik, S. Pustelny, J. Zachrowski, and V. V. Yashchuk, "Nonlinear magneto-optical rotation with frequency modulated light in the geophysical field range," *Phys. Rev. A*, vol. 73, pp. 53404-53411, 2006.

[4] T. L. Gustavson, P. Bouyer, and M. A. Kasevich, "Precision Rotation Measurements with an Atom Interferometer Gyroscope," *Phys. Rev. Letters*, vol. 78, pp. 2046-2049, 1997.

[5] S. Bize, P. Laurant, M. Abgrall, H. Marion, I. Maksimovic, I. Cacciapuoti, J. Grunert, C. Vinn, F. Pereira dos Santos, P. Rosenbusch, P. Lemonde, G. Santarelli, P. Wolf, A. Clarion, A. Luiten, M. Tobar, and C. Salomon, "Cold atom clocks and applications," *J. Phys B*, vol. 38, pp. S449-478, 2005.

[6] H. Häffner, C.F. Roos, and R. Blatt, "Quantum computing with trapped ions," *Physics Reports*, vol. 469, pp. 155-203, 2008.

[7] J. P. Home, D. Hanneke, J. D. Jost, J. M. Amini, D. Leibfried, and D. J. Wineland, "Complete methods set for scalable ion trap quantum information processing," *Science* vol. 325**,** pp.1227-1230, 2009.

[8] D. J. Wineland, "Quantum information processing and quantum control with trapped atomic ions," *Phys. Scr*, vol. T137, pp. 1- 11, 2009.

[9] M. Kuznetzov, "VECSEL Semiconductor Lasers: A Path to High-Power, Quality Beam and UV to IR Wavelength by Design," in *Semiconductor Disk Lasers. Physics and Technology*, Oleg G. Okhotnikov, Ed., WILEY-VCH Verlag GmbH & Co. KGaA, Weinheim, 2010, pp. 1-72.

[10] A. Laurain, M. Myara, G. Beaudoin, I. Sagnes, and A. Garnache, "Multiwatt-power highly-coherent compact single-frequency tunable vertical-external-cavity-surface-emitting-semiconductor-laser", *Optics Express*, vol. 18, pp. 14627-14636, 2010.

[11] S. Ranta, M. Tavast, T. Leinonen, R Epstein, and M Guina, "Narrow linewidth 1118/559 nm VECSEL based on strain compensated GaInAs/GaAs quantum-wells for laser cooling of Mg-ions," *Opt. Mat. Express*, vol. 2, pp. 1011-1019, 2012.

[12] A. Garnache, A. A. Kachanov, F. Toceckel, and R Houdre, "Diode pumped broadband vertical-external-cavity surface-emitting semiconductor laser applied to high sensitivity intracavity absorption spectroscopy," *J. Opt. Soc. Am. B*, vol. 17, pp. 1589-1598, 2000.

[13] M. A. Holm, D. Ferguson, and M. D. Dawson, "Actively stabilized single frequency vertical-external-cavity AlGaAs laser," *IEEE Photon. Technol. Lett.*, vol. 11, pp. 1551–1553, 1999.

[14] R. H. Abram, K. S. Gardner, E. Riis, and A. I. Ferguson, "Narrow linewidth operation of a tunable optically pumped semiconductor laser," *Opt. Express*, vol. 12, pp. 5434–5439, 2004.

[15] B. Cocquelin, D. Holleville, G. Lucas-Leclin, I. Sagnes, A. Garnache, M. Myara, and P. Georges, "Tunable single-frequency operation of a diode-pumped vertical external-cavity laser at the cesium D2 line," *Appl. Phys. B*, vol. 95, pp. 315–321, 2009.

[16] F. A. Camargo, J. Barrientos, G. Baili, L. Morvan, D. Dolfi, D. Holleville, S. Guerandel, I. Sagnes, P. Georges, and G. Lucas-Leclin, "Coherent Dual-Frequency Emission of a Vertical External-Cavity Semiconductor Laser at the Cesium D2 Line," *IEEE Photonics Tech. Letters*, vol. 24, pp. 1218-1220, 2012.

[17] J. Paul, Y. Kaneda, T.-L. Wang, C. Lytle, J. V. Moloney, and R. J. Jones, "Doppler-free spectroscopy of mercury at 253.7 nm using a high-power, frequency-quadrupled, optically pumped external-cavity semiconductor laser," *Optics Letters*, vol. 36, pp. 61-63, 2011.

[18] A. R. Albrecht, D. Seletskiy, C. P. Hains, J. G. Cederberg, A. Di Lieto, M. Tonelli, G. Balakrishnan, and M. Sheik-Bahae, "Intracavity Laser Cooling Using a VECSEL," in *Quantum Electronics and Laser Science Conference (QELS)* San Jose, CA, 2012, session High Field Phenomena & Laser Cooling (QTh4E).

[19] S. Ranta, M. Tavast, T. Leinonen, N. Van Lieu, G. Fetzer, and M. Guina, "1180 nm VECSEL with output power beyond 20 W," *Electronics Letters*, vol. 49, pp.59-60, 2013.

[20] A. Friedenauer, F. Markert, H. Schmitz, L. Petersen, S. Kahra, M. Herrmann, Th. Udem, T. W. Hänsch, T. Schätz, "High power all solid state laser system near 280 nm," *Appl. Phys. B*, vol. 84, pp.371-373, 2006.

[21] B. Hemmerling, F. Gebert, Y. Wan, D. Nigg, I.V. Sherstov, and P. O. Schmidt**, "**A single laser system for ground-state cooling of $^{25}Mg^{+}$," *Appl. Phys. B*, vol. 104, pp. 583–590, 2011.

[22] C. D'Orgeville, F. Rigaut, and B. L. Ellerbroek, "LGS AO photon return simulations and laser requirements for the Gemini LGS AO program," *Proc. SPIE*, vol. 4007, pp. 131-141, 2000.

[23] J. Drummond, J. Telle, C. Denman, P. Hillman, and A. Tuffli, "Photometry of a Sodium Laser Guide Star at the Starfire Optical Range," *Publications of the Astronomical Society of the Pacific*, vol. 116, pp.278–289, 2004.

[24] J. Ge, B. P. Jacobsen, J. R. P. Angel, P. C. McGuire, T. Roberts, B. A. McLeod, and M. Lloyd-Hart, "Simultaneous measurements of sodium column density and laser guide star brightness," *Proc. SPIE*, vol. 3353, pp. 242-253, 1998.

[25] A. C. Tropper and S. Hoogland, "Extended cavity surface-emitting semiconductor lasers," *Progress in Quantum Electronics*, vol. 30, pp. 1-43, 2006.

[26] C. Borgentun, C. Hessenius, J. Bengtsson, M. Fallahi, and A. Larsson, "Widely Tunable High-Power Semiconductor Disk Laser With Nonresonant AR-Assisted Gain Element on Diamond Heat Spreader," *IEEE Photonics J.*, vol. 3, pp. 946-953, 2011.

[27] S. Calvez, J. E. Hastie, M. Guina, O. G. Okhotnikov, and M. D. Dawson, "Semiconductor disk lasers for the generation of visible and ultraviolet radiation," *Laser & Photon. Rev.* vol. 3, pp. 407–434, 2009.

[28] A. J. Maclean, A. J. Kemp, S. Calvez, J. Kim, T. Kim, M. D. Dawson, and D. Burns, "Continuous Tuning and Efficient Intracavity Second-Harmonic Generation in a Semiconductor Disk Laser With an Intracavity Diamond Heatspreader," *IEEE J. Quantum Electronics*, vol. 44, pp. 216-225, 2008.

[29] S. Hilbich, W. Seelert, V. Ostroumov, C. Kannengiesser, R. Elm, and J. Mueller, "New wavelengths in the yellow orange range between 545 nm to 580 nm generated by an intracavity frequency-doubled optically pumped semiconductor laser," *Proc. of SPIE*, vol. 6451, pp. 64510C-1-64510C-7, 2007.

[30] S. Lutgen, M. Kuehnelt, U. Steegmueller, P. Brick, T. Albrecht, W. Reill, J. Luft, B. Kunert, S. Reinhard, K. Volz, and W. Stolz, "Green semiconductor disk laser with 0.7W cw output power" *Proc. of SPIE*, vol. 5737, pp. 109-112, 2005.

[31] L. E. Hunziker, Q. Shu, D. Bauer, C. Ihli, G. J. Mahnke, M. Rebut, J. R. Chilla, A. L. Caprara, H. Zhou, E. S. Weiss, and M. K. Reed, "Power-

Copyright (c) 2013 IEEE. Personal use is permitted. For any other purposes, permission must be obtained from the IEEE by emailing pubs-permissions@ieee.org.

This is the author's version of an article that has been published in this journal. Changes were made to this version by the publisher prior to publication.
The final version of record is available at http://dx.doi.org/10.1109/JQE.2013.2270912

scaling of optically-pumped semiconductor lasers," *Proc. of SPIE*, vol. 6451, pp. 64510A-1-64510A-6, 2007.

[32] L. E. Hunziker, C. Ihli, and D. S. Steingrube, "Miniaturization and power scaling of fundamental mode optically pumped semiconductor lasers," *IEEE J. Sel. Topics in Quantum Electronics*, vol. 13, pp. 610-618, 2007.

William J. Alford received his B.S. degree in physics in 1979 from the University of Arizona, Tucson, AZ. He received his M.S. and Ph.D. degrees in physics in 1981 and 1984 from the University of Colorado, Boulder, CO.

He was with Sandia National Labs from 1984 to 2001, initially as a postdoc and subsequently as a member of technical staff. He carried out laser and nonlinear optics research and development while at Sandia. He was with Coherent Technologies, Inc. (later Lockheed Martin Coherent Technologies) from 2001 to 2011. He carried out laser and nonlinear optics research and development and managed the laser and nonlinear optics group while at CTI. He is currently a consultant on lasers and nonlinear optics based out of Lafayette, Colorado.

Dr. Alford is a member of the Optical Society of America.

Gregory J. Fetzer received his B. S., M. S., and Ph.D. degrees in electrical engineering in 1980, 1982, and 1990 from Colorado State University, Fort Collins, CO.

He joined Areté Associates in 1997 and has been involved in a wide variety of electro-optics system development efforts. He currently leads efforts in laser radar, laser absorption spectroscopy, hollow optical waveguides, laser induced fluorescence, and a variety of other sensor-based activities at the Longmont, Colorado office of Areté Associates.

Dr. Fetzer is a member of the Optical Society of America and SPIE.

Ryan J. Epstein received a PhD in condensed matter physics from UC Santa Barbara in 2005. He was with Areté Associates from 2007 until 2012 where he was involved in LIDAR and laser system development. He is currently with Lockheed Martin in Littleton Colorado..

Sandalphon received his B.S. degree in physics in 1985 from San Diego State University, San Diego, CA. He received his M.S. and Ph.D. degrees in Optical Sciences in 1990 and 1997 from the University of Arizona, Tucson, AZ.

He worked for large and small companies in R&D for optical data storage, biometrics, and remote sensing. In 2009 he founded Cinnabar Optics LLC to consult on advanced R&D optoelectronic systems.

Dr. Sandalphon is a member of the Optical Society of America.

Neil Van Lieu received his B.S. degree in optics in 1990 from the University of Rochester, Rochester, New York.

He joined Areté Associates in 2007, after previous R&D, engineering, design, and manufacturing experience at various organizations, in the fields of laser fusion, biomedicine, thin film coating, vacuum technology, flat panel displays, polarization optics, telecommunications, spectroscopy, and unconventional energy exploration. He currently creates opto-mechanical systems for a variety of lasers, laser radar, and electro-optical sensors in the Longmont, Colorado office of Areté Associates**.**

Sanna Ranta received her M.Sc. degree in Science and Engineering in 2009 from Tampere University of Technology (TUT), Finland, where she is currently working towards a Doctorate degree. She joined Optoelectronics Research Centre at TUT in 2005 initially as an undergraduate student, and after graduation as a postgraduate student. Her research interests include design and fabrication of visible and near infrared vertical external-cavity surface-emitting semiconductor lasers.

Miki Tavast was born in Tampere, Finland in 1986. He joined the Optoelectronics Research Centre at the Tampere University of Technology in 2009 and is currently working on the epitaxial growth of III-V semiconductors. In the course of this work he has coauthored six refereed journal articles. Currently, he is working towards his Masters degree.

Tomi Leinonen joined Tampere University of Technology in 1999 and has since been involved in the development of numerous edge and surface emitting semiconductor lasers. He received his M.Sc. and D.Sc. in 2002 and 2007 in Tampere, and is currently the principal investigator of 1100-1200 nm and visible high-power Vertical-External-Cavity Surface-Emitting Lasers. He has published 30 papers in international peer-reviewed journals and has over 50 international peer-reviewed conference publications (2 invited).

Mircea Guina obtained the Ph.D. degree in physics from Tampere University of Technology, Finland, in 2002. In 2008 he was appointed professor and Head of the semiconductor technology division of the Optoelectronics Research Centre, Tampere University of Technology. His research interests include the development of new epitaxial techniques, such as site controlled epitaxy and epitaxy of novel III-V heterostructures, and the development of novel optoelectronic devices, with current focus on visible and mid-IR VECSELs and high efficiency solar cells. He has published more than 100 journal papers, several book chapters, holds 4 international patents, and has given numerous invited talks at major optoelectronics conferences. He is the chairman of COST Action MP0805 and the Director of the International Summer School "New Frontiers in Optical Technologies", which he established in 2003.

Copyright (c) 2013 IEEE. Personal use is permitted. For any other purposes, permission must be obtained from the IEEE by emailing pubs-permissions@ieee.org.

Publication 4

S. Ranta, M. Tavast, T. Leinonen, N. Van Lieu, G. Fetzer, and M. Guina, "1180 nm VECSEL with output power beyond 20 W," *Electronics Letters*, vol. 49, no. 1, pp. 59–60, 2013

© 2013 The Institution of Engineering and Technology. Reproduced with permission.

1180 nm VECSEL with output power beyond 20 W

S. Ranta, M. Tavast, T. Leinonen, N. Van Lieu, G. Fetzer and M. Guina

We report the highest power result for an optically-pumped single-chip vertical external-cavity surface-emitting laser with emission near 1180 nm. The gain mirror was grown by molecular beam epitaxy and incorporated a strain compensated GaInAs/GaAs/GaAsP active region. An intra-cavity diamond heat spreader was attached to the gain mirror for thermal management. In free-running operation, the laser emitted more than 20 W at a mount temperature of about 12 ºC. The output spectrum was centred between 1165–1190 nm depending on the mount temperature and pump power. By using an intracavity birefringent filter, we were able to narrow the full width at half-maximum linewidth to ≤1 nm and at the same time achieved approximately 14 W of output power near 1178 nm. Moreover, the lasing wavelength could be tuned over more than 40 nm.

Introduction: High-power lasers emitting at 1160–1200 nm [1–3] have recently gained increased attention due to their ability to generate yellow-orange radiation via second harmonic generation (SHG).

Vertical external-cavity surface-emitting lasers (VECSELs) that use GaInAs/GaAs/GaAsP gain mirrors have proven to be suitable for high power operation near 1000–1120 nm spectral range [4–5]. However, the high lattice strain associated with the high indium (In) composition of the GaInAs quantum wells (QWs) has hampered the use of this material system for longer wavelengths (1160–1200 nm) that are required for generating yellow-orange radiation. The highest output power reported for an 1175 nm GaInAs/GaAs/GaAsP VECSEL gain material grown by metal-organic vapour-phase epitaxy (MOVPE) is ~8 W [3]. Alternatively, we have developed GaInNAs/GaAs/GaAsN gain material by molecular beam epitaxy (MBE), where the QWs are less strained, which led to the demonstration of 11 W at ~1180 nm [6].

In this Letter, we demonstrate that MBE-grown GaInAs/GaAs/GaAsP gain chip is also capable of emitting high output powers at the challenging wavelength of ~1180 nm, which corresponds to yellow spectral range after SHG.

Experimental setup: The VECSEL consisted of a gain mirror and a curved output coupler that formed a straight I-cavity, as shown in Fig. 1. The radius of curvature (RoC) of the coupler was 150 mm, and the spacing between the gain chip and the cavity end mirror was ~150 mm.

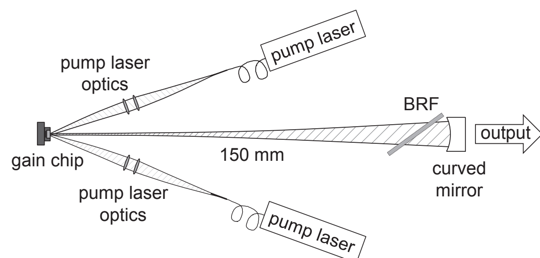

Fig. 1 *Illustration of the I-cavity laser setup. The birefringent filter (BRF) was used in the wavelength tuning experiment.*

The GaInAs/GaAs/GaAsP gain medium was grown by MBE and comprised a total of 10 QWs with a target In composition of ~37% (nominal) in order to reach the 1178 nm emission wavelength during laser operation. The gain mirror design was similar to the 1120 nm structure described in [7] except for the increased amount of In in the QWs and the use of 2 nm thicker strain compensation layers. In comparison to the structure reported in [7], we reduced the QW growth temperature from 545 °C to 460 °C to avoid relaxation of the QWs; a lower growth temperature increases the critical thickness of the GaInAs layer [8].

In order to remove the heat efficiently, the gain mirror was cut into 2.5 mm × 2.5 mm chips that were capillary bonded [9] from the epi-side to an intra-cavity diamond (3 mm × 3 mm × 0.3 mm) heat spreader. The bonded chip was then attached to a copper mount. The mount was cooled with a 30-percent-by-volume ethanol-water solution that flew at a rate of 1 l/min during laser operation. The diamond surfaces were specified to be flat and parallel to each other but in reality we noticed that the surfaces formed a slight wedge (<1°); this was observed by inspecting laser beam reflections from the two surfaces.

The VECSEL was pumped with two fibre-coupled 808-nm diode laser pump modules that were capable of providing a combined incident pump power of approximately 100 W when focused to a 540 µm (diameter) sized spot. The focused laser beams were adjusted with the aid of a camera to form a single spot on the gain mirror.

Results: In order to find the optimal laser configuration for high power operation, the VECSEL output power was measured using various partially reflecting cavity end mirrors (95.5–98.5%; RoC = 150 mm). The coolant was set to 5 °C for this experiment, and the mount temperature was monitored with a thermocouple, since the temperature varied with the pump laser power. The resulting output power for each cavity output coupler as a function of the incident pump power is plotted in Fig. 2. The highest output powers and slope efficiencies were achieved with a 97% reflective output coupler resulting in ~20.5 W of output power and ~33% slope efficiency with a mount temperature of 12.3 °C. The measurement was repeated using the 97% reflective mirror at a coolant temperature of -10 °C in order to achieve even higher output powers. This configuration produced 23 W and a mount temperature of ~0 °C.

The increase in output power in comparison to what was reported in [6] is likely due to a combination of two factors. First, there is no nitrogen in gain mirror that can cause non-radiative recombination and limit the performance. Secondly, we used a redesigned mount thereby improving heat removal. The heat dissipation from the new mount was limited by the cooling system flow capacity.

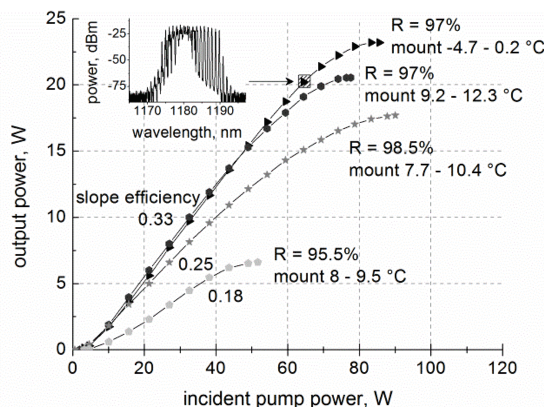

Fig. 2 *Output power characteristics for different reflectivities (R) of the cavity end mirror and mount temperatures.*
Inset Spectrum measured at the indicated operating point.

The VECSEL emission spectrum was recorded at various output power levels using 97% reflective output coupler. For a mount temperature of 9–12 °C (coolant set to 5 °C), the centre of the emission was observed to redshift by ~25 nm from 1165 nm to 1190 nm when the incident pump power was increased from 1.9 W (threshold) to 77 W (20.5 W output). For a mount temperature of -4–0 °C (coolant set to -10 °C) the corresponding redshift extended from 1160 to 1188 nm corresponding to a variation of the output power from threshold to 23.2 W. The wavelength shift was caused by the increased operating temperature with increasing pump power. The inset of Fig. 2 shows the measured spectrum at the output power of 20.2 W (64.4 W pump power) and mount temperature of -0.9 °C. The distinct peaks seen in the output spectrum are a result of an etalon effect caused by the intra-cavity diamond; the peak spacing of ~1 nm corresponds to the free spectral range of the diamond.

A 1.5 mm thick uncoated BRF (quartz), positioned at Brewster's angle inside the cavity, was used to tune the output wavelength and to

narrow the emission linewidth. The midpoint of the BRF was located ~10 mm away from the curved cavity end mirror. A 98.5% output coupler was chosen to compensate for losses caused by the BRF. The coolant temperature was 5 °C, and the measurement was performed at 85.6 W and 43.6 W pump powers. Corresponding mount temperatures for these pump powers were 11–13 °C and 9–10 °C for 85.6 W and 43.6 W, respectively.

The measured tuning curves are shown in Fig. 3. The highest output power of ~14.2 W was reached at 85.6 W pump power at ~1179 nm. The emission spectra had a full width at half-maximum (FWHM) linewidth of ≤1 nm for this pump power. The tuning bandwidth was ~40 nm (FWHM). A slightly wider tuning bandwidth of 45 nm was achieved at 43.6 W pump power. The VECSEL emitted a maximum of ~7 W at ~1170 nm in ≤0.6 nm wide spectrum for a pump power of 43.6 W.

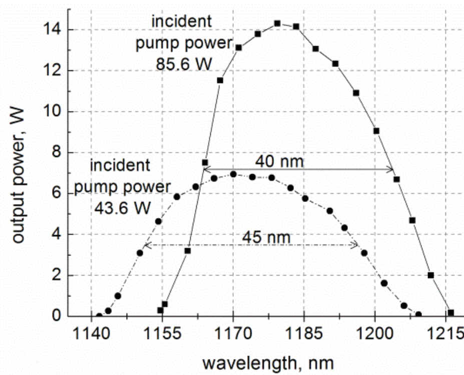

Fig. 3 *Wavelength tuning curves measured with a 98.5% reflective cavity end mirror and a 1.5 mm thick BRF at 85.6 W (mount at 11–13 °C) and 43.6 W (mount at 9–10 °C) pump powers.*

Conclusion: We have achieved more than 20 W of output power from a single-chip VECSEL emitting at around 1180 nm. The key element for this demonstration was the MBE-grown GaInAs/GaAs/GaAsP gain chip. Emission line narrowed output was obtained over a 40 nm tuning range using an intra-cavity BRF.

Acknowledgments: This work was supported by Areté Associates, TEKES Brightlase (project 40048/12), graduate school of Tampere University of Technology, and Jenny and Antti Wihuri Foundation.

S. Ranta, M. Tavast, T. Leinonen and M. Guina (*Optoelectronics Research Centre, Tampere University of Technology, Korkeakoulunkatu 3, FIN-33101 Tampere, Finland*)

E-mail: sanna.ranta@tut.fi

N. Van Lieu and G. Fetzer (*Areté Associates, 2500 Trade Center Ave Suite A, Longmont, CO 80503, United States*)

References

1 Fan, L., Hessenius, C., Fallahi, M., Hader, J., Li, H., Moloney, J.V., Stolz, W., Koch, S.W., Murray, J.T., and Bedford, R. : ‘Highly strained InGaAs/GaAs multiwatt vertical-external-cavity surface-emitting laser emitting around 1170 nm’ *Appl. Phys. Lett.*, 2007, **91**, p. 131114

2 - nen, A., and Guina, M. : ‘7.4W yellow GaInNAs-based semiconductor disk laser’, *Electron. Lett.*, 2011, **47**, (20), pp.1139–1140

3 Fallahi, M., Fan, L., Kaneda, Y., Hessenius, C., Hader, J., Li, H., Moloney, J.V., Kunert, B., Stolz, W., Koch, S.W., Murray, J., and Bedford, R. : ‘5-W yellow laser by intracavity frequency doubling of high-power vertical-external-cavity surface-emitting laser’, *IEEE Photon. Technol. Lett.*, 2008, **20**, (20), pp.1700–1702

4 Heinen, B., Wang, T.-L., Sparenberg, M., Weber, A., Kunert, B., Hader, J., Koch, S.W., Moloney, J.V., Koch, M., and Stolz, W. : ‘106 W continuous-wave output power from vertical-external-cavity surface-emitting laser’, *Electron. Lett.*, 2012, **48**, (9), pp. 516–517

5 Rudin, B., Rutz, A., Hoffmann, M., Maas, D.J.H.C., Bellancourt, A.-R., Gini, E., Südmeyer, T., and Keller, U. : ‘Highly efficient optically pumped vertical-emitting semiconductor laser with more than 20 W average output power in a fundamental transverse mode’, *Opt. Lett.*, 2008, **33**, (22), pp. 2719–2721

6 Korpijärvi, V.-M., Leinonen, T., Puustinen, J., Härkönen, A., and Guina, M.D. : ‘11 W single gain-chip dilute nitride disk laser emitting around 1180 nm’, *Opt. Express*, 2010, **18**, (25), pp. 25633–25641

7 Ranta, S., Tavast, M., Leinonen, T., Epstein, R., and Guina, M. : ‘Narrow linewidth 1118/559 nm VECSEL based on strain compensated GaInAs/GaAs quantum-wells for laser cooling of Mg-ions’, *Opt. Mater. Express*, 2012, **2**, (8), pp. 1011–1019

8 Wang, S.M., Andersson, T.G., and Ekenstedt, M.J. : ‘Temperature-dependent transition from two-dimensional to three-dimensional growth in highly strained $In_xGa_{1-x}As/GaAs$ ($0.36 \le x \le 1$) single quantum wells’, *Appl. Phys. Lett.*, 1992, **61**, (26), pp. 3139–3141

9 Liau, Z.L. : ‘Semiconductor wafer bonding via liquid capillarity’, *Appl. Phys. Lett.*, 2000, **77**, (5), pp. 651–653

Publication 5

S. Ranta, A. Härkönen, T. Leinonen, L. Orsila, J. Lyytikäinen, G. Steinmeyer, and M. Guina, "Mode-locked VECSEL emitting 5 ps pulses at 675 nm," *Optics Letters*, vol. 38, no. 13, pp. 2289–2291, 2013.

© 2013 Optical Society of America. Reproduced with permission.

This paper was published in Optics Letters and is made available as an electronic reprint with the permission of OSA. The paper can be found at the following URL on the OSA website: http://www.opticsinfobase.org/ol/abstract.cfm?uri=ol-38-13-2289. Systematic or multiple reproduction or distribution to multiple locations via electronic or other means is prohibited and is subject to penalties under law.

Mode-locked VECSEL emitting 5 ps pulses at 675 nm

Sanna Ranta,[1,*] Antti Härkönen,[1] Tomi Leinonen,[1] Lasse Orsila,[1] Jari Lyytikäinen,[1] Günter Steinmeyer[2,1] and Mircea Guina[1]

[1] Optoelectronics Research Centre, Tampere University of Technology, Korkeakoulunkatu 3,33720 Tampere, Finland
[2] Max Born Institute for Nonlinear Optics and Short Pulse Spectroscopy, Max-Born-Straße 2a, 12489 Berlin, Germany
**Corresponding author: sanna.ranta@tut.fi*

Received Month X, XXXX; revised Month X, XXXX; accepted Month X, XXXX; posted Month X, XXXX (Doc. ID XXXXX); published Month X, XXXX

A picosecond GaInP/AlGaInP/GaAs vertical external-cavity surface-emitting laser at 675 nm is reported. The laser is mode-locked with a GaInP/AlGaInP/GaAs saturable absorber mirror and emitted ~5.1 ps pulses at a 973 MHz repetition rate and an average power of 45 mW. To our knowledge, this is the first demonstration of a passively mode-locked vertical external-cavity surface-emitting laser emitting fundamental laser radiation at the visible part of the spectrum.

OCIS Codes: (140.4050) Mode-locked lasers, (140.5960) Semiconductor lasers, (140.7270) Vertical emitting lasers, (140.7300) Visible lasers

Passively mode-locked vertical external-cavity surface-emitting lasers (VECSELs [1]) have been extensively studied for their advantageous properties, such as short pulses [2], high average power, compact footprint [3], and high repetition rate [4]. The standard mode-locking technique for VECSELs utilizes semiconductor saturable absorber mirrors (SESAMs) [5]. Impressive mode-locking results were demonstrated at ~1 μm wavelength range with GaInAs/GaAs gain and SESAM structures [2–4]. Alternative material systems such as InP and GaSb widen the available spectral range, enabling passively mode-locked VECSELs at 850 nm [6,7], 1.2 μm [8], 1.3 μm [9,10], 1.5 μm [11,12], and at 2 μm [13]. In this Letter, we present a 675 nm VECSEL passively mode-locked by a SESAM, which, to the best of our knowledge, emits at the shortest wavelength that has ever been reported for a mode-locked VECSEL with direct emission.

The VECSEL gain mirror structure used in this study consists of a GaInP/AlGaInP active region and an $AlAs/Al_{0.45}Ga_{0.55}As$ distributed Bragg reflector (DBR) and is similar to the one described in [14]. The active region is anti-resonant at the lasing wavelength at room temperature. No strain compensation is utilized in the structure. The gain is provided by 20 compressively strained (0.42% misfit) $Ga_{0.46}In_{0.54}P$ QWs with a thickness of 6 nm and room-temperature photoluminescence (PL) emission at 660 nm. The QWs are arranged in 10 groups of 2 QWs each and are placed uniformly at the antinodes of the optical field in the laser resonator. The groups are separated by an optical length of λ/2. Within each QW group, the two QWs are separated by a 7 nm thick $(Al_{0.6}Ga_{0.4})_{0.51}In_{0.49}P$ barrier layer. The QW groups are separated by $(Al_{0.6}Ga_{0.4})_{0.51}In_{0.49}P$ spacer layers with a thickness of 81 nm. In order to prevent oxidation of aluminum containing compounds, the structure is capped with a 10 nm thick $Ga_{0.52}In_{0.48}P$ layer. The DBR is designed for high reflection at 670 nm and consists of 40.5 pairs of alternating λ/4 AlAs and $Al_{0.45}Ga_{0.55}As$ layers.

The SESAM comprises one compressively-strained (0.86% misfit) $Ga_{0.4}In_{0.6}P$ QW with a 5 nm thickness, embedded within an $(Al_{0.6}Ga_{0.4})_{0.51}In_{0.49}P$ cavity. The $(Al_{0.6}Ga_{0.4})_{0.51}In_{0.49}P$ layer situated near the semiconductor–air surface and the layer next to the DBR are 36 and 26 nm thick, respectively. A 5 nm thick GaAs cap is used to protect the surface against rapid oxidization of the Al-containing layer. The DBR is similar to the one used for the gain mirror structure. No strain compensation is utilized, and the structure is anti-resonant at the lasing wavelength at room temperature.

The gain mirror and SESAM structures were grown on 2 inch (001) GaAs substrates by solid-source molecular beam epitaxy. The structures were characterized by measuring reflectance and photoluminescence intensity directly from as-grown samples at normal incidence (Fig. 1). From the measurement in Fig. 1(b), we deduced a 1−1.2% maximum nonlinear reflectivity change for the SESAM. The absorption recovery time of the SESAM was reduced by ion irradiation, inducing similar defect densities that previously provided sub-10 ps recovery times for GaAs-based samples at several IR operating wavelengths [15]. Given the unavailability of suitable mode-locked laser systems at 670 nm, it is currently impossible for us to verify the nonlinear SESAM characteristics.

The gain chip was cut to a size of 2.5 × 2.5 mm² and capillary bonded [16] from the epi-side to a 3 × 3 × 0.25–0.35 mm³ wedged diamond heat spreader. The gain element was clamped to a copper mount with circular aperture. For increasing the heat conductance, we used a thin indium foil between the heat spreader and the copper mount. The diamond was coated with a 2-layer TiO_2/SiO_2 anti-reflective coating to reduce pump and signal reflectance from the surface.

After processing, the mounted gain chip was placed in a Z-shaped cavity (Fig. 2), with the SESAM acting as one of the end mirrors and a curved output coupler as the opposite end mirror. The laser was pumped through the diamond heat spreader with a continuous-wave (*cw*) 532 nm laser. During pumping, the laser was cooled by water circulating through the copper mount at 10 °C. The pump spot diameter on the gain chip was ~115 μm, and the laser mode diameter on the SESAM was ~20 μm.

The average output power of the laser was measured with a thermal power meter, either using the SESAM or a

highly reflective mirror instead [Fig 3(a)]. The *cw* lasing threshold was reached at 2.25 W, with a maximum output of 143 mW at 5.5 W pump power and 10 °C water cooling temperature. The slope efficiency was 4.5%. Using a lower cooling temperature of 5 °C for the gain chip, the maximum output power increased to 186 mW at 5.9 W pumping. Inserting the SESAM as cavity end mirror, the lasing threshold increased to 3.6 W, and the maximum output power decreased to 45 mW at 5.2 W pump, yielding a slope efficiency of 3.2%. These mode-locking results were obtained at 10 °C cooling water temperature. The output power deteriorated after several hours of operation in the mode-locked as well as *cw* mode. Slight modification of the gain chip position restored high output powers, which indicates a slow degradation of the gain chip at elevated pump levels. A typical laser pulse train, measured with a 20 GHz sampling oscilloscope and a 40 GHz photo diode (New Focus Model 1004) is shown in Fig 3(b), indicating clean single-pulse mode-locked operation. The same signal was analyzed with a 26.5 GHz spectrum analyzer using a resolution bandwidth of 100 kHz. Fig. 4(a) indicates a nearly flat spectral response with apparent sinusoidal variations that originate from a mismatch of the source impedance of the diode (100 Ω). The fundamental intermode beat at 972.7 MHz was analyzed in more detail employing a 1 GHz photodiode at a resolution bandwidth of 100 Hz [Fig. 4(b)] and exhibits a >60 dB side band mode suppression ratio. The spectrum contains side peaks at 200 kHz offset frequency, which clearly relate to an amplitude modulation of the pump laser, see inset in Fig. 4 (b).

The laser output was further analyzed by optical characterization methods. Fig. 5 shows the optical spectrum centered at 675.8 nm and the beam profile measured with a CCD camera. The spectral width is 0.14 ± 0.05 nm full width at half maximum (FWHM), and the beam profile appears to be clean yet slightly elliptic. Pulse shapes were characterized with an SHG-based intensity autocorrelator. The autocorrelation trace exhibits a width of ~10 ps [Fig. 6(a)], with extended wings that are incompatible with symmetric Gaussian or hyperbolic secant pulses. We employed the PICASO method [17] to obtain an estimate for the underlying pulse structure and duration. This method indicates an asymmetric optical pulse shape with a FWHM width of 5.1 ps [Fig. 6(b)], which is 3.75 times above the transform limit. Based on this pulse shape, we estimate a laser peak power of 15 W. This retrieved pulse shape agrees favorably with both, the spectrum in Fig. 5 and the measured autocorrelation in Fig. 6(a). Moreover, the retrieved pulse shape agrees widely with the expected temporal relaxation dynamics of the SESAM. It needs to be emphasized that all positive optical and electronic indications of mode-locking immediately vanish if the SESAM is replaced by the HR mirror. With the SESAM, however, indications for incomplete or partial mode-locking were neither observed in the autocorrelations nor the rf characterization.

In conclusion, we have demonstrated mode-locking of a red VECSEL, emitting 5.1 ps pulses at 675 nm with a SESAM as a passive mode-locker. The maximum average output power of 45 mW was obtained at the fundamental repetition rate of 972.7 MHz. These results open a new perspective on developing practical picoseconds lasers with high-average powers emitting in the red as they are required for a number of important applications in life-science, including fluorescent lifetime microscopy [18] and imaging techniques exploiting nonlinear optical absorption [19]. In the future, the laser could be in-well pumped [20] with 660 nm broad-area diode lasers or barrier-pumped with high-power blue laser diodes [21] for enhanced efficiency and practicality.

This work was financially supported by the graduate school of Tampere University of Technology, Academy of Finland (project grants #251018 and #128844) and the Jenny and Antti Wihuri Foundation. The authors thank S. Calvez, J. Hastie, and M. Dawson, University of Strathclyde for their early contributions to development of the gain chips. We acknowledge inspiring discussions with A. Tropper, University of Southampton, which motivated us to develop SESAMs for red wavelengths. We also thank EpiCrystals Ltd for loan of the fast photodiode used in the measurements.

References

1. M. Kuznetsov, F. Hakimi, R. Sprague, and A. Mooradian, IEEE Photon. Technol. Lett. **9**, 1063–1065 (1997).
2. P. Klopp, U. Griebner, M. Zorn, and M. Weyers, Appl. Phys. Lett. **98**, 071103 (2011).
3. B. Rudin, V. J. Wittwer, D. J. H. C. Maas, M. Hoffmann, O. D. Sieber, Y. Barbarin, M. Golling, T. Südmeyer, and U. Keller, Opt. Express **18**, 27582–27588 (2010).
4. K. G. Wilcox, A. H. Quarterman, V. Apostolopoulos, H. E. Beere, I. Farrer, D. A. Ritchie, and A. C. Tropper, Opt. Express **20**, 7040–7045 (2012).
5. U. Keller, K. J. Weingarten, F. X. Kärtner, D. Kopf, B. Braun, I. D. Jung, R. Fluck, C. Hönninger, N. Matuschek, and J. Aus der Au, IEEE J. Sel. Top. Quant. Electron. **2**, 435–453 (1996).
6. K. G. Wilcox, Z. Mihoubi, S. Elsmere, A. Quarterman, H. D. Foreman, S. Hashimoto, T. Südmeyer, U. Keller, and A. Tropper, Electron. Lett. **44**, 1469–1470 (2008).
7. M. A. Holms, P. Cusumano, D. Burns, A. I. Ferguson, and M. D. Dawson, in *Summaries of Papers Presented at the Conference on Lasers and Electro-Optics, 1999. CLEO '99* (1999), pp. 153–154.
8. J. Rautiainen, V.-M. Korpijärvi, J. Puustinen, M. Guina, and O. G. Okhotnikov, Opt. Express **16**, 15964–15969 (2008).
9. A. Rutz, V. Liverini, D. J. H. C. Maas, B. Rudin, A.-R. Bellancourt, S. Schön, and U. Keller, Electron. Lett. **42**, 926–927 (2006).
10. J. Rautiainen, J. Lyytikäinen, L. Toikkanen, J. Nikkinen, A. Sirbu, A. Mereuta, A. Caliman, E. Kapon, and O. G. Okhotnikov, IEEE Photon. Technol. Lett. **22**, 748–750 (2010).
11. S. Hoogland, A. Garnache, I. Sagnes, B. Paldus, K. J. Weingarten, R. Grange, M. Haiml, R. Paschotta, U. Keller, and A. C. Tropper, Electron. Lett. **39**, 846–847 (2003).
12. H. Lindberg, M. Sadeghi, M. Westlund, S. Wang, A. Larsson, M. Strassner, and S. Marcinkevicius, Opt. Lett. **30**, 2793–2795 (2005).
13. A. Härkönen, C. Grebing, J. Paajaste, R. Koskinen, J.-P. Alanko, S. Suomalainen, G. Steinmeyer, and M. Guina, Electron. Lett. **47**, 454-456 (2011).
14. J. Hastie, S. Calvez, M. Dawson, T. Leinonen, A. Laakso, J. Lyytikäinen, and M. Pessa, Opt. Express **13**, 77–81 (2005).

15. M. J. Lederer, V. Kolev, B. Luther-Davies, H. H. Tan, and C. Jagadish, J. Phys. D: Appl. Phys. **34**, 2455 (2001).
16. Z. L. Liau, Appl. Phys. Lett. **77**, 651–653 (2000).
17. J. W. Nicholson and W. Rudolph, J. Opt. Soc. Am. B **19**, 330–339 (2002).
18. A. Periasamy, P. Wodnicki, X. F. Wang, S. Kwon, G. W. Gordon, and B. Herman, Rev. Sci. Instrum. **67**, 3722–3731 (1996).
19. T. Liu, J. Wang, G. I. Petrov, V. V. Yakovlev, and H. F. Zhang, Med. Phys. **37**, 1518–1521 (2010).
20. N. Schulz, B. Rösener, R. Moser, M. Rattunde, C. Manz, K. Köhler, and J. Wagner, Appl. Phys. Lett. **93**, 181113 (2008).
21. A. Smith, J. E. Hastie, H. D. Foreman, T. Leinonen, M. Guina, and M. D. Dawson, Electron. Lett. **44**, 1195–1196 (2008).

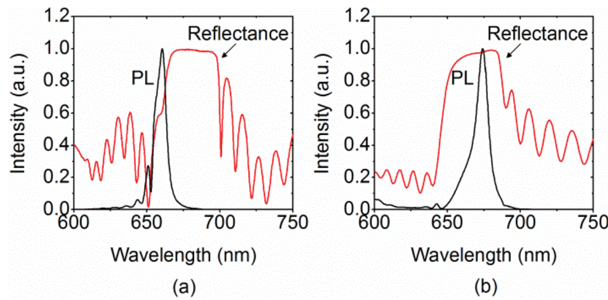

Fig. 1. Normalized photoluminescence (PL) and reflectance of (a) the VECSEL gain mirror and (b) the SESAM.

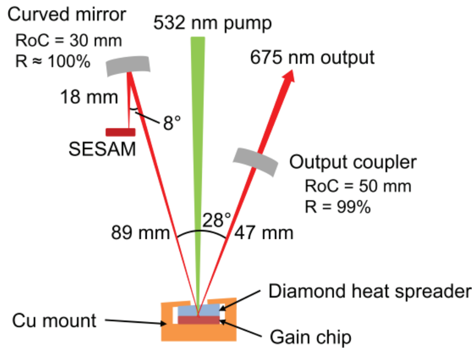

Fig. 2. Laser cavity setup. RoC = Radius of curvature, R = reflectivity.

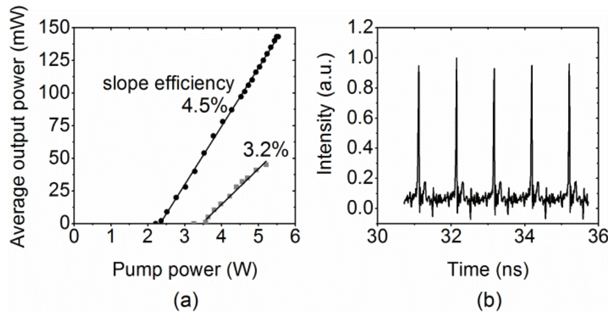

Fig. 3. (a) Laser output power as a function of incident 532 nm pump power for the laser without (black dots) and with (gray squares) the SESAM inserted in the cavity at 10 °C water cooling. A linear regression was calculated at 2.4–5.5 W and 3.6–5.2 W pump power range, respectively. (b) Pulse train measured with a 20 GHz sampling oscilloscope at 4.5 W pump power.

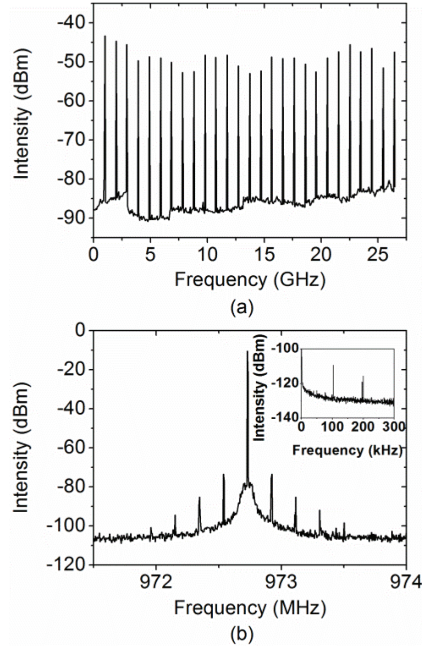

Fig. 4. Radio frequency spectrum measured with (a) 40 GHz photodiode using 100 kHz resolution bandwidth, and (b) 1 GHz photodiode using 100 Hz resolution bandwidth. The 200 kHz side bands in (b) are caused by a spurious modulation of the pump laser, see inset. Resolution bandwidth: 2 Hz. The 100 kHz noise component shown in the inset was present also when the pump laser was turned off, indicating that it originated from an external noise source, not from the pump laser. Therefore it is not shown in the RF spectrum of the laser.

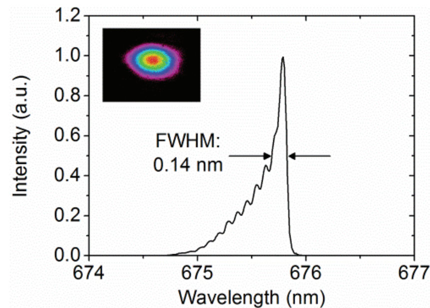

Fig. 5. Optical spectrum and beam profile (inset) of the mode-locked laser for a pump power of 5.2 W.

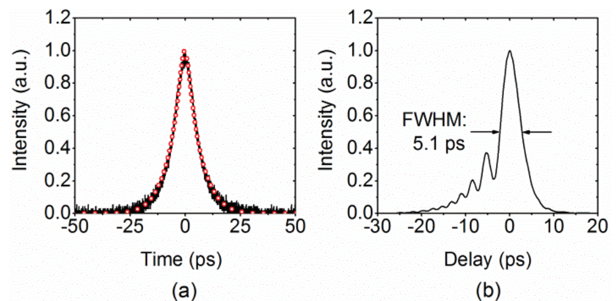

Fig. 6. (a) Measured intensity autocorrelation trace (black line) and the simulated autocorrelation of the optical pulses (red circles). (b) Reconstructed optical pulse shape using the PICASO method.

Full references

1. M. Kuznetsov, F. Hakimi, R. Sprague, and A. Mooradian, "High-power (>0.5-W CW) diode-pumped vertical-external-cavity surface-emitting semiconductor lasers with circular TEM00 beams," IEEE Photon. Technol. Lett. **9**, 1063–1065 (1997).
2. P. Klopp, U. Griebner, M. Zorn, and M. Weyers, "Pulse repetition rate up to 92 GHz or pulse duration shorter than 110 fs from a mode-locked semiconductor disk laser," Appl. Phys. Lett. **98**, 071103 (2011).
3. B. Rudin, V. J. Wittwer, D. J. H. C. Maas, M. Hoffmann, O. D. Sieber, Y. Barbarin, M. Golling, T. Südmeyer, and U. Keller, "High-power MIXSEL: an integrated ultrafast semiconductor laser with 6.4 W average power," Opt. Express **18**, 27582–27588 (2010).
4. K. G. Wilcox, A. H. Quarterman, V. Apostolopoulos, H. E. Beere, I. Farrer, D. A. Ritchie, and A. C. Tropper, "175 GHz, 400-fs-pulse harmonically mode-locked surface emitting semiconductor laser.," Opt. Express **20**, 7040–7045 (2012).
5. U. Keller, K. J. Weingarten, F. X. Kärtner, D. Kopf, B. Braun, I. D. Jung, R. Fluck, C. Hönninger, N. Matuschek, and J. Aus der Au, "Semiconductor saturable absorber mirrors (SESAM's) for femtosecond to nanosecond pulse generation in solid-state lasers," IEEE J. Sel. Top. Quant. Electron. **2**, 435–453 (1996).
6. K. G. Wilcox, Z. Mihoubi, S. Elsmere, A. Quarterman, H. D. Foreman, S. Hashimoto, T. Südmeyer, U. Keller, and A. Tropper, "Passively modelocked 832 nm vertical-external-cavity surface-emitting semiconductor laser producing 15.3 ps pulses at 1.9 GHz repetition rate," Electron. Lett. **44**, 1469–1470 (2008).
7. M. A. Holms, P. Cusumano, D. Burns, A. I. Ferguson, and M. D. Dawson, "Mode-locked operation of a diode-pumped, external-cavity GaAs/AlGaAs surface emitting laser," in *Summaries of Papers Presented at the Conference on Lasers and Electro-Optics, 1999. CLEO '99* (1999), pp. 153–154.
8. J. Rautiainen, V.-M. Korpijärvi, J. Puustinen, M. Guina, and O. G. Okhotnikov, "Passively mode-locked GaInNAs disk laser operating at 1220 nm," Opt. Express **16**, 15964–15969 (2008).
9. A. Rutz, V. Liverini, D. J. H. C. Maas, B. Rudin, A.-R. Bellancourt, S. Schön, and U. Keller, "Passively modelocked GaInNAs VECSEL at centre wavelength around 1.3 µm," Electron. Lett. **42**, 926–927 (2006).
10. J. Rautiainen, J. Lyytikäinen, L. Toikkanen, J. Nikkinen, A. Sirbu, A. Mereuta, A. Caliman, E. Kapon, and O. G. Okhotnikov, "1.3-µm mode-locked disk laser with wafer fused gain and SESAM structures," IEEE Photon. Technol. Lett. **22**, 748–750 (2010).
11. S. Hoogland, A. Garnache, I. Sagnes, B. Paldus, K. J. Weingarten, R. Grange, M. Haiml, R. Paschotta, U. Keller, and A. C. Tropper, "Picosecond pulse generation with 1.5 µm passively modelocked surface-emitting semiconductor laser," Electron. Lett. **39**, 846–847 (2003).
12. H. Lindberg, M. Sadeghi, M. Westlund, S. Wang, A. Larsson, M. Strassner, and S. Marcinkevicius, "Mode locking a 1550 nm semiconductor disk laser by using a GaInNAs saturable absorber," Opt. Lett. **30**, 2793–2795 (2005).
13. A. Härkönen, C. Grebing, J. Paajaste, R. Koskinen, J.-P. Alanko, S. Suomalainen, G. Steinmeyer, and M. Guina, "Modelocked GaSb disk laser producing 384 fs pulses at 2 µm wavelength," Electron. Lett. **47**, 454-456 (2011).
14. J. Hastie, S. Calvez, M. Dawson, T. Leinonen, A. Laakso, J. Lyytikäinen, and M. Pessa, "High power CW red VECSEL with linearly polarized TEM00 output beam," Opt. Express **13**, 77–81 (2005).
15. M. J. Lederer, V. Kolev, B. Luther-Davies, H. H. Tan, and C. Jagadish, "Ion-implanted InGaAs single quantum well semiconductor saturable absorber mirrors for passive mode-locking," J. Phys. D: Appl. Phys. **34**, 2455 (2001).
16. Z. L. Liau, "Semiconductor wafer bonding via liquid capillarity," Appl. Phys. Lett. **77**, 651–653 (2000).
17. J. W. Nicholson and W. Rudolph, "Noise sensitivity and accuracy of femtosecond pulse retrieval by phase and intensity from correlation and spectrum only (PICASO)," J. Opt. Soc. Am. B **19**, 330–339 (2002).
18. A. Periasamy, P. Wodnicki, X. F. Wang, S. Kwon, G. W. Gordon, and B. Herman, "Time-resolved fluorescence lifetime imaging microscopy using a picosecond pulsed tunable dye laser system," Rev. Sci. Instrum. **67**, 3722–3731 (1996).
19. T. Liu, J. Wang, G. I. Petrov, V. V. Yakovlev, and H. F. Zhang, "Photoacoustic generation by multiple picosecond pulse excitation," Med. Phys. **37**, 1518–1521 (2010).
20. N. Schulz, B. Rösener, R. Moser, M. Rattunde, C. Manz, K. Köhler, and J. Wagner, "An improved active region concept for highly efficient GaSb-based optically in-well pumped vertical-external-cavity surface-emitting lasers," Appl. Phys. Lett. **93**, 181113 (2008).
21. A. Smith, J. E. Hastie, H. D. Foreman, T. Leinonen, M. Guina, and M. D. Dawson, "GaN diode-pumping of red semiconductor disk laser," Electron. Lett. **44**, 1195–1196 (2008).

Tampereen teknillinen yliopisto
PL 527
33101 Tampere

Tampere University of Technology
P.O.B. 527
FI-33101 Tampere, Finland

ISBN 978-952-15-3391-4
ISSN 1459-2045